Analysis of a model microswimmer with applications to blebbing cells and mini-robots

Qixuan Wang & Hans G. Othmer

Journal of Mathematical Biology

ISSN 0303-6812
Volume 76
Number 7

J. Math. Biol. (2018) 76:1699-1763
DOI 10.1007/s00285-018-1225-y

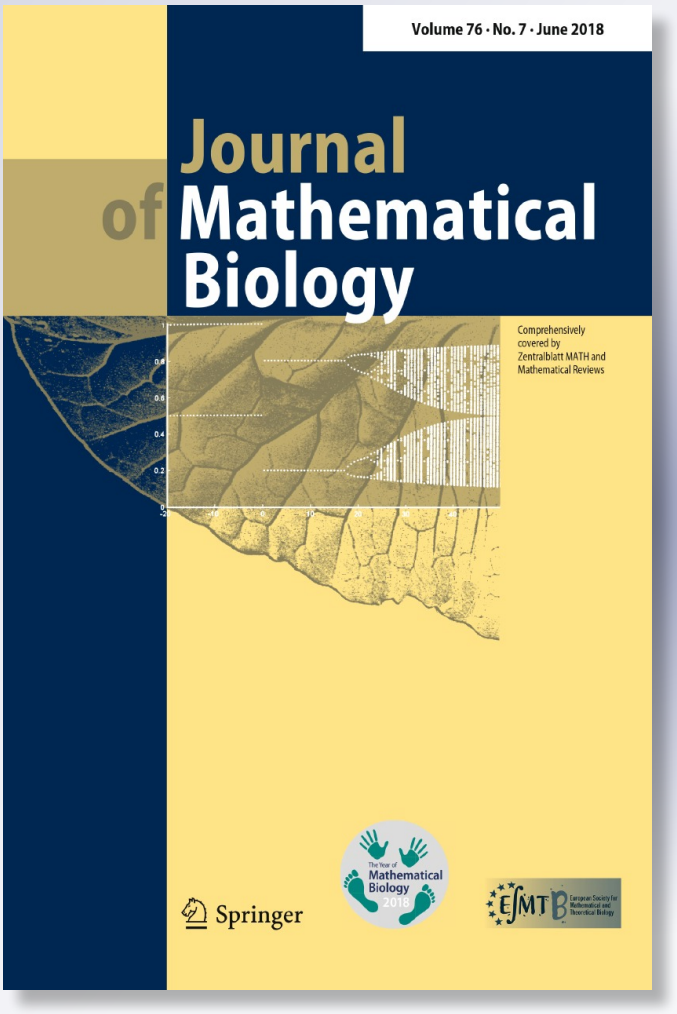

Springer

J. Math. Biol. (2018) 76:1699–1763
https://doi.org/10.1007/s00285-018-1225-y

Mathematical Biology

Analysis of a model microswimmer with applications to blebbing cells and mini-robots

Qixuan Wang[1] · **Hans G. Othmer**[2]

Received: 6 October 2016 / Revised: 5 January 2018 / Published online: 1 March 2018

Abstract Recent research has shown that motile cells can adapt their mode of propulsion depending on the environment in which they find themselves. One mode is swimming by blebbing or other shape changes, and in this paper we analyze a class of models for movement of cells by blebbing and of nano-robots in a viscous fluid at low Reynolds number. At the level of individuals, the shape changes comprise volume exchanges between connected spheres that can control their separation, which are simple enough that significant analytical results can be obtained. Our goal is to understand how the efficiency of movement depends on the amplitude and period of the volume exchanges when the spheres approach closely during a cycle. Previous analyses were predicated on wide separation, and we show that the speed increases significantly as the separation decreases due to the strong hydrodynamic interactions between spheres in close proximity. The scallop theorem asserts that at least two degrees of freedom are needed to produce net motion in a cyclic sequence of shape changes, and we show that these degrees can reside in different swimmers whose collective motion is studied. We also show that different combinations of mode sharing can lead to significant differences in the translation and performance of pairs of swimmers.

Supported in part by NSF Grants DMS 0817529 and 1311974, NIH Grants GM29123 and 54-CA-210190, and a grant from the Simons Fdn to H. G. Othmer, and by NIH Grant R01GM107264 and NSF Grant DMS1562176 to Qing Nie.

✉ Qixuan Wang
qixuanw@uci.edu

Hans G. Othmer
othmer@math.umn.edu

1 540R Rowland Hall, University of California, Irvine, Irvine, USA

2 School of Mathematics, 270A Vincent Hall, University of Minnesota, Minneapolis, USA

Keywords Low Reynolds number swimming · Self-propulsion · Amoeboid swimming · Robotic swimmers · *Pushmepullyou* · Reflection method

Mathematics Subject Classification 92B05 · 76D07 · 76D10 · 76M45 · 76Z99

Contents

1 Introduction

Locomotion of cells, both individually and collectively, is an important process in development, tissue regeneration, the immune response, cancer metastasis, and wound healing. The motion of an individual cell is classified as either mesenchymal or amoeboid, depending on how it interacts mechanically with its environment (Binamé et al. 2010). The mesenchymal mode is used by cells such as fibroblasts that have a well-organized cytoskeleton, which comprises the actin filaments, intermediate filaments, and microtubules, and use strong adhesions to transmit force to their surroundings via integrin-mediated adhesion complexes. Mesenchymal movement usually involves the extension of broad flat lamellipodia and/or pseudopodia and is driven by actin polymer-

ization at the leading edge. Amoeboid motion involves a less structured cytoskeleton and weaker surface interactions, and leads to speeds up to forty times faster than those resulting from mesenchymal motion (Renkawitz and Sixt 2010). In this mode cells may use pseudopodia, but can also use protrusions such as blebs (Fig. 1) which involve blister-like extensions of the membrane. Leukocytes, which normally use the mesenchymal mode in the extracellular matrix (ECM), can migrate *in vivo* in the absence of integrins, using a 'flowing and squeezing' mechanism (Lämmermann et al. 2008). Cells of the slime mold *Dictyostelium discoideum* (Dd) can move either by extending pseudopodia or by blebbing, and they monitor the stiffness of their surroundings to determine the mode: pseudopodia in a compliant medium and blebbing in stiffer media (Zatulovskiy et al. 2014). Furthermore, blebbing cells are efficient in their chemotactic response to cyclic-AMP, producing nearly all of their blebs upgradient. In certain tumor cells, knockdown of secreted MMPs, which are enzymes that degrade the ECM, produces only a small reduction in speed because cells compensate for the decreased proteolysis by undergoing a 'mesenchymal-to-amoeboid transition (MAT) (Wolf et al. 2003; Friedl and Wolf 2003). The MAT can also be triggered by changes in the adhesiveness of the ECM (Friedl and Alexander 2011; van Zijl et al. 2011). Moreover, cells such as Dd and neutrophils can swim in a fluid environment (Barry and Bretscher 2010), and a model of swimming by such cells appears in Wang and Othmer (2016). In fact, some cells move only by blebbing. Certain carcinoma cells in suspension spontaneously polarize and forms blebs at the leading edge, and while they cannot move on 2D substrates, they can move in 3D (Bergert et al. 2012).

Thus numerous cell types display enormous plasticity in the choice of locomotory mode, in that they sense the mechanical properties of the environment and adjust the balance between the modes by adjusting the balance between signal transduction pathways that control the structure of the cytoskeleton (Renkawitz et al. 2009; Bergert et al. 2012; Fackler and Grosse 2008). Crawling and swimming are the extremes on a continuum of strategies, but cells sense their environment and use the most efficient strategy in a given context. While blebbing is frequently thought of as a 'push–pull' mechanism in which a cell expands at the front, followed by contraction at the rear, another type of blebbing called 'stable-bleb migration', has recently been observed in progenitor cells of the gastrulating zebrafish embryo (Maiuri et al. 2015; Ruprecht et al. 2015). In this mode cells form a balloon-like protrusion at their front, and these cells can move more rapidly than other cells in the embryo.

The fact that some cells can use very complicated shape changes for locomotion leads to a question posed by experimentalists, which is 'How does deformation of the cell body translate into locomotion?' (Renkawitz and Sixt 2010). Two examples are shown in Fig. 1. In (a) is shown a cell that blebs and moves very little, and in (b) is a Dd cell that uses a combination of blebs at the front and contraction at the rear to move in a tissue-like environment. Figure 1c shows the different modes used by cells in different environments. In this paper we analyze a simple model of the push–pull type for movement in a fluid by blebbing, motivated by the recent experimental findings mentioned above. Protrusions and other shape changes require forces that must be correctly orchestrated in space and time to produce net motion—protrusions on cells in (a) are not, while those in (b) are—and to understand this orchestration one must couple the cellular dynamics with the dynamics of the surrounding fluid or ECM.

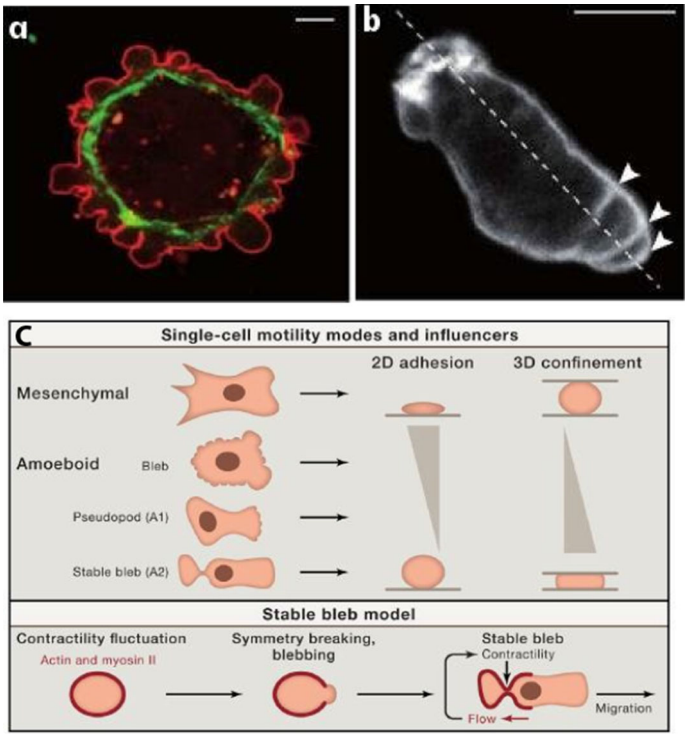

Fig. 1 **a** Blebbing on a melanoma cell: myosin (green) localizes under the blebbing membrane (red). **b** The actin cortex of a blebbing Dd cell migrating to the lower right. Arrowheads indicate the successive blebs and arcs of the actin cortex (from Charras and Paluch 2008). **c** A schematic of the various modes of movement (from Welch 2015) (color figure online)

At the spatial scale of cells and the speeds at which they move, the exterior fluid problem is a low Reynolds number (LRN) flow. LRN flows have been extensively studied in the context of bacterial and sperm movement. Taylor Taylor (1952) treated the flagellum as an infinite cylinder executing small-amplitude oscillations, and Hancock Hancock (1953) developed a large-amplitude theory using singular solutions to the Stokes equations situated along the center line of a flagellum, to describe the motion in three dimensions. This 'slender-body theory' was further developed by Higdon (1979) to account for hydrodynamic interactions between the flagellum and the cell head, and Phan-Thien et al. (1987) used the boundary-element method to allow for non-spherical heads and non-slender flagella. The current state of knowledge is reviewed in Lauga and Powers (2009) and Elgeti et al. (2015).

A separate path in cell locomotion at LRN was stimulated by Purcell's seminal article (Purcell 1977) and by interest in mini-robots. Several models of LRN swimmers that do not rely on slender-body theory exist. There is *Purcell's two-hinge swimmer*, the Najafi–Golestanian *accordion* model in which three spheres of fixed size are connected by movable links (Najafi and Golestanian 2004; Alexander et al. 2009), the *push-me-pull-you* swimmer (PMPY) (Avron et al. 2005), in which two spheres

that can expand or contract radially are connected by an extensible arm, and a three-sphere volume-exchange or *breather* model in which the spheres are linked by rigid connectors but exchange volume (Wang et al. 2012). In Wang and Othmer (2015) we compared the performance of these models, and showed that generally the PMPY model is the most efficient.[1]

In many earlier analyses of two- or three-sphere models, the spheres are treated as point particles that generate point forces, which in effect means that the separation between them is large enough that hydrodynamic interactions between the spheres can be neglected. Thus the conclusions reached in these analyses are not directly applicable to models of cells that swim by blebbing, nor to realistic robotic swimmers. Hydrodynamic interactions between spheres of fixed size have been studied for almost a century, and analytical results are available for a pair of spheres connected by a rigid rod (a dumbbell) (Stimson and Jeffery 1926). Approximation methods for other configurations center on either a truncated multipole expansion of the Green's function or on the method of reflections, both described in Kim and Karrila (1991). An analysis of hydrodynamic interactions as a function of the ratio of the sphere radius to the separation between spheres, is done for the accordion model in both Newtonian and non-Newtonian fluids in Curtis and Gaffney (2013).

In this paper we use the basic PMPY swimmer as a model of blebbing or for mini-robots to study the swimming behaviors of solitary and group swimmers at LRN. Our objective is to understand the effect of higher-order hydrodynamic interactions between spheres in a PMPY swimmer, and for this we use the reflection method (Kim and Karrila 1991). In Sect. 3 we investigate the difference between the higher-order solution and the asymptotic solution both analytically and numerically, and show that the asymptotic solution may severely underestimate the effectiveness of a PMPY swimmer. There we also compare its swimming behavior to existing experimental data on swimming Dd amoebae. In Sect. 4 we apply the reflection method to a system consisting of one active PMPY swimmer and a passive buoyant object. We discuss the hydrodynamic effect of the velocity field generated by the PMPY swimmer on the passive object and vice versa, we numerically investigate how effectively the swimmer can pursue the passive object, and we study the higher-order hydrodynamic effects on a tracer trajectory. In Sect. 5 we apply the reflection method to a system of two PMPY models, one in which the swimmers are collinear and the other a planar system, and we discuss the higher-order hydrodynamic interactions between the two active swimmers. In Sect. 6 we review the *scallop theorem*, which is the fundamental principle of LRN swimming, and discuss how this extends to the hydrodynamic interactions amongst several swimmers, each unable to swim on its own. We also discuss how different combinations of shape change modes affect the collective swimming behavior of such swimmers. Throughout we only consider the regime in which there is sufficient spacing between units so as to justify the neglect of the lubrication effects that arise when objects in relative motion are in close proximity. Such effects are discussed by various authors (Brenner 1961; Cooley and O'Neill 1969a, b) in other contexts.

[1] The measures of performance that are used here and in the literature do not include the work needed to move material between spheres in the PMPY and breather models, and thus the accordion model suffers by comparison in this respect.

2 Swimming at low Reynolds number

Hereafter we suppose that the swimmer is immersed in an infinite, incompressible fluid of density ρ and viscosity μ, that is at rest at infinity. The Navier–Stokes equations for the fluid velocity $\mathbf{u}$ are (Childress 1977)

$$\rho\frac{\partial \mathbf{u}}{\partial t} + \rho(\mathbf{u}\cdot\nabla)\mathbf{u} = \nabla\cdot\mathbb{T} + \mathbf{f}_{\text{ext}} = -\nabla p + \mu\Delta\mathbf{u} + \mathbf{f}_{\text{ext}}, \tag{2.1}$$

$$\nabla\cdot\mathbf{u} = 0 \tag{2.2}$$

where

$$\mathbb{T} = -p\mathbf{I} + \mu(\nabla\mathbf{u} + (\nabla\mathbf{u})^T)$$

is the Cauchy stress tensor and $\mathbf{f}_{\text{ext}}$ is the external force field. We further assume that the swimmer is self-propelled and does not rely on any exterior force, and therefore we require that $\mathbf{f}_{\text{ext}} = 0$ throughout. Either the swimmer is neutrally buoyant or the gravitational force is included in the pressure.

When converted to dimensionless form and the symbols re-defined, these equations read

$$\text{ReSl}\frac{\partial \mathbf{u}}{\partial t} + \text{Re}(\mathbf{u}\cdot\nabla) = -\nabla p + \mu\Delta\mathbf{u}, \quad \nabla\cdot\mathbf{u} = 0, \tag{2.3}$$

where the Reynolds number based on a characteristic length scale L and a characteristic speed scale U is $\text{Re} = \rho\text{LU}/\mu$. In addition, $\text{Sl} = \omega L/U$ is the Strouhal number and ω is a characteristic frequency of the shape changes. When $\text{Re} \ll 1$ the convective momentum term in equation (2.3) can be neglected, but the time variation requires that $\text{ReSl} = \omega\rho L^2/\mu$. When both terms are neglected, which we assume throughout, the low Reynolds number (LRN) flow is governed by the Stokes equations

$$\mu\Delta\mathbf{u} - \nabla p = \mathbf{0}, \quad \nabla\cdot\mathbf{u} = 0. \tag{2.4}$$

Throughout we consider small cells such as Dd, whose small size and low speed lead to LRN flows (Wang and Othmer 2015), and in this regime time does not appear explicitly, there are no inertial effects, and bodies move by exploiting the viscous resistance of the fluid. As a result, time-reversible deformations produce no motion, which is known as the "scallop theorem" (Purcell 1977). Under the assumptions of an infinite fluid domain with $\mathbf{u} = \mathbf{0}$ at infinity and the absence of external forces, there is no net force or torque on a self-propelled swimmer in the Stokes regime, and therefore movement is a purely geometric process: the net displacement of a swimmer during a stroke is independent of the rate at which the stroke is executed, as long as the Reynolds number remains small enough.

Let $D(t) \subset \mathbb{R}^3$ be a closed, compact set occupied by the swimmer at time t, and let $\partial D(t)$ denote its prescribed time-dependent boundary. In reality amoeboid swimming cells may take up or release fluid, but we assume that the prescribed motion of the boundary is such that the volume of the swimmer is conserved under all deformations.

A *swimming stroke* is specified by a time-dependent sequence of shapes, and it is *cyclic* if the initial and final shapes are identical, i.e., $\partial D(0) = \partial D(T)$, where T is the period. The swimmer's boundary velocity $\mathbf{V}$ relative to fixed coordinates can be written as a part $\mathbf{v}$ that defines the intrinsic shape deformations, and a rigid motion part $\mathbf{U} + \boldsymbol{\Omega} \times \mathbf{x}$, where $\mathbf{U}$, $\boldsymbol{\Omega}$ are the rigid translation and rotation, resp.. If $\mathbf{u}$ denotes the velocity field in the fluid exterior to D, then a standard LRN self-propulsion problem is: *given a cyclic shape deformation specified by* $\mathbf{v}$, *solve the Stokes equations* (2.4) *subject to*

$$\int_{\partial D} \sigma \cdot \mathbf{n} = 0, \quad \int_{\partial D} \mathbf{x} \times (\sigma \cdot \mathbf{n}) = \mathbf{0}, \quad \mathbf{u}|_{\mathbf{x}\in\partial D} = \mathbf{V} = \mathbf{v} + \mathbf{U} + \boldsymbol{\Omega} \times \mathbf{x},$$
$$\mathbf{u}|_{\mathbf{x}\to\infty} = \mathbf{0}$$

where $\mathbf{n}$ is the exterior normal, and the integrals are the force- and torque-free conditions.

3 The solitary PMPY swimmer

The simplest PMPY model consists of two spheres that can expand or contract radially, and an extensible, massless rod connecting them (Fig. 2).

The standard assumptions on the domain and the fluid, which is described by the Stokes' Equations (2.4), apply here. Let $R_i(t)$ be the radius of the ith sphere ($i = 1, 2$) and $l(t)$ the length of the rod. The prescribed motion of each sphere consists of two parts: a rigid translation along the x-axis at velocity $\mathbf{U}_i = U_i \mathbf{e}_x$, and a radial expansion or contraction: $\dot{R}_i$. Thus the no-slip boundary conditions on the surfaces of the two spheres can be expressed as:

$$\mathbf{u}(\mathbf{r}_i; t) = U_i(t)\mathbf{e}_x + \dot{R}_i(t)\hat{\mathbf{r}}_i \quad \text{at} \quad |\mathbf{r}_i| = R_i(t), \quad i = 1, 2 \tag{3.1}$$

where $\mathbf{r}_i$ is the radius vector with origin at the center of the ith sphere (Fig. 2) and $\hat{\mathbf{r}}_i$ is the outward unit vector along the $\mathbf{r}_i$ direction. The instantaneous velocity of the swimmer is defined as the average of the velocities of the two spheres

$$\overline{\mathbf{U}} = \frac{\mathbf{U}_1 + \mathbf{U}_2}{2} = \frac{U_1 + U_2}{2}\mathbf{e}_x, \tag{3.2}$$

although other measures such as the velocity of the center of mass could also be used. The instantaneous velocity would change in the latter case, but the net translation during a cycle would not.

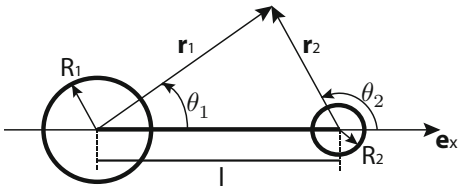

Fig. 2 Geometry of the pushmpullyou model

The rate of change of the length of the connecting rod is $\dot{l}(t)$, and thus the velocities of the two spheres are related by:

$$U_2 - U_1 = \dot{l}. \tag{3.3}$$

We assume that the total volume $V_1 + V_2 \equiv V_T$ is conserved during the motion, and thus the radii of the spheres satisfy the constraint

$$R_1^3(t) + R_2^3(t) \equiv \frac{3}{4\pi} V_{\mathrm{T}}. \tag{3.4}$$

In addition, the PMPY swimmer is force- and torque-free, and while the swimmer's linear geometry automatically guarantees that it is torque-free in the absence of asymmetric shear forces, the force-free constraint is non-trivial. Let $\mathbf{F}_i(t)$ be the hydrodynamic force due to drag and expansion exerted on the ith sphere at time t—then the constraint is that

$$\sum_{i=1,2} \mathbf{F}_i(t) \equiv \mathbf{0}. \tag{3.5}$$

It is clear that extension and contraction of the rod produces a direct effect on the translation of either sphere, whereas the expansion only has an indirect effect. If sphere 1 expands this has no direct effect on its movement since the expansion is radially symmetric, but the flow generated affects the second sphere. Simultaneously, the conservation of volume condition produces a reduction in size of the second sphere, which induces a flow that affects the first sphere. In the LRN regime these effects are felt instantaneously.[2]

The shape changes for a PMPY swimmer are described by $\dot{l}$, $\dot{R}_1$ and $\dot{R}_2$, but in view of (3.4) two degrees of freedom define its motion. A cyclic stroke of a PMPY swimmer is determined by a periodic profile $(\dot{l}(t), \dot{R}_1(t))$ for $t \in [0, T]$, and a solution of the swimmer problem entails finding the relation between the swimmer's velocity $\overline{\mathbf{U}}$ and the controls $(\dot{l}, \dot{R}_1)$. In the general analysis that follows we assume that the controls are chosen so that the motion is not time reversible. An example of how the choice of phase difference between $\dot{l}(t)$ and $\dot{R}_1(t)$ affects the efficiency when both vary sinusoidally is given later.

3.1 Scaling the PMPY problem

The PMPY model contains three length scales: the radii of the spheres R_1, R_2 and the length of the connecting arm l. The geometry of the model requires that the two spheres never overlap, hence $R_1 + R_2 < l$. As previously defined, $Re = \rho L U/\mu \ll 1$, and therefore all lengths in the model must be small enough to ensure that

[2] The reader can easily show that in the absence of volume exchange the net translation after a periodic extension and contraction of the rod produces no motion. This provides the simplest example of the scallop theorem discussed later.

$$R_1, R_2, l \ll \frac{\mu}{\rho U}.$$

However even if this LRN pre-condition is satisfied, the relations among the lengths R_1, R_2, l are also crucial in the swimming problem, and different relations may lead to different regimes of interaction (Kim and Karrila 1991). We assume that the radii of the two spheres are comparable, i.e., $O(R_1) \sim O(R_2)$, which rules out the possibility of interactions between a large sphere and a very small one (this case is discussed in Kim and Karrila (1991)). This leaves three major scenarios: the spheres are in close proximity in part of the cycle, *i.e.*, $R_1(t)+R_2(t) \sim l(t)$ in part of the cycle; the spheres are widely-separated spheres throughout the cycle, where $R_1(t)+R_2(t) \ll l(t)$, and an intermediate regime. In the first regime the flow in the gap region dominates when the spheres nearly touch in part of the cycle, and the lubrication approximation provides the leading terms in an asymptotic expansion (Kim and Karrila 1991). If the spheres are also well-separated in part of the cycle this leads to a difficult matching problem that is not attempted here. We only consider the intermediate regime in which the separation never enters the lubrication regime, but is also not in the infinitely-separated regime throughout the cycle, as this has been studied previously (Avron et al. 2005). Our objective is to use the reflection method to determine corrections to the problem with very large separation.

Since the length scales involved are time-dependent, some care is needed in setting an appropriate scaling for the lengths. The primary criterion that must be met is that $(R_1(t) + R_2(t))/l(t) < 1$ throughout the cycle. Define

$$R_M = \max_t\{R_i(t)\}_{i=1,2}, \quad L_m = \min_t\{l(t)\}$$

and

$$\delta = R_M/L_m,$$

We then nondimensionalize the radii and rod lengths by R_M and L_m, resp.,

$$\hat{R}_i = \frac{R_i}{R_M} \leq 1, \quad \hat{l} = \frac{l}{L_m} \geq 1, \tag{3.6}$$

and we assume that the amplitudes of both rod displacement and radius changes are of the same order of R_M. Thus we let $\xi = \dot{l}$ and $\zeta_i = \dot{R}_i$, and apply the following scaling:

$$\hat{\xi} = \frac{T}{R_M}\xi, \quad \hat{\zeta}_i = \frac{T}{R_M}\zeta_i$$

Next, we nondimensionalize other length scales by R_M as well, and time by the period T to obtain

$$\hat{\mathbf{x}} = \frac{\mathbf{x}}{R_M}, \quad \hat{\nabla} = R_M\nabla, \quad \hat{t} = \frac{t}{T}, \quad \hat{\mathbf{u}} = \frac{T}{R_M}\mathbf{u}, \quad \hat{\mathbf{U}}_i = \frac{T}{R_M}\mathbf{U}_i, \quad \hat{\boldsymbol{\Omega}}_i = T\boldsymbol{\Omega}_i.$$

Finally, the drag force $\mathbf{F}$ exerted on a sphere of radius R in a quiescent fluid is related to the sphere velocity $\mathbf{U}$ via $\mathbf{F} = 6\pi\mu R\mathbf{U}$, which leads to the following scaling for forces:

$$\hat{\mathbf{F}} = \frac{T}{6\pi\mu R_M^2}\mathbf{F} = \hat{R}\hat{\mathbf{U}}. \tag{3.7}$$

3.2 The reflection method

In previous analyses of the PMPY swimmer the spheres are infinitely-separated, and thus treated as the source of point forces. The free space Green's function, or Stokeslet, for the Stokes problem is

$$\mathbf{G}(\mathbf{x}, \mathbf{x}_0) = \frac{1}{r}\left[\mathbf{I} + \frac{\mathbf{rr}}{r^2}\right] = \frac{1}{r}\left[\mathbf{I} + \hat{\mathbf{r}}\hat{\mathbf{r}}\right]. \tag{3.8}$$

Here $\mathbf{I}$ is the unit second-rank tensor, $\mathbf{r} = \mathbf{x} - \mathbf{x}_0$, $r = |\mathbf{x} - \mathbf{x}_0|$ and $\hat{\mathbf{r}} = \mathbf{r}/r$. Thus the velocity field generated at a point $\mathbf{x}$ by a point force $\mathbf{F}$ at $\mathbf{x}_0$ is

$$\mathbf{u}(\mathbf{x}) = \frac{\mathbf{G}(\mathbf{x}, \mathbf{x}_0)}{8\pi\mu} \cdot \mathbf{F}(\mathbf{x}_0). \tag{3.9}$$

When combined with the flow field generated by expansion of the spheres (*cf.* Appendix A), this leads to the following approximation for the velocity of the swimmer (Avron et al. 2005).

$$\overline{U} = \frac{R_1 - R_2}{2(R_1 + R_2)}\dot{l} + \left(\frac{R_1}{l}\right)^2 \dot{R}_1 \tag{3.10}$$

The first and second terms are the leading order terms that result from the cyclic change of the rod length and the contraction and expansion of the spheres, resp.. If we nondimensionalize this solution we obtain

$$\hat{\overline{U}} = \frac{\hat{R}_1 - \hat{R}_2}{2(\hat{R}_1 + \hat{R}_2)}\hat{\xi} + \left(\frac{\hat{R}_1}{\hat{l}}\right)^2 \delta^2 \hat{\xi}_1. \tag{3.11}$$

Thus the effect of changes in the rod length for widely-separated spheres is $O(1)$, while the leading term of sphere volume change is $O(\delta^2)$. Thus Eq. (3.10) is only accurate to $O(1)$, and therefore at least the $O(\delta)$ and $O(\delta^2)$ terms that result from the movement of the spheres should be taken into account. In regard to higher-order terms, (3.11) suggests that corrections resulting from rod length change may add $O(\delta)$ and $O(\delta^2)$ terms, while those from sphere volume change only appear in the $O(\delta^3)$ terms. The effect is that higher-order interactions resulting from rod length changes play a more important role than the volumetric changes for a single PMPY swimmer. As will be shown later, the relative importance of these factors changes in other situations.

One approach to obtaining the higher-order effects of the interactions between the spheres in the PMPY model, both from their relative motion and the volume changes, is the reflection method (Kim and Karrila 1991). A general description of the algorithm underlying this method is as follows.

- **The 0th reflection** The 0th reflection for either sphere is simply the superposition of this sphere alone in whatever background flow, call it $\mathbf{u}_\infty$, exists. In other words, in this step no interaction between the spheres are taken into consideration. We denote the velocity field that results from translation and expansion/contraction of the ith sphere by $\mathbf{u}_i^{(0)}(\mathbf{x})$, and the sum of these is the new field $\mathbf{u}^{(0)}(\mathbf{x})$.
- **The 1st reflection** However, in the combined field $\mathbf{u}^{(0)}(\mathbf{x})$ the no-slip boundary conditions on each sphere are not met and to correct this one computes a new field by solving two new Stokes problems: one with the boundary value $-\mathbf{u}_1^{(0)}(\mathbf{x})$ on sphere 2, and one with the value $-\mathbf{u}_2^{(0)}(\mathbf{x})$ on sphere 1. This leads to two new fields $\mathbf{u}_{12}^{(1)}(\mathbf{x})$ and $\mathbf{u}_{21}^{(1)}(\mathbf{x})$, and the first reflection field is $\mathbf{u}^{(1)}(\mathbf{x}) = \mathbf{u}_{12}^{(1)}(\mathbf{x}) + \mathbf{u}_{21}^{(1)}(\mathbf{x})$.
- **The 2nd reflection** In the second reflection two new corrections that satisfy $-\mathbf{u}_{12}^{(1)}(\mathbf{x})$ and $-\mathbf{u}_{21}^{(1)}(\mathbf{x})$, on sphere 1 and 2, respectively, are computed, and are called $\mathbf{u}_{121}^{(2)}(\mathbf{x})$, and $\mathbf{u}_{212}^{(2)}(\mathbf{x})$. The resulting second reflection field is $\mathbf{u}^{(2)}(\mathbf{x}) = \mathbf{u}_{121}^{(2)}(\mathbf{x}) + \mathbf{u}_{212}^{(2)}(\mathbf{x})$.
- Repeat until the desired accuracy is achieved.

This process has been proven to converge very rapidly for finite domains (Luke 1989).

We denote the translational and rotational velocities of sphere i that result from the nth reflection as $\mathbf{U}_i^{(n)}$ and $\boldsymbol{\Omega}_i^{(n)}$, resp., and the stress on sphere i by $\mathbb{T}_i^{(n)}$. To compute $\mathbf{U}_i^{(n)}$ and $\boldsymbol{\Omega}_i^{(n)}$, we use the reciprocal theorem (Stone and Samuel 1996), which states that $\nabla \cdot (\mathbb{T}_j^{(n-1)} \cdot \mathbf{U}_i^{(n)}) = \nabla \cdot (\mathbb{T}_i^{(n)} \cdot \mathbf{u}_j^{(n-1)})$, and from this and a similar equivalence for the torques it follows that

$$\mathbf{U}_i^{(n)} = \frac{1}{4\pi R_i^2} \int_{S_i} \mathbf{u}_j^{(n-1)}(\mathbf{x})\, \mathrm{d}S(\mathbf{x}) \tag{3.12}$$

$$\boldsymbol{\Omega}_i^{(n)} = \frac{3}{8\pi R_i^3} \int_{S_i} \mathbf{n} \times \mathbf{u}_j^{(n-1)}(\mathbf{x})\, \mathrm{d}S(\mathbf{x}). \tag{3.13}$$

Since we are considering spheres, equivalent expressions obtained by use of Faxén's law (Kim and Karrila 1991) are

$$\mathbf{U}_i^{(n)} = \left(1 + \frac{R_i^2}{6}\nabla^2\right)\mathbf{u}_j^{(n-1)}\Big|_{\mathbf{x}=\mathbf{x}_i} \tag{3.14}$$

$$\boldsymbol{\Omega}_i^{(n)} = \frac{1}{2}\nabla \times \mathbf{u}_j^{(n-1)}\Big|_{\mathbf{x}=\mathbf{x}_i} \tag{3.15}$$

In a self-propulsion problem at LRN the flows vanish at infinity, and in this context the velocity generated by a sphere of radius R centered at $\mathbf{x}_0$, subject to the force $\mathbf{F}$, and 'expanding' at the rate $\dot{R} = \mathrm{d}R/\mathrm{d}t$ is (*cf.* Appendix A):

$$\mathbf{u}^{(0)}\big(\mathbf{r};\, R, \mathbf{F}, \dot{R}\big) = \frac{1}{24\pi\mu r}\Big[\big(3+\frac{R^2}{r^2}\big)\mathbf{F} + 3\big(1-\frac{R^2}{r^2}\big)\big(\mathbf{F}\cdot\widehat{\mathbf{r}}\big)\widehat{\mathbf{r}}\Big] + \dot{R}\Big(\frac{R}{r}\Big)^2\widehat{\mathbf{r}}. \tag{3.16}$$

The first term and second terms in Eq. (3.16) result from the drag force $\mathbf{F}$ and the radial change $\dot{R}$, resp., and we denote them by $\mathbf{u}^{(0)}\{\mathbf{F}\}$ and $\mathbf{u}^{(0)}\{\dot{R}\}$:

$$\begin{aligned}
\mathbf{u}^{(0)}\big(\mathbf{r};\, R, \mathbf{F}, \dot{R}\big) &= \mathbf{u}^{(0)}\{\mathbf{F}\}(\mathbf{r};\, R) + \mathbf{u}^{(0)}\{\dot{R}\}(\mathbf{r};\, R)\\
\mathbf{u}^{(0)}\{\mathbf{F}\}(\mathbf{r};\, R) &= \frac{1}{24\pi\mu r}\Big[\big(3+\frac{R^2}{r^2}\big)\mathbf{F} + 3\big(1-\frac{R^2}{r^2}\big)\big(\mathbf{F}\cdot\widehat{\mathbf{r}}\big)\widehat{\mathbf{r}}\Big]\\
\mathbf{u}^{(0)}\{\dot{R}\}(\mathbf{r};\, R) &= \dot{R}\Big(\frac{R}{r}\Big)^2\widehat{\mathbf{r}}.
\end{aligned}$$

For the symmetric geometry of the PMPY model, $\mathbf{F}_i = F_i\mathbf{e}_x$. Therefore the angular velocities $\boldsymbol{\Omega}_1$ and $\boldsymbol{\Omega}_2$ both vanish, while each reflection contributes to the translational velocity. In the zeroth reflection, i.e., when we consider the ith sphere ($i = 1, 2$) of the PMPY model alone immersed in the fluid, the radial expansion will not result in any rigid motion, but the drag force $\mathbf{F}_i$ leads to the translational component

$$\mathbf{U}_i^{(0)} = \frac{1}{6\pi\mu R_i}\mathbf{F}_i \tag{3.17}$$

The first reflection is computed as follows. Given the velocity of sphere j, we have to find the solution of a Stokes problem with velocity $-\mathbf{u}_j^{(0)}$ on the surface of sphere i and vanishing at infinity, and from that compute the translational and rotational velocities at the first reflection. Once again, $\boldsymbol{\Omega}_i^{(1)} = \mathbf{0}$ due to the symmetry of the model, and by using (3.16) in (3.12), the translational component is

$$\begin{aligned}
\mathbf{U}_i^{(1)} = \frac{1}{4\pi R_i^2}\int_{S_i}\mathbf{u}_j^{(0)}\,\mathrm{d}S &= \frac{1}{4\pi R_i^2}\int_{S_i}\mathbf{u}^{(0)}\{\mathbf{F}\}(\mathbf{r};\, R_j)\,\mathrm{d}S\\
&+ \frac{\dot{R}_j}{4\pi}\Big(\frac{R_j}{R_i}\Big)^2\int_{S_i}\frac{\mathbf{x}-\mathbf{x}_j}{|\mathbf{x}-\mathbf{x}_j|^3}\,\mathrm{d}S(\mathbf{x})
\end{aligned} \tag{3.18}$$

We denote the first and second terms in Eq. (3.18) as $\mathbf{U}_i^{(1,f)}$ and $\mathbf{U}_i^{(1,e)}$, resp., and then Eq. (3.18) can be written as

$$\mathbf{U}_i^{(1)} = \mathbf{U}_i^{(1,f)} + \mathbf{U}_i^{(1,e)}$$

$\mathbf{U}_i^{(1,f)}$ is the result of the drag force $\mathbf{F}_j$, and it has been well studied. The result is given by the Rotne–Prager–Yamakawa (RPY) approximation (Yamakawa 1970; Wajnryb et al. 2013; Zuk et al. 2014; Liang et al. 2013):

$$\begin{aligned}
\mathbf{U}_i^{(1,f)} = \frac{1}{8\pi\mu l}\Big[&\Big(1+\frac{R_1^2+R_2^2}{3l^2}\Big)\mathbf{I}\\
&+\Big(1-\frac{R_1^2+R_2^2}{l^2}\Big)\frac{(\mathbf{x}_i-\mathbf{x}_j)\otimes(\mathbf{x}_i-\mathbf{x}_j)}{|\mathbf{x}_i-\mathbf{x}_j|^2}\Big]\mathbf{F}_j
\end{aligned} \tag{3.19}$$

and together with the relations $\mathbf{U}_i^{(1,f)} = U_i^{(1,f)}\mathbf{e}_x$ and $\mathbf{F}_j = F_j\mathbf{e}_x$, we find that

$$\mathbf{U}_i^{(1,f)} = \frac{1}{4\pi\mu l}\Big[1 - \frac{R_1^2 + R_2^2}{3l^2}\Big]F_j. \tag{3.20}$$

$\mathbf{U}_i^{(1,e)}$ is due to the expansion $\dot{R}_j$, which can be calculated directly (Appendix B) or by Faxen's law,

$$\mathbf{U}_i^{(1,e)} = (-1)^i \dot{R}_j \Big(\frac{R_j}{l}\Big)^2 \mathbf{e}_x \tag{3.21}$$

which is precisely the radial expansion term in Avron's solution [Eq. (3.10)]. This completes the first reflection, and Eqs. (3.17, 3.20, 3.21) give the following approximation of the translational velocities of the spheres after one reflection

$$\begin{aligned} U_i \sim U_i^{(0)} + U_i^{(1)} = \frac{F_i}{6\pi\mu R_i} + \frac{F_j}{4\pi\mu l}\Big(1 - \frac{R_1^2 + R_2^2}{3l^2}\Big) \\ + (-1)^i \dot{R}_j \Big(\frac{R_j}{l}\Big)^2. \end{aligned} \tag{3.22}$$

The nondimensional version of Eq. (3.22) is

$$\hat{U}_i \sim \frac{\hat{F}_i}{\hat{R}_i} + \frac{3}{2}\delta\frac{\hat{F}_j}{\hat{l}}\Big(1 - \delta^2\frac{\hat{R}_1^2 + \hat{R}_2^2}{3\hat{l}^2}\Big) + (-1)^i\delta^2\Big(\frac{\hat{R}_j}{\hat{l}}\Big)^2\hat{\zeta}_j, \tag{3.23}$$

and together with the Eqs. (3.5, 3.3) we obtain the following closed system:

$$\begin{pmatrix} -1 & 0 & \dfrac{1}{\hat{R}_1} & \Gamma \\ 0 & -1 & \Gamma & \dfrac{1}{\hat{R}_2} \\ 1 & -1 & 0 & 0 \\ 0 & 0 & 1 & 1 \end{pmatrix} \begin{pmatrix} \hat{U}_1 \\ \hat{U}_2 \\ \hat{F}_1 \\ \hat{F}_2 \end{pmatrix} = \begin{pmatrix} \Gamma_2 \\ -\Gamma_1 \\ -\hat{\xi} \\ 0 \end{pmatrix} \tag{3.24}$$

where

$$\Gamma \equiv \delta\frac{3}{2\hat{l}}\Big(1 - \delta^2\frac{\hat{R}_1^2 + \hat{R}_2^2}{3\hat{l}^2}\Big) \quad \text{and} \quad \Gamma_i \equiv \delta^2\Big(\frac{\hat{R}_i}{\hat{l}}\Big)^2\hat{\zeta}_i.$$

It is easy to see that the matrix in (3.24) is non-singular and can be inverted explicitly. Therefore the solution of (3.24) can be expressed as a power series in δ.

To determine the contribution of higher reflections, we compute the second reflection. The translational velocity that results from drag forces from the 0th through the 2nd reflections for sphere 1 is found to be (Kim and Karrila 1991):

$$\sum_{n=0}^{2} U_1^{(n,f)} = \frac{F_1}{6\pi\mu R_1}\Big(1 - \frac{15R_1R_2^3}{4l^4}\Big) + \frac{F_2}{4\pi\mu l}\Big(1 - \frac{R_1^2+R_2^2}{3l^2}\Big) + O\big(\frac{1}{l^5}\big), \tag{3.25}$$

and after nondimensionalization this reads

$$\sum_{n=0}^{2} \hat{U}_1^{(n,f)} = \frac{\hat{F}_1}{\hat{R}_1}\Big(1 - \frac{15}{4}\delta^4\frac{\hat{R}_1\hat{R}_2^3}{\hat{l}^4}\Big) + \frac{3}{2}\delta\frac{\hat{F}_2}{\hat{l}}\Big(1 - \delta^2\frac{\hat{R}_1^2+\hat{R}_2^2}{3\hat{l}^2}\Big) + O\big(\delta^5\big). \tag{3.26}$$

A comparison of this with the first two terms in (3.23) shows that the translational velocity from the first reflection is accurate through $O(\delta^4)$. One can show that a second reflection for the component due to the radial expansion will lead to the correction $U_i^{(2,e)}$ of $O(\delta^5)$ (*cf* Appendix B), and thus the solution is accurate through $O(\delta^4)$ after one reflection.

The perturbation expansions of the solution to Eq. (3.24) to $O(\delta^4)$ order are:[3]

$$\begin{aligned} U_1 \sim & -\frac{R_2}{R_1+R_2}\xi + \delta\frac{3R_1R_2(R_1-R_2)}{2(R_1+R_2)^2 l}\xi \\ & + \frac{\delta^2}{l^2}\Big[\frac{9R_1^2R_2^2(R_1-R_2)}{2(R_1+R_2)^3}\xi - R_2^2\zeta_2\Big] \\ & + \delta^3\frac{R_1R_2(R_1-R_2)}{2(R_1+R_2)^4 l^3}\Big(25R_1^2R_2^2 - R_1^4 - R_2^4 - 2R_1^3R_2 - 2R_1R_2^3\Big)\xi \\ & + O(\delta^4) \end{aligned} \tag{3.27}$$

$$\begin{aligned} U_2 \sim & \frac{R_1}{R_1+R_2}\xi + \delta\frac{3R_1R_2(R_1-R_2)}{2(R_1+R_2)^2 l}\xi \\ & + \frac{\delta^2}{l^2}\Big[\frac{9R_1^2R_2^2(R_1-R_2)}{2(R_1+R_2)^3}\xi + R_1^2\zeta_1\Big] \\ & + \delta^3\frac{R_1R_2(R_1-R_2)}{2(R_1+R_2)^4 l^3}\Big(25R_1^2R_2^2 - R_1^4 - R_2^4 - 2R_1^3R_2 - 2R_1R_2^3\Big)\xi \\ & + O(\delta^4) \end{aligned} \tag{3.28}$$

$$\begin{aligned} -F_1 = F_2 \sim & \frac{R_1R_2}{R_1+R_2}\xi + 3\frac{\delta}{l}\Big(\frac{R_1R_2}{R_1+R_2}\Big)^2\xi + 9\frac{\delta^2}{l^2}\Big(\frac{R_1R_2}{R_1+R_2}\Big)^3\xi \\ & + \frac{\delta^3}{l^3}\frac{(R_1R_2)^2}{(R_1+R_2)^4}\Big(25R_1^2R_2^2 - R_1^4 - R_2^4 - 2R_1^3R_2 - 2R_1R_2^3\Big)\xi \\ & + O(\delta^4) \end{aligned} \tag{3.29}$$

[3] In the remainder we omit the $\hat{}$ on nondimensionalized quantities for simplicity unless units are given, but since δ appears in the equations this should not lead to any confusion.

Finally, the velocity of the PMPY model, correct to $O(\delta^4)$, and subject to the pair of controls (ξ, ζ_1), is

$$\begin{aligned}\overline{U} = \frac{R_1 - R_2}{2(R_1 + R_2)}\Big[1 + 3\frac{\delta}{l}\frac{R_1 R_2}{R_1 + R_2} + 9\frac{\delta^2}{l^2}\Big(\frac{R_1 R_2}{R_1 + R_2}\Big)^2 \\ + \frac{\delta^3}{l^3}\Big(\frac{R_1 R_2}{R_1 + R_2}\Big)^3\Big(25 - \frac{R_1^2}{R_2^2} - \frac{R_2^2}{R_1^2} - 2\frac{R_1}{R_2} - 2\frac{R_2}{R_1}\Big)\Big]\xi \\ + \delta^2\Big(\frac{R_1}{l}\Big)^2\zeta_1 + O(\delta^4). \qquad (3.30)\end{aligned}$$

If we compare Eq. (3.30) with Eq. (3.11), we see that the earlier analysis ignores all effects due to finite separation of the spheres, and thus (3.11) is only valid to the zeroth-order in δ.

3.3 Power expenditure and the performance of a PMPY

Next we consider the power $P(t)$ required to propel the swimmer. For a PMPY model, the power P comprises two parts: P_D that results from the drag force on the spheres, and P_V that results from the radial expansion of the spheres. P_D is given by

$$P_D = F_1 U_1 + F_2 U_2$$

which can be simplified by the force-free condition (Eq. 3.5) and the geometric relation between the two spheres (Eq. 3.3) to the form

$$P_D = F_2\big(U_2 - U_1\big) = F_2\dot{l}.$$

The stress on the surface of a sphere expanding at the rate $\dot{R}(t)$ in a Newtonian fluid is obtained as follows (Brennen 2013). The continuity equation in the exterior fluid implies that the radial velocity $v_r = dR/dt$ has the form

$$v_r = \frac{F(t)}{r^2}.$$

The forces per unit area on the sphere acting at the sphere-fluid interface are the interior pressure p_i, the fluid stress force

$$\mathbb{T}_{rr} = \Big(-p + 2\mu\frac{\partial v_r}{\partial r}\Big)\Big|_{r=R}$$

due to the exterior fluid motion, and a tension τ due to interfacial forces equal to

$$\frac{2\tau}{R}.$$

We neglect both the pressure difference across the interface and the interfacial tension, and therefore the force is

$$\mathbb{T}_{rr} = 2\mu \frac{\partial v_r}{\partial r} = -4\frac{\mu}{R}\frac{dR}{dt}.$$

Therefore the power required to expand a sphere is

$$-\int_S \mathbb{T}_{\mathbf{rr}} v_r \, ds = 16\pi\mu R\dot{R}^2$$

Therefore for the PMPY model we have

$$P_V = 16\pi\mu\left(R_1\dot{R}_1^2 + R_2\dot{R}_2^2\right)$$

and thus the power expended to propel a PMPY at time t is

$$P = P_D + P_V = F_2\dot{l} + 16\pi\mu\left(R_1\dot{R}_1^2 + R_2\dot{R}_2^2\right). \tag{3.31}$$

We nondimensionalize P as

$$\hat{P} = \frac{1}{6\pi\mu}\frac{T^2}{R_M^3}P$$

so that while $P = FU$ in dimensional form, after nondimensionalization we also have $\hat{P} = \hat{F}\hat{U}$. Thus the nondimensional version of Eq. (3.31) is

$$P = F\xi + \frac{8}{3}\left(R_1\zeta_1^2 + R_2\zeta_2^2\right) \tag{3.32}$$

with hat notation omitted. While P_V is determined, P_D depends on the perturbation, which in turn depends on δ. A first order approximation to P is given in Avron et al. (2005), which after nondimentionalization reads

$$P = \frac{R_1R_2}{R_1+R_2}\xi^2 + \frac{8}{3}\left(R_1\zeta_1^2 + R_2\zeta_2^2\right) + O(\delta), \tag{3.33}$$

while higher-order approximations can be obtained by using the results for F obtained from Eqs. (3.24) or (3.29) into Eq. (3.32).

Finally we define the performance $\mathscr{P}$ of a stroke as the ratio of the translation per cycle to the energy expended in a cycle, *viz.*

$$\mathscr{P} = \frac{\left|\int_0^T \overline{U}(t)\,dt,\right|}{\int_0^T P(t)\,dt}. \tag{3.34}$$

which has the units of $force^{-1}$. $\mathscr{P}$ measures the energy required for the PMPY to swim a certain distance in a cycle, and a large value of $\mathscr{P}$ indicates an energy-saving stroke. The nondimensional form of $\mathscr{P}$ is

$$\hat{\mathscr{P}} = \frac{6\pi\mu R_M^2}{T}\mathscr{P} = \frac{|\int_0^1 \hat{\overline{U}}\, d\hat{t}|}{\int_0^1 \hat{P}\, d\hat{t}}$$

3.4 A comparison of the solutions

Next we compare the asymptotic solution given by Eq. (3.10), the solution obtained by the reflection method [Eq. (3.24)] and the solution given by Eq. (3.30), for a prescribed loop in the control space described by $(\dot{l}, \dot{R}_1)$. We use the sinusoidal circuits

$$\begin{aligned} R_1(t) &= (2 + \sin 2\pi t)\,\mu\text{m}, \quad R_2(0) = 3\,\mu\text{m}, \quad l \\ &= (l_0 + \cos 2\pi t)\,\mu\text{m}, \quad \text{for } 0\,\text{min} \le t \le 1\,\text{min} \end{aligned} \tag{3.35}$$

with typical length unit μm and time unit min—these set the length and time scales for a realistic biological LRN swimmer, such as Dd amoebae (Van Haastert 2011), as will be seen later in this section. For this protocol one finds that

$$R_M \sim 3.24\,\mu\text{m}, \quad L_m = (l_0 - 1)\,\mu\text{m}, \quad \delta \sim \frac{3.24}{l_0 - 1}, \quad T = 1\,\text{min}\,.$$

Since the radius of sphere 2 is maximum when $R_1 = 1\,\mu$m at $t = .75$ min, R_M is achieved at this time. The results for scaled translation $X(t) = \int_0^t \overline{U}\, dt$ and scaled power $P(t)$ in a period for different values of l_0 are shown in Fig. 3a–e , and the relation between the scaled performance $\mathscr{P}$ and l_0 is given in Fig. 3f.

One can check that the spheres never touch under the protocol at (3.35) by computing the minimum of the gap $l - (R_1 + R_2)$, which is $\sim 0.9\,\mu$m at $t = 0.45$min for $l_0 = 7\,\mu$m, and larger for larger l_0's. In Fig. 3 we see that both the scaled translation X and the power P computed via the first reflection and its $O(\delta^3)$ approximation (black dots and red solid lines, resp.,) agree very well. On the other hand, the asymptotic approximation for the translation given by Eq. (3.10) and shown in Fig. 3a–c, (blue lines) deviates from them significantly when l_0 is small. In contrast, the scaled power of the Avron approximation coincides closely with that of the higher-order approximations (Fig. 3d–e), because most of the time, $P_V > P_D$, yet the higher-order corrections only contribute to P_D [Eq. (3.31)]. Computations that show the separate contributions of P_V and P_D are given in Appendix C. Finally, the scaled performance deviates from the reflection results significantly when the spheres are relatively close (Fig. 3f).

When the minimal gap between the spheres is small (large δ), the first reflection adds a significant correction to the asymptotic solution, as shown in Fig. 3a, d, and the effect of additional reflections should be checked. In the simulation of Fig. 3a, d, $\delta^4 = 8.5 \times 10^{-2}$, which is comparable to the net translation, which suggests that a second reflection may be necessary to guarantee the accuracy of the system. We compare the results obtained with the first reflection to those with the leading order term (i.e., δ^4 term) from the second reflection included, in Appendix C. Simulation results shown in Fig. 4 show that under the protocol given by Eq. (3.35) and with $l_0 = 7$, $\delta = 0.54$, the difference between the net translation $X(1)$ computed by the foregoing two approximations is 8.9×10^{-3}, smaller than either δ^4 or the net translation

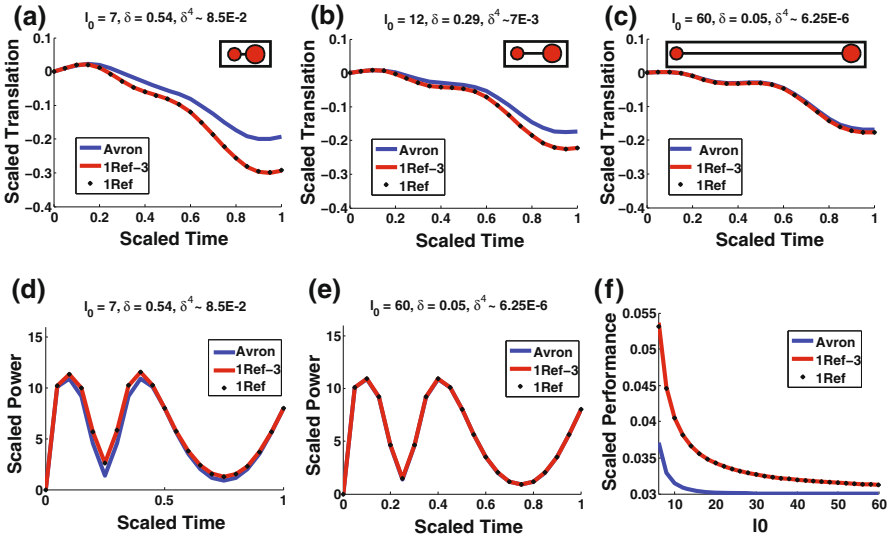

Fig. 3 A comparison of the asymptotic Avron solution (blue lines), the solution obtained by the reflection method (1Ref, black dots) and its perturbation analysis up to $O(\delta^4)$ order (1Ref-3, red lines). **a**–**c** The scaled translation $X(t) = \int_0^t \overline{U}\, dt$ within a period for $l_0 = 7, 12, 60\,\mu$m. The initial profile of the swimmer is shown in the box. **d**, **e** The scaled power $P(t)$ within a period, with $l_0 = 7, 60\,\mu$m. **f** The scaled performance $\mathscr{P}$ of PMPY with respect to l_0 (color figure online)

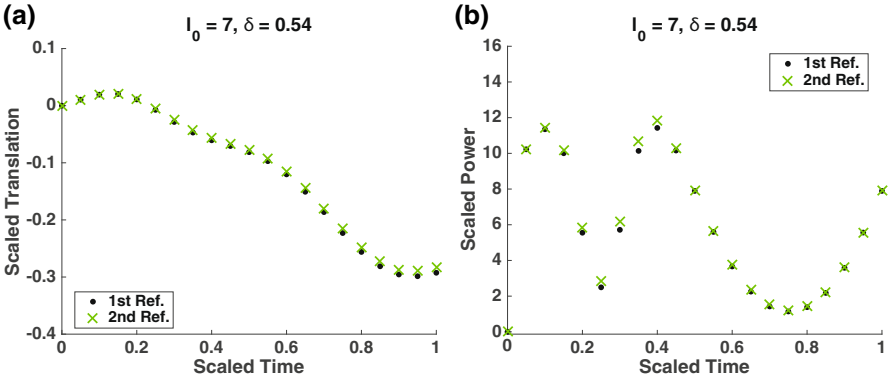

Fig. 4 A comparison of the solution obtained with the first reflection only (black dots) and with the leading order term from second reflection included (green crosses). **a** The scaled translation $X(t) = \int_0^t \overline{U}\, dt$ within a period. **b** The scaled power $P(t)$ within a period (color figure online)

$X(1)$. This indicates that even for a PMPY swimmer with a relatively small separation of the spheres ($\delta = 0.54$), the first reflection gives a solution with acceptable accuracy. In the following sections (Sects. 4–6), all solutions are obtained with the first reflection and we restrict the system to the regime $\delta \leq 0.54$.

As pointed out earlier (Wang and Othmer 2015), PMPY adopts a mixed control strategy in $(\dot{l}, \dot{R})$, which makes it superior to other linked-sphere models that adopt combinations of a single type of control. In fact, PMPY is the only model studied there

for which the net translation $X = \int_0^1 \overline{U}\, dt \sim O(1)$ over a period. This can be seen in Fig. 3a–c, in that the net translation X does not vanish as the length of the connecting rod increases. For $l \to \infty$, we have $\delta \to 0$, and Eq. (3.30) gives the estimate

$$\lim_{\delta\to 0} \overline{U} = \frac{R_1 - R_2}{2(R_1 + R_2)}\xi \sim O(1), \quad \lim_{\delta\to 0} X = \lim_{\delta\to 0} \int_0^T \overline{U}(t)\, dt \sim O(1)$$

For the stroke prescribed by Eq. (3.35), we have the estimate $X \sim -0.17$ as $l_0 \to \infty$, $\delta \to 0$. On the other hand, the power P does not change much as l_0 changes, and taken together, we have the estimate for the performance of PMPY in the limit $l_0 \to \infty$, $\delta \to 0$ of about $\mathscr{P} \sim 0.03$.

As a final check on the validity of the solutions, we determine whether the flow regime for the PMPY model computations satisfies $\mathrm{Re} \ll 1$ and $\mathrm{ReSl} \ll 1$, which is required for a LRN swimmer. We assume that the medium is water ($\rho \sim 10^3 \mathrm{kg}\cdot\mathrm{m}^{-3}$, $\mu \sim 10^{-3}\mathrm{Pa}\cdot\mathrm{s}$), and test two sets of L and U from our simulations ($L = 6\,\mu\mathrm{m}$, $U \sim -1.2\,\mu\mathrm{m}/\,\mathrm{min}$ from Fig. 3a, or $L = 60\,\mu\mathrm{m}$, $U \sim -0.6\,\mu\mathrm{m}/\,\mathrm{min}$ from Fig. 3c). In either case we have $\mathrm{Re} \ll 1$ and $\mathrm{ReSl} \ll 1$ ($\mathrm{Re} \sim O(10^{-6})$, $\mathrm{ReSl} \sim O(10^{-6})$ in Fig. 3a, and $\mathrm{Re} \sim O(10^{-6})$, $\mathrm{ReSl} \sim O(10^{-5})$ in Fig. 3c).

The foregoing results are for a fixed phase difference, and next we investigate the effect of changing the phase difference between the two controls $\dot{l}$ and $\dot{R}_1$. We consider the following class of sinusoidal cycles

$$\begin{aligned} R_1(t) &= (2 + \sin 2\pi t)\,\mu\mathrm{m}, \quad R_2(0) = 3\,\mu\mathrm{m}, \\ l &= (l_0 + \sin(2\pi t + \phi))\,\mu\mathrm{m}, \quad \text{for } 0\ \mathrm{min} \le t \le 1\ \mathrm{min}, \end{aligned}$$

where $\phi \in [0, 2\pi]$ is the phase difference. The scaled net translation and performance with respect to ϕ is shown in Fig. 5, from which we see that the maxima of both scaled net translation and performance are reached at a phase difference of $\phi = k\pi + \pi/2$, $k \in \mathbb{Z}$. In contrast, when $\phi = k\pi$, $k \in \mathbb{Z}$, the net translation after one cycle equals zero, which naturally leads to zero performance as well. This stems from the fact that in these cases the shape deformation become time reversible, and according to the scallop theorem, no net translation results.

To compare our analysis with experimental observations, we use the data on swimming amoebae from Van Haastert (2011), where it is reported that Dd amoebae move in a fluid environment by side protrusions. Typically the cell body is elongated, and single or multiple protrusions cyclically propagate along the cell (Wang and Othmer 2016). Although the shape deformation mode of these amoebae cell is not exactly the same as a PMPY model, however similar to a PMPY, such a traveling protrusion mode does exploit mass transfer along an elongated body. It is reported that amoebae using this swimming mode have maximum cell body length $\sim 25\,\mu\mathrm{m}$, average cell body width $\sim 6\,\mu\mathrm{m}$, a typical stroke has period ~ 1 min, and a typical swimming velocity $\sim 3\,\mu\mathrm{m}/\,\mathrm{min}$. Using this data, we approximate

$$L \sim 25\,\mu\mathrm{m}, \quad T \sim 1\,\mathrm{min}, \quad R \sim 6\,\mu\mathrm{m}, \quad U \sim 3\,\mu\mathrm{m}/\,\mathrm{min}$$

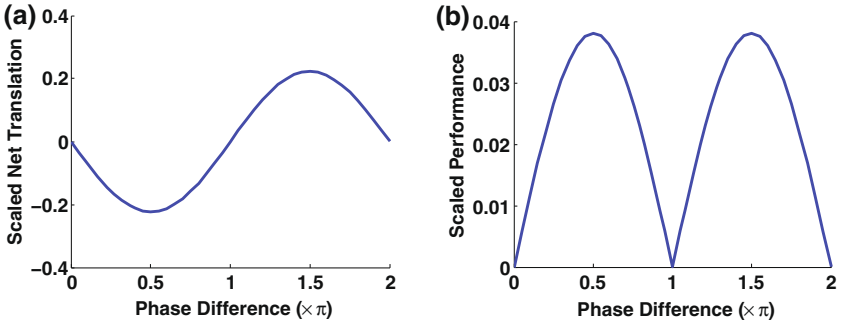

Fig. 5 The scaled net translation (**a**) and performance (**b**) with respect to phase difference between the two controls $\dot{l}$ and $\dot{R}_1$, with $l_0 = 12$, computed using the first reflection

thus $\delta \sim R/L \sim 0.24$, $\hat{U} \sim TU/R \sim 0.5$ and the scaled net translation within a period $\hat{X} = X/R \sim 0.5$, which is about the same scale as for a PMPY swimmer. In fact, as can be seen from Fig. 3a, if the spheres are not too separated in the model, the scaled net translation of a PMPY can reach $X \sim 0.3$. On the other hand, other linked-sphere models that also have elongated shape and adopt large-scale shape deformations can only result in $X \sim O(\delta^2)$ (Wang and Othmer 2015), which is far less than a PMPY or a swimming amoebae as observed. This suggests that the PMPY model merits further investigation.

We summarize our results in this section as follows.

1. The first reflection adds a significant correction to the order-one asymptotic solution for the net translation when the minimal gap between the spheres of a PMPY swimmer is small.
2. A comparison of the solution that includes the leading order terms from the second reflection with the solution for only one reflection shows that the latter provides sufficient accuracy even for relatively small separations.
3. PMPY adopts a mixed control strategy, which leads to an $O(1)$ net translation. Therefore, it can swim even with widely separated spheres.
4. The LRN approximation is appropriate for the foregoing computations, and the behavior of the PMPY is comparable to that of a swimming amoebae.
5. The translation and performance of the PMPY swimmer are maximized when the stroke controls $\dot{l}$ and $\dot{R}_1$ have a phase difference of $\phi = k\pi + \pi/2,\ k \in \mathbb{Z}$; while there is no net translation if the controls are in phase, i.e., $\phi = k\pi,\ k \in \mathbb{Z}$;

4 A PMPY swimmer in the presence of a passive buoyant obstacle

In an extension of the previous results that leads to several interesting applications, we next analyze a PMPY swimmer that interacts with an untethered, passive, neutrally-buoyant object nearby. To simplify the computation of the interaction, we suppose that this object is a rigid sphere, and that there is no external force or torque imposed on it. The geometry of the system is shown in Fig. 6, where one sees that there are six characteristic lengths: the radius of each sphere (R_i, $i = 1, 2, 3$) and the

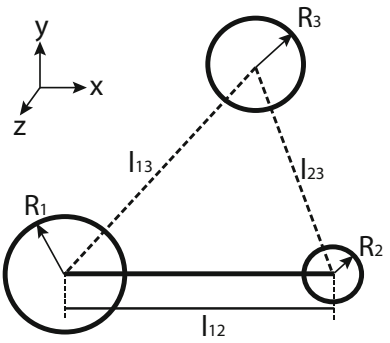

Fig. 6 The geometry of the system of a PMPY swimmer and a passive, neutrally-buoyant spherical object

lengths between any pair of spheres: (l_{ij}, $i, j = 1, 2, 3$). For scaling purposes we define

$$R_M = \max_t\{R_i(t)\}_{i=1,2,3}, \quad L_m = \min_t\{l_{12}(t)\}, \quad \delta = \frac{R_M}{L_m}.$$

To apply the reflection method to this system, we require that $\delta < 1$ as before, and in addition, we only consider the regime $l_{13}, l_{23} > L_m$. Thus all non-dimensionalization relations in Sect. 3.1 apply. The following discussion is similar to that in Sect. 3.2, except that one more sphere is now involved in the system. We assume that the centers of all three spheres lie in the xy-plane, and that the active swimmer moves along the x-axis initially (Fig. 6). In this configuration the torque and angular velocities must be taken into account unless the three spheres are co-linear. However, the motion of the spheres will remain in the plane defined by their initial positions since the axis of rotation of a sphere is orthogonal to that plane. Thus the problem remains effectively two-dimensional, but this plays no role in the analysis.

4.1 The linear and angular velocities after the first reflection

At the zeroth-order reflection, in which no hydrodynamic interactions between the spheres are considered, the results for the swimmer are the same as in the absence of a passive object, and the velocity field for each sphere is given by Eqs. (3.16, 3.17). At this order the linear and angular velocities of sphere 3 are

$$\mathbf{U}_3^{(0)} = \boldsymbol{\Omega}_3^{(0)} = \mathbf{0}, \quad \mathbf{u}_3^{(0)} \equiv \mathbf{0} \tag{4.1}$$

At the first reflection, each sphere is subject to the flows generated by the other spheres. Since $\mathbf{u}_3^{(0)} \equiv \mathbf{0}$, the calculation of rigid motions for sphere 1 and 2 in the first reflection are identical to Sect. 3.2 – thus we have:

$$\mathbf{U}_1^{(1)} = \left(1 + \frac{R_1^2}{6}\nabla^2\right)\left(\mathbf{u}_2^{(0)} + \mathbf{u}_3^{(0)}\right)\Big|_{\mathbf{x}=\mathbf{x}_1} = \frac{\mathbf{F}_2}{4\pi\mu l_{12}}\left(1 - \frac{R_1^2 + R_2^2}{3l_{12}^2}\right) - \dot{R}_2\left(\frac{R_2}{l_{12}}\right)^2$$

$$\boldsymbol{\Omega}_1^{(1)} = \frac{1}{2}\nabla \times \left(\mathbf{u}_2^{(0)} + \mathbf{u}_3^{(0)}\right)\Big|_{\mathbf{x}=\mathbf{x}_1} = \mathbf{0}$$
$$\mathbf{U}_2^{(1)} = \left(1 + \frac{R_2^2}{6}\nabla^2\right)\left(\mathbf{u}_1^{(0)} + \mathbf{u}_3^{(0)}\right)\Big|_{\mathbf{x}=\mathbf{x}_2} = \frac{\mathbf{F}_1}{4\pi\mu l_{12}}\left(1 - \frac{R_1^2 + R_2^2}{3l_{12}^2}\right) + \dot{R}_1\left(\frac{R_1}{l_{12}}\right)^2$$
$$\boldsymbol{\Omega}_2^{(1)} = \frac{1}{2}\nabla \times \left(\mathbf{u}_1^{(0)} + \mathbf{u}_3^{(0)}\right)\Big|_{\mathbf{x}=\mathbf{x}_2} = \mathbf{0}.$$

From this one sees that at the first reflection, the presence of the passive sphere at a sufficient distance does not affect the swimmer, but the converse is not true—the effect of the swimmer on the passive sphere is non-zero after the first reflection. Its translational velocity $\mathbf{U}_3^{(1)}$ is given by the sum of the contributions from translation and expansion of the swimmer's spheres, *viz.*,

$$\mathbf{U}_3^{(1)} = \sum_{i=1,2} \mathbf{U}_{3,i}^{(1,f)} + \mathbf{U}_{3,i}^{(1,e)} \tag{4.2}$$

where

$$\mathbf{U}_{3,i}^{(1,f)} = \left(1 + \frac{R_3^2}{6}\nabla^2\right)\mathbf{u}\{\mathbf{F}_i\}\Big|_{\mathbf{x}=\mathbf{x}_3} = \frac{1}{8\pi\mu l_{i3}}\left[\left(1 + \frac{R_i^2 + R_3^2}{3l_{i3}^2}\right)\mathbf{F}_i + \left(1 - \frac{R_i^2 + R_3^2}{l_{i3}^2}\right)(\mathbf{F}_i \cdot \mathbf{d}_{i3})\mathbf{d}_{i3}\right] \tag{4.3}$$
$$\mathbf{U}_{3,i}^{(1,e)} = \frac{1}{2}\nabla \times \left(R_i^2\dot{R}_i\frac{\mathbf{x} - \mathbf{x}_i}{|\mathbf{x} - \mathbf{x}_i|^3}\right)\Big|_{\mathbf{x}=\mathbf{x}_3} = \dot{R}_i\left(\frac{R_i}{l_{i3}}\right)^2\mathbf{d}_{i3} \tag{4.4}$$

and

$$\mathbf{d}_{i3} = \frac{\mathbf{x}_3 - \mathbf{x}_i}{|\mathbf{x}_3 - \mathbf{x}_i|}, \quad l_{i3} = |\mathbf{x}_3 - \mathbf{x}_i|.$$

Although sphere 1 and 2 are rotation-free after the first reflection, one finds that the translation of sphere 1 and 2 contributes to the rotation of $\boldsymbol{\Omega}_3^{(1)}$, while their expansion has no effect on $\boldsymbol{\Omega}_3^{(1)}$. The detailed calculation of $\boldsymbol{\Omega}_3^{(1)}$ is straightforward and is given in Appendix D. The result is that

$$\boldsymbol{\Omega}_3^{(1)} = \sum_{i=1,2} \frac{F_i}{8\pi\mu l_{i3}^3}\left[\left(\mathbf{x}_3 - \mathbf{x}_i\right) \cdot \mathbf{e}_y\right]\mathbf{e}_z. \tag{4.5}$$

To summarize the analysis for the first reflection, we first solve for the motion of the swimmer and the forces it exerts using the system (3.24), and use the results in Eqs. (4.2, 4.5) to obtain the motion of sphere 3.

4.2 Accuracy of the system

For the PMPY, as we mentioned earlier, up to the first reflection, the passive buoyant sphere 3 has no effect on the PMPY model. It follows from Sect. 3.2, that after the first reflection the translational velocities of the two spheres of the PMPY (U_1, U_2), together with the translational velocity of the PMPY ($\overline{\mathbf{U}}$), are accurate up to δ^3 order. The leading order of $\overline{\mathbf{U}}$ is of $O(1)$, as shown by Eq. (3.30). Because $\boldsymbol{\Omega}_i^{(0)} = \boldsymbol{\Omega}_i^{(1)} = \mathbf{0},\ i = 1, 2$, we neglect the rotation effect of the PMPY.

Similar to the analysis of the PMPY, neglecting the second and higher reflections for the passive sphere 3 results in the translational velocity $\mathbf{U}_3 \sim \mathbf{U}_3^{(0)} + \mathbf{U}_3^{(1)}$ accurate up to order δ^3. Moreover, the effects from the self-deformable PMPY model on sphere 3 starts to show up from the first reflection ($\mathbf{U}_3^{(0)} = \mathbf{0}$), thus an estimate of the leading term of $\mathbf{U}_3$ is

$$\sum_{i=1,2} \frac{3}{4} \frac{\mathbf{F}_i + \big(\mathbf{F}_i \cdot \mathbf{d}_{i3}\big)\mathbf{d}_{i3}}{l_{i3}} \delta \sim O(\delta)$$

For the angular velocity we have $\boldsymbol{\Omega}_3 \sim \boldsymbol{\Omega}_3^{(0)} + \boldsymbol{\Omega}_3^{(1)} = \boldsymbol{\Omega}_3^{(1)}$, and thus the leading order of $\boldsymbol{\Omega}_3$ can be estimated as follows:

$$\sum_{i=1,2} \frac{3\mathbf{F}_i}{4l_{i3}^3} \Big[\big(\mathbf{x}_3 - \mathbf{x}_i\big) \cdot \mathbf{e}_y\Big] \mathbf{e}_z \delta^3 \sim O(\delta^3)$$

In the wide-separation regime, i.e., when $\delta \ll 1$, it is clear that the angular velocity of the passive sphere 3 ($\boldsymbol{\Omega}_3 \sim O(\delta^3)$) can be neglected compared to its translational velocity $\mathbf{U}_3 \sim O(\delta)$ or the translational velocity of PMPY ($\overline{\mathbf{U}} \sim O(1)$).

To investigate the second reflection, we must first compute all the velocities — $\mathbf{u}_{ij}^{(1)}$ for $i, j = 1, 2, 3,\ i \neq j$—that result from putting sphere j into the flow $\mathbf{u}_i^{(0)}$. Since $\mathbf{u}_3^{(0)} \equiv \mathbf{0}$ [Eq. (4.1)], we have $\mathbf{u}_{3j}^{(1)} \equiv \mathbf{0}$ for $j = 1, 2$. On the other hand, when we put sphere 2 or 3 into $\mathbf{u}_1^{(0)}$, the resulting flow $\mathbf{u}_{1j}^{(1)}$ is a superposition of two parts:

$$\mathbf{u}_{1j}^{(1)} = \mathbf{u}_{1j}^{(1)}\{\mathbf{F}_1\} + \mathbf{u}_{1j}^{(1)}\{\dot{R}_1\}$$

where $\mathbf{u}_{1j}^{(1)}\{\mathbf{F}_1\}$ results from the drag force $\mathbf{F}_1$ exerted on sphere 1, and its leading term is of the order δ^4 (Kim and Karrila 1991); $\mathbf{u}_{1j}^{(1)}\{\dot{R}_1\}$ results from the radial deformation of sphere 1, and its leading term is of the order δ^5. Hence $\mathbf{u}_{1j}^{(1)} \sim O(\delta^4)$ and similarly, $\mathbf{u}_{2j}^{(1)} \sim O(\delta^4)$ as well. Thus for sphere 1:

$$\begin{aligned}
\mathbf{U}_1^{(2)} &= \Big(1 + \frac{R_1^2}{6}\nabla^2\Big)\big(\mathbf{u}_{12}^{(1)} + \mathbf{u}_{13}^{(1)} + \mathbf{u}_{23}^{(1)} + \mathbf{u}_{32}^{(1)}\big)\Big|_{\mathbf{x}=\mathbf{x}_1} + O(\delta^4) \\
\boldsymbol{\Omega}_1^{(2)} &= \frac{1}{2}\nabla \times \big(\mathbf{u}_{12}^{(1)} + \mathbf{u}_{13}^{(1)} + \mathbf{u}_{23}^{(1)} + \mathbf{u}_{32}^{(1)}\big)\Big|_{\mathbf{x}=\mathbf{x}_1} + O(\delta^5)
\end{aligned}$$

with similar results for sphere 2 and 3 as well. In conclusion, the results we obtained from Sect. 4.1 are accurate up to the δ^3 term.

Finally, it is easily seen that the results obtained in Sect. 4.1 can be applied to a system consisting of a PMPY model and N passive neutrally-buoyant spheres, as long as the spheres are separated sufficiently. We number the two spheres in the PMPY model as sphere 1 and 2, as usual, and the others from sphere 3 to sphere $N+2$. For each of the N passive spheres, $\mathbf{u}_i^{(0)} \equiv 0$ $(i = 3, 4, \ldots, N+2)$ in the zeroth reflection, from which we conclude that: up to the first reflection,

1. The PMPY model does not "see" the other spheres:

$$\boldsymbol{\Lambda}_i^{(1)} = \boldsymbol{\Lambda}_{i,j}^{(1,f)} + \boldsymbol{\Lambda}_{i,j}^{(1,e)} + \sum_{n=3}^{N+2} \left(\boldsymbol{\Lambda}_{i,n}^{(1,f)} + \boldsymbol{\Lambda}_{i,n}^{(1,e)} \right) = \boldsymbol{\Lambda}_{i,j}^{(1,f)} + \boldsymbol{\Lambda}_{i,j}^{(1,e)}$$

   where $i, j = 1, 2,\ i \neq j$ and $\boldsymbol{\Lambda}$ stands for $\mathbf{U}$ or $\boldsymbol{\Omega}$.
2. Each passive sphere only "sees" the PMPY model and "sees" no other spheres:

$$\begin{aligned} \boldsymbol{\Lambda}_n^{(1)} &= \sum_{i=1,2} \left(\boldsymbol{\Lambda}_{n,i}^{(1,f)} + \boldsymbol{\Lambda}_{n,i}^{(1,e)} \right) + \sum_{3 \le m \le N+2}^{m \neq n} \left(\boldsymbol{\Lambda}_{n,m}^{(1,f)} + \boldsymbol{\Lambda}_{n,m}^{(1,e)} \right) \\ &= \sum_{i=1,2} \left(\boldsymbol{\Lambda}_{n,i}^{(1,f)} + \boldsymbol{\Lambda}_{n,i}^{(1,e)} \right) \end{aligned}$$

   where $n \in 3, 4, \ldots, N+2$ and $\boldsymbol{\Lambda}$ stands for $\mathbf{U}$ or $\boldsymbol{\Omega}$.

4.3 Chasing an object

The scenario of a micro-swimmer swimming with a passive object has many applications. For example, can a microorganism that locates a target object (nutrient, a bacterium, etc.), capture the object within a reasonable time period? To be specific, the micro-swimmer should be able to swim fast enough to reach the target object, and the object, as it is passive, should not be pushed away faster than the micro-swimmer swims, especially when they are close.

We consider a scenario in which a PMPY swims toward a passive sphere directly in front of it, in simulating a microorganism chasing an object. As we discussed in Sect. 3.4, a PMPY is an effective swimmer—with a translational velocity $\overline{\mathbf{U}}$ scaled as $O(1)$—and approximates the swimming behavior of Dd amoebae (Van Haastert 2011), which feed on bacteria. This indicates that a PMPY can swim a distance within a reasonable time period by consuming a reasonable amount of energy. As was discussed in Sect. 4.2, the leading order term of $\mathbf{U}_3$ for the movement of the passive sphere 3 that results from the hydrodynamic interaction with the PMPY is

$$\mathbf{U}_3 \sim \mathbf{U}_3^{(1)} \sim \sum_{i=1,2} \frac{3}{4} \frac{\mathbf{F}_i + (\mathbf{F}_i \cdot \mathbf{d}_{i3})\mathbf{d}_{i3}}{l_{i3}} \delta \tag{4.6}$$

Since the spheres are collinear we have $\mathbf{d}_{13} = \mathbf{d}_{23}$, and the force-free constraint of the PMPY gives $\mathbf{F_1} = -\mathbf{F}_2$, both of which lie along $\mathbf{d}_{13}$. Therefore we have the following estimate of the translational velocity $\mathbf{U}_3$:

$$\mathbf{U}_3 \sim -\frac{3}{2}\mathbf{F}_1\left(\frac{1}{l_{13}} - \frac{1}{l_{23}}\right)\delta = -\frac{3}{2}\mathbf{F}_1\frac{l_{12}}{l_{13}l_{23}}\delta,$$

and by using Eq. (3.29) we have

$$\mathbf{U}_3 \sim \frac{3}{2}\frac{l_{12}}{l_{13}l_{23}}\frac{R_1R_2}{R_1+R_2}\delta\xi. \tag{4.7}$$

From Eq. (4.7) we see that when the passive sphere 3 is far from the PMPY, i.e., $l_{13} \gg 1$, $l_{23} \gg 1$, $\mathbf{U}_3$ scales much less than $O(\delta)$, and only when the PMPY is close to the target can $\mathbf{U}_3$ increase to $O(\delta)$. Therefore, with the estimates of the translational velocities of the PMPY and the passive sphere giving $\overline{\mathbf{U}} \sim O(1)$ and $\mathbf{U}_3 < O(\delta)$, we confirm that a PMPY can easily catch up with its passive target. Moreover, we note that although in problems like nutrient supply, the target objects are likely to be much smaller than the microswimmer, this size relation is not required here. As we can see from the Eq. (4.7), the size of the passive sphere (R_3) does not enter the leading order term of $\mathbf{U}_3$. In fact, from Eqs. (4.3, 4.4), R_3 only shows up in the $O(\delta^3)$ term, and as long as $R_3/l_{i3} \sim O(1)$, $i = 1, 2$, the above analysis and conclusions still hold.

To numerically investigate the effects of the PMPY on the passive sphere 3, we consider the following system (Fig. 7a). At $t = 0$ the passive sphere 3 is at a distance d_0 from the leading sphere (i.e., sphere 2), and for $t > 0$ the PMPY swimmer executes the following cyclic deformations.

$$\begin{aligned} R_1(t) &= (2 - \sin 2\pi t)\,\mu\text{m}, \quad R_2(0) = 3\,\mu\text{m}, \quad R_3 \equiv 2\,\mu\text{m}, \quad l_{12} \\ &= (l_0 + \cos 2\pi t)\,\mu\text{m} \end{aligned} \tag{4.8}$$

for $0\ \text{min} \le t \le 1\ \text{min}$. With this stroke the PMPY swimmer moves in the positive x direction and pushes the passive sphere in that direction. We take $l_0 = 12\,\mu\text{m}$, $d_0 = 20\,\mu\text{m}$, which allows the PMPY swimmer to execute a few cycles before it gets too close to sphere 3, that is, when $l_{23} \le L_m$. The system profile gives $R_M \sim 3.24\,\mu\text{m}$, $L_m = 11\,\mu\text{m}$, $\delta \sim 0.29$. The translation of the PMPY is computed by Eq. (3.24), while that of sphere 3 is computed from Eqs. (4.3, 4.4), therefore $\delta^4 \sim 7E - 3$. After 13.5 cycles, the PMPY model swims a scaled distance of $X_{\text{PMPY}} \sim 3.13$, while the passive sphere only moves a scaled distance $X_3 = 0.29$ (Fig. 7b, c). Thus $X_3/X_{\text{PMPY}} \sim 0.087$, which is even less than the estimated ratio $U_3/\overline{U} \sim O(\delta)$. One sees in (b) that the trajectory of the passive sphere (blue solid line in Fig. 7b) is only slightly tilted as compared to that of the PMPY swimmer (red solid line in Fig. 7b). This reflects the fact that sphere 3 oscillates back and forth, and the oscillations grow as the swimmer approaches the sphere, as seen in Fig. 7c. Thus the swimmer can easily catch up with the passive object.

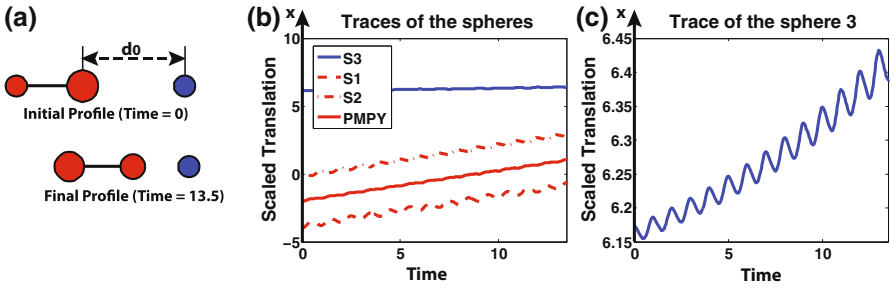

Fig. 7 Simulation of a PMPY swimmer and a passive sphere, arranged collinearly. **a** Initial and final profiles of the system. **b** Translation of all components in the 13.5 cycles. **c** Translation of S3 within 13.5 cycles (color figure online)

4.4 Tracer trajectories

Another important application of this swimmer-object interaction problem is swimmer–tracer scattering, in which the swimming of micro-organisms stirs the surrounding fluid (Dunkel et al. 2010). This is important in controlling and enhancing nutrient uptake, and leads to enhanced tracer diffusion observed in swimmer suspensions (Wu and Libchaber 2000; Leptos et al. 2009; Sokolov et al. 2009; Kurtuldu et al. 2011; Miño et al. 2011). Experimental observations show that trajectories of tracers in a suspension of swimmers are often nearly-closed loops (Leptos et al. 2009), and theoretical arguments and simulation predictions have emerged to elucidate this phenomenon (Underhill et al. 2008; Rushkin et al. 2010; Ishikawa et al. 2010; Lin et al. 2011; Zaid et al. 2011). In particular, the PMPY model has been used in the study of swimmer–tracer scattering, where an asymptotic analysis based on the stroke-averaged behavior of the PMPY, together with some simulations, illustrate the near closed-loop of a triangular shape of the tracer (Dunkel et al. 2010). In this section we apply the reflection analysis elaborated in Sects. 4.1 and 4.2 to further investigate the tracer trajectories induced by a PMPY swimmer.

4.4.1 The instantaneous velocity of the tracer sphere

The swimmer–tracer interaction is easily found by asymptotic analysis when the swimmer and the tracer are far apart (Dunkel et al. 2010; Pushkin et al. 2013; Yeomans et al. 2014). As is the case for a PMPY swimmer, when a spherical object is far away from it, i.e., $l_{13}, l_{23} \gg 1$, the asymptotic estimate is given by Eq. (4.6), and the instantantaneous velocity of the tracer sphere as a function of its location is shown in Fig. 8. In this case the velocity field is the same as the asymptotic behavior of the velocity field generated by a single PMPY (Dunkel et al. 2010).

In this snapshot the connecting rod is expanding ($\dot{l} > 0$), and one sees that the velocity field is divided into four domains. A tracer sphere located in the two shaded domains will be attracted to the PMPY and repulsed if it is located in the two unshaded domains.

The reflection analysis allows us to observe the situation when the PMPY and the tracer sphere get close to each other, as long as $\delta < 1$ still holds. Moreover, as we

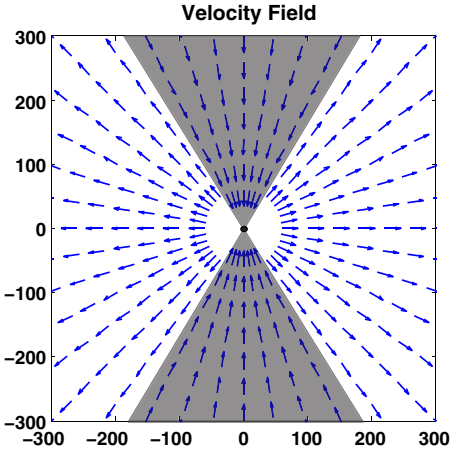

Fig. 8 A snapshot of the instantaneous velocity field generated by a PMPY swimmer and felt by a tracer sphere when the latter is far away from the swimmer. In this simulation the PMPY is located at the origin, with an instantaneous profile $R_1 = R_2 = 2\,\mu\text{m}$, $l = 6\,\mu\text{m}$, the connecting rod is expanding (i.e., $\dot{l} > 0$), and the expansion/contraction of the spheres in the PMPY is neglected as it only generates $O(\delta^2)$ order terms. The tracer sphere has radius $R_3 = 2.5\,\mu\text{m}$. Arrows only show the direction, not the magnitude, of the velocity

showed in Sect. 4.1, the velocity of the tracer sphere $\mathbf{U}_3$ consists of two parts: $\mathbf{U}_3^{(f)}$ that results from the drag forces on the two spheres in the swimmer [Eq. (4.3)], and $\mathbf{U}_3^{(e)}$, which results from the radial changes [Eq. (4.4)]. To further investigate the separate effects of drag and expansion when the tracer sphere is close to the PMPY, we show the instantaneous velocity of the tracer sphere in different stages of movement of the swimmer in Fig. 9. Figure 9a, b show the velocity field when the PMPY connecting rod is expanding without radial changes, and the spheres of the PMPY are either of unequal sizes (a) or equal sizes (b). Comparing Fig. 9a, b with Fig. 8 we see that even at small separations, the local velocity varies little from the far-field behaviors. The reason for this similarity is that other than the leading $O(1)$ term, the next term in $\mathbf{U}_3^{(f)}$ [Eq. (4.3)] is an $O(\delta^3)$ term, which decreases very rapidly as l_{13} and l_{23} increase. However, a blown-up view of the velocity fields shows that the $O(\delta^3)$ term does give rise to a tangential velocity when the tracer sphere is close to the swimmer, as it must. This is clear at the border of the shaded and unshaded regions shown in Fig. 8 (shown by arrows in the green boxes in Fig. 9c, d). This rotation of the velocity filed is larger when the PMPY has unequal-sized spheres and the tracer sphere is near the larger one (Fig. 9c). Figure 9e, f show the velocity field when the PMPY undergoes radial changes without changes in the length of the connecting rod. Again we consider unequal-sized spheres (Fig. 9e) and equal-sized spheres (Fig. 9f) at one instant. In the asymptotic analysis (Fig. 8) the effects on the tracer sphere that result from radial changes in the swimmer are not considered, as they only give rise to $O(\delta^2)$ terms [Eq. (4.4)]. However, as we can see from Fig. 9e, f, expansion and contraction of the swimmer have significant effects on the tracer sphere, and therefore should be taken into account.

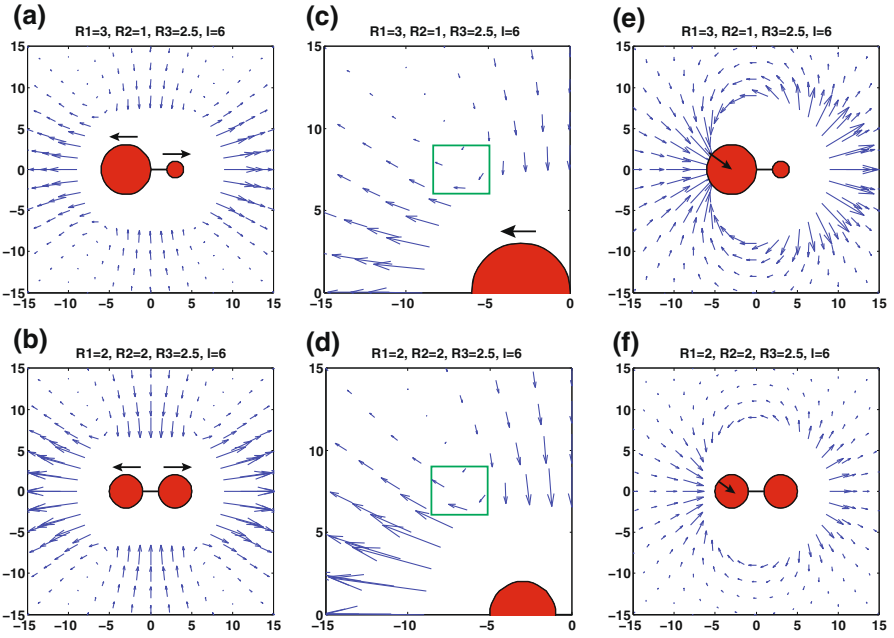

Fig. 9 The instantaneous velocity of a tracer sphere that results from a swimming PMPY, when the tracer sphere is close to the PMPY. The arrows in all panels are scaled uniformly, thus arrows show both direction and magnitudes. **a**, **b** The connecting rod is instantaneously expanding at $\dot{l} = 2\pi$ μm/min, and there is no expansion/contraction in the PMPY. **c**, **d** A blown-up view of panel **a**, **b** near sphere 1 in the PMPY. **e**, **f** Sphere 1 is instantaneously shrinking at $\dot{R}_1 = -2\pi$ μm/min while sphere 2 is expanding. The connecting rod is neither expanding nor contracting in the PMPY (color figure online)

Finally, when the two shape changes governed by $\dot{l}$ and $\dot{R}_1$ are combined, as occurs in most of the simulations, the $O(\delta^2)$ term in the tracer's velocity clearly gives rise to a large change from the asymptotic solution when the tracer is close to the PMPY (compare Fig. 8 and 10). In particular, depending on the instantaneous system profile, the effects resulting from the sphere expansion/contraction might overcome that from the rod length changes (Fig. 10a), and therefore an asymptotic analysis is not sufficient for the study of swimmer–tracer interactions when they are close together.

4.4.2 The long-term behavior of the tracer

As we mentioned earlier, experimental observations show that trajectories of tracers in a suspension of swimmers often look loop-like (Leptos et al. 2009), but a loop-like trajectory will not enhance nutrient supply. In fact, simulations of Rhodobacter sphaeroids (Shum et al. 2010) have shown that when the tracer is far away from the straight path of the swimmer, the loop-like trajectory is approximately true with the net displacement between the initial and final locations considerably shorter than the characteristic trajectory size. On the other hand, when the tracer is close to the swimmer path, it is clearly pulled forward by the swimmer (Pushkin et al. 2013;

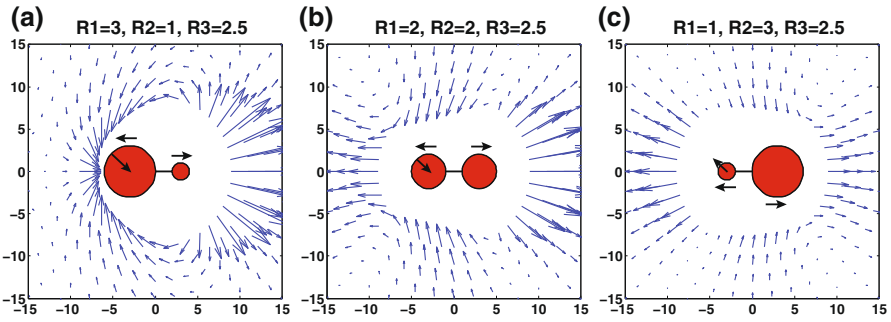

Fig. 10 The instantaneous velocity of a tracer sphere that results from a PMPY swimmer when the tracer sphere is close to the PMPY and higher-order effects are included. The arrows in all panels are scaled uniformly, thus arrows show both direction and magnitude. **a** The connecting rod is instantaneously expanding at $\dot{l} = 2\pi\ \mu\text{m/min}$ and sphere 1 is shrinking at $\dot{R}_1 = -2\pi\ \mu\text{m/min}$. **b** $\dot{l} = 2\pi\ \mu\text{m/min}$, $\dot{R}_1 = -2\pi\ \mu\text{m/min}$. **c** $\dot{l} = 2\pi\ \mu\text{m/min}$, $\dot{R}_1 = 2\pi\ \mu\text{m/min}$

Yeomans et al. 2014). Here we ask the question: how can the tracer scattering, i.e., the net displacement of the tracer, be improved as a swimmer passes?

We first repeat the swimmer–tracer simulation using a PMPY swimmer and a rigid sphere as a tracer. The results—again with the translation of the PMPY computed by Eq. (3.24) and that of sphere 3 by Eqs. (4.3, 4.4)—are given in Fig. 11a, where the system profiles are:

$$l(t) = (20 + \cos(2\pi t))\,\mu\text{m},\ \ R_1 = (2 - \sin(2\pi t))\,\mu\text{m},$$
$$R_2(0) = 3\,\mu\text{m},\ \ R_3 \equiv 0.5\,\mu\text{m},$$

The PMPY swims along the x-axis, from $x = -1000\,\mu\text{m}$ to $x = 1000\,\mu\text{m}$, and the tracer sphere 3 is initially located at $(0, Y_0)$, where $6\,\mu\text{m} \le Y_0 \le 20\mu\text{m}$. In order to compare different trajectories, in this part we set $L_m = \min\{Y_0, \min_t\{l_{12}(t)\}\}$ and we give the values of δ for some of the trajectories in Fig. 11a, and the simulation results (Figs. 11 and 12) are dimensional ones. The result is qualitatively similar to what is obtained from the simulations of Rhodobacter sphaeroids (Shum et al. 2010), that is, the tracer is pushed backwards slightly when more distant from the PMPY swimming path, and clearly pulled forward when close to the path. Its trajectory has three distinct branches, and a close-up view of a part of the trajectory (Fig. 11a′) shows that the tracer undergoes a spiral oscillatory motion, which is qualitatively similar to existing results (Dunkel et al. 2010; Pushkin et al. 2013; Yeomans et al. 2014). The blow-up in Fig. 11c shows the position of the tracer sphere relative to the swimmer's position in the upper panels and the corresponding position along the quasi-loop in the lower panels. While the net translation direction of the tracer per swimmer cycle is determined by its relative position to the swimmer (tracer movement: forward/downward/backward ∼ location: in front of/above/behind), the amplitude of the tracer oscillations is determined by its distance to the swimmer, as can be expected.

According to an asymptotic analysis (Pushkin et al. 2013), the tracer trajectory should approximate a closed loop, but simulation results show that when the tracer

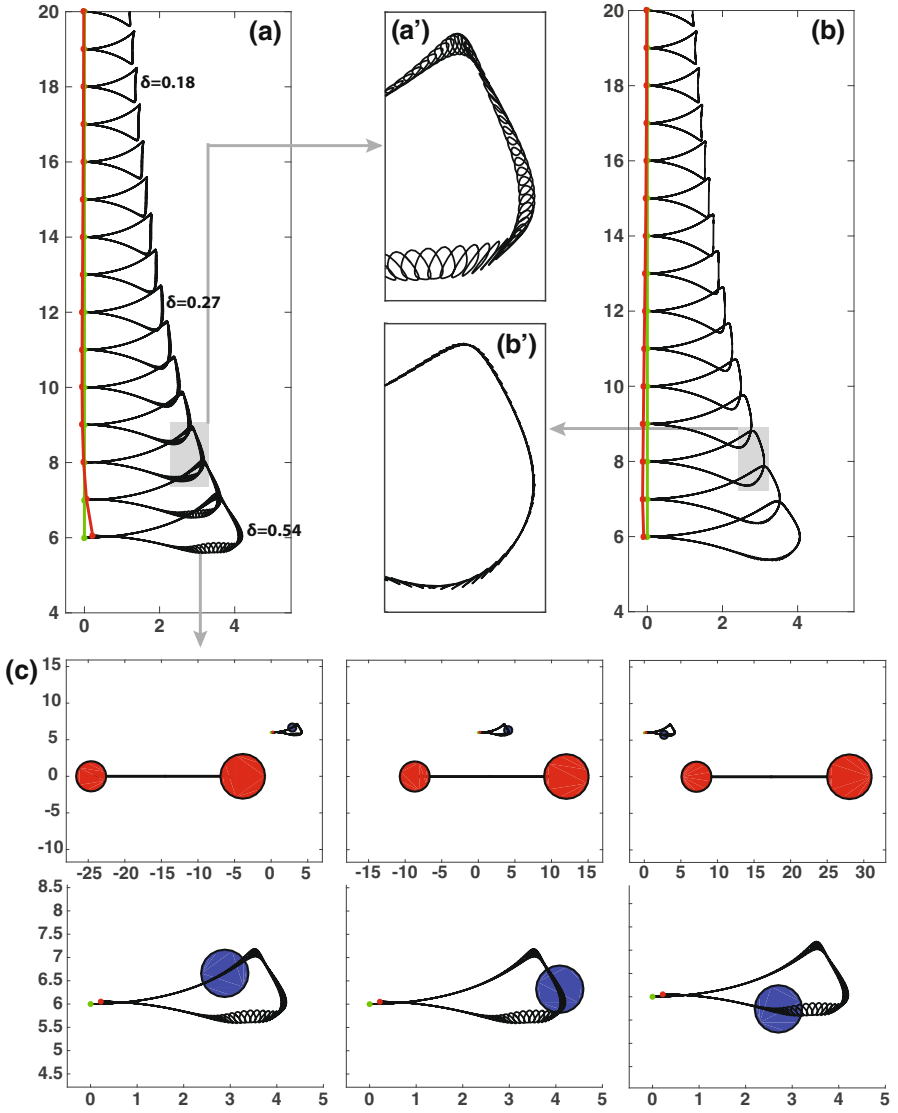

Fig. 11 The tracer loop when a PMPY swimmer moves in a straight line. The green lines give the starting points of the tracer while the red lines give the end points. These curves are computed at increments of $\Delta Y_0 = 1\,\mu$m, and the black lines show the tracer trajectories. **a**–**a**′ The tracer loop of sphere 3, computed with $\mathbf{U}_3 = \mathbf{U}_3^{(f)} + \mathbf{U}_3^{(e)}$. **b**–**b**′ The tracer loop of sphere 3, computed with $\mathbf{U}_3 \sim \mathbf{U}_3^{(f)}$ only. **c** Snap-shots of the system in **a** with the tracer initially located at (0, 6) and the enlarged view of sphere 3 showing its location in the loop (color figure online)

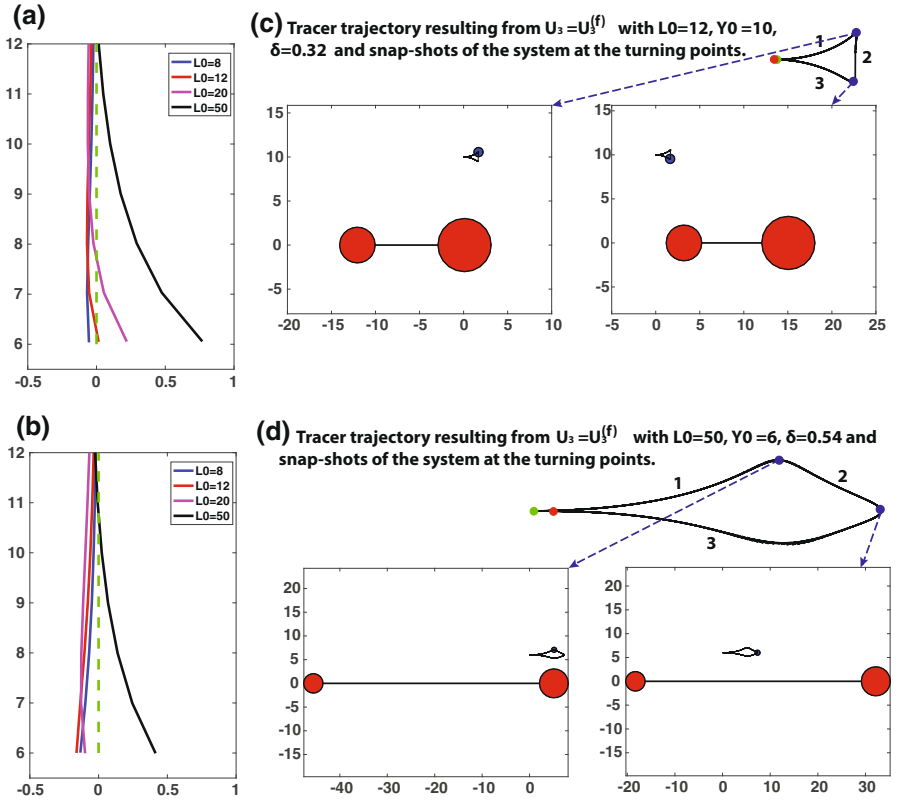

Fig. 12 **a** The tracer sphere's starting (green dashed line) and ending points (solid lines) when a PMPY swims along the x-axis, with $L_0 = 8, 12, 20, 50\,\mu$m (blue, red, magenta, and black solid lines). The lines are computed with $\Delta Y_0 = 1\,\mu$m. The translational velocity of the tracer sphere is calculated as $\mathbf{U}_3 = \mathbf{U}_3^{(f)} + \mathbf{U}_3^{(e)}$. **b** $\mathbf{U}_3 \sim \mathbf{U}_3^{(f)}$. **c** The tracer trajectory with $L_0 = 12\,\mu$m, $Y_0 = 10\,\mu$m and $\mathbf{U}_3 \sim \mathbf{U}_3^{(f)}$ only. Snap-shots of the system at the turning points of the tracer trajectory. **d** As in **c** but with $L_0 = 50\,\mu$m, $Y_0 = 6\,\mu$m (color figure online)

is close to the PMPY path, its trajectory is not fully closed (Shum et al. 2010 and Fig. 11a). This indicates that the scattering is primarily determined by higher order terms in the hydrodynamical interaction between the PMPY and the tracer. Simulations of the instantaneous profile of the system (Figs. 9 and 10) show that when the tracer is close to the PMPY, the $O(\delta^2)$ term resulting from sphere expansion and contraction induces a significant distortion to the instantaneous velocity field of the tracer. To compare the effects of rod length changes versus volume changes on the long-term behavior of the tracer, we ran the long-term swimmer–tracer simulation again with the same strokes but with the translational velocity of the tracer computed from the flow generated by rod length changes only, i.e., $\mathbf{U}_3 \sim \mathbf{U}_3^{(f)}$ [Eq. (4.3)]. The result is shown in Fig. 11b, from which we see that the tracer is still pushed backward slightly, even when close to the PMPY swimming path. A comparison of Fig. 11a, b shows that the effect of the drag force, which is $O(\delta)$ at leading order, [Eq. (4.3)], produces an

essentially closed loop-like trajectory of the tracer, and thus makes little contribution to tracer scattering. On the other hand, the forward motion of the tracer is primarily due to the sphere expansion/contraction with a leading term $O(\delta^2)$ [Eq. (4.4)]. Moreover, a close-up view of the trajectory (Fig. 11b′) shows that the tracer still undergoes an oscillatory motion when subject only to the velocity field due to rod shortening and lengthening, but not in a spiral manner.

Next we investigate whether the rod length of the PMPY swimmer also has an effect on the tracer scattering behavior. In the following simulations we consider the system profiles

$$l(t) = (L_0 + \cos(2\pi t))\,\mu\text{m}, \;\; R_1 = (2 - \sin(2\pi t))\,\mu\text{m},$$
$$R_2(0) = 3\,\mu\text{m}, \;\; R_3 \equiv 0.5\,\mu\text{m},$$

with $L_0 = 8, 12, 20, 50\,\mu$m. The simulation results, with $\mathbf{U}_3 = \mathbf{U}_3^{(f)} + \mathbf{U}_3^{(e)}$ calculated from Eqs. (4.3, 4.4) are given in Fig. 12a. There one sees that the longer the rod is, or equivalently, the further the two spheres in the swimmer are apart, the more the tracer is pulled forward, especially when it is close to the swimmer's path.

Because we found earlier that the PMPY sphere expansion/contraction contributes significantly to the movement of the tracer, we repeat the simulations in Fig. 12a but with $\mathbf{U}_3 \sim \mathbf{U}_3^{(f)}$ computed by Eq. (4.3) only, which approximates the asymptotic behavior. The results are shown in Fig. 12b, from which we see that even without the sphere expansion/contraction, the tracer is still clearly dragged forward when it is close to the swimming path of a long PMPY ($L_0 = 50\,\mu$m). To understand this behavior, we compare two tracer trajectories, both of which result from $\mathbf{U}_3 \sim \mathbf{U}_3^{(f)}$ only. One starts with $L_0 = 12\,\mu$m and $Y_0 = 10\,\mu$m (Fig. 12c), i.e, the PMPY spheres are not far apart and the tracer is not very close to the swimmer's path, and the other starts with $L_0 = 50\,\mu$m and $Y_0 = 6\,\mu$m (Fig. 12d), i.e, the PMPY spheres are far apart and the tracer is close to the swimmer's path. In Fig. 12c the trajectory of the tracer approximates an isosceles triangle and the base (side 2 in the figure) corresponds to the part of the trajectory in which the tracer is essentially directly over the swimmer. On the other hand, when L_0 is large, as in Fig. 12d, the trajectory of the tracer is very different, and in particular, we see that side 2 of the triangle-like trajectory is stretched horizontally, which reflects an enhanced pulling effect on the tracer. In either case, side 2 of the trajectory loop essentially reflects the tracer motion when it is above the swimmer, and therefore the comparison between Fig. 12c and d indicates that the separation of spheres in the PMPY results in an increased pulling effect on the tracer if it is close enough to the swimmer's path.

The foregoing results when a tracer is close enough to the infinite PMPY swimming path can be summarized as follows.

1. Despite having a leading $O(\delta)$ term, rod length changes of the PMPY swimmer lead to an essentially closed-loop trajectory of the tracer, and thus contribute little to tracer scattering, i.e., to the long-term net displacement of the tracer. Thus the scattering is primarily induced by the sphere volume changes with leading $O(\delta^2)$ term.

2. Increasing the sphere separation in a PMPY swimmer will enhance the tracer scattering.

These findings have implications for strategies for how to improve tracer scattering. The first suggests that to induce scattering, transporting mass between different parts of the body is more efficient than expending energy on extending/contracting body length. The second suggests that a longer, more slender swimmer gives rise to a larger amplitude of scattering than shorter ones. However, we should point out that (a) changes in body length may be coupled to mass transport, and (b) it may require more energy to transport mass through a long body. Thus further investigation of shape and stroke design of the micro swimmer are needed, but this is the subject of future research.

5 Swimming with a friend

In this section we consider the hydrodynamic interactions between two PMPY swimmers in an infinite fluid domain, as shown in Fig. 13. To fix the geometry, we introduce a fixed Cartesian frame and we assign a body frame to each swimmer. $\{\mathbf{0}; \mathbf{e}_x, \mathbf{e}_y, \mathbf{e}_z\}$ is attached to PMPY I and has its origin $\mathbf{0}$ at the center $\mathbf{x}_1$ of sphere 1, and has $\mathbf{e}_x$ along the direction of the connecting rod; while $\{\mathbf{0}'; \mathbf{e}_{x'}, \mathbf{e}_{y'}, \mathbf{e}_{z'}\}$ is attached to PMPY II and has its origin $\mathbf{0}'$ at the center $\mathbf{x}_3$ of sphere 3, and $\mathbf{e}_{x'}$ along the direction of its connecting rod. The relationship between the two frames is given by

$$\begin{cases} \mathbf{e}_{x'} = \cos\phi\mathbf{e}_x + \sin\phi\mathbf{e}_y \\ \mathbf{e}_{y'} = -\sin\phi\mathbf{e}_x + \cos\phi\mathbf{e}_y \\ \mathbf{e}_{z'} = \mathbf{e}_z \end{cases}$$

where ϕ is the angle between the two connecting rods: $\phi = \arccos(\mathbf{d}_{12} \cdot \mathbf{d}_{34})$ and $\mathbf{d}_{ij} = (\mathbf{x}_j - \mathbf{x}_i)/|\mathbf{x}_j - \mathbf{x}_i|$.

5.1 Analysis of the two-swimmer system

The basic steps in the analysis of the two PMPY swimmer system are the same as in previous sections, and therefore we only sketch the analysis up to the first reflection. In the zeroth reflection, no hydrodynamic interactions are considered, and therefore

$$\mathbf{U}_i^{(0)} = \frac{1}{6\pi\mu R_i}\mathbf{F}_i, \quad \boldsymbol{\Omega}_i^{(0)} = \mathbf{0}. \tag{5.1}$$

The translational velocities after the first reflection are given by

$$\mathbf{U}_i^{(1)} = \sum_{j\neq i}\left[\mathbf{U}_{i,j}^{(1,f)} + \mathbf{U}_{i,j}^{(1,e)}\right] \tag{5.2}$$

$$\mathbf{U}_{i,j}^{(1,f)} = \frac{1}{8\pi\mu l_{ij}}\left[\left(1 + \frac{R_i^2 + R_j^2}{3l_{ij}^2}\right)\mathbf{F}_j + \left(1 - \frac{R_i^2 + R_j^2}{l_{ij}^2}\right)(\mathbf{F}_j \cdot \mathbf{d}_{ji})\mathbf{d}_{ji}\right] \tag{5.3}$$

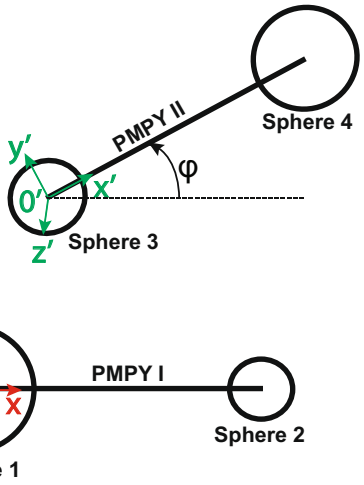

Fig. 13 The geometry of two PMPY swimmers in $\mathbb{R}^3$

$$\mathbf{U}_{i,j}^{(1,e)} = \dot{R}_j \Big(\frac{R_j}{l_{ij}}\Big)^2 \mathbf{d}_{ji} \tag{5.4}$$

where $l_{ij} = |\mathbf{x}_i - \mathbf{x}_j|$ and $\mathbf{d}_{ji} = (\mathbf{x}_i - \mathbf{x}_j)/l_{ij}$. The corresponding angular velocities are

$$\boldsymbol{\Omega}_{\alpha}^{(1)} = \sum_{i=1,2} \frac{F_i}{8\pi\mu l_{i\alpha}^3} \Big[\big(\mathbf{x}_\alpha - \mathbf{x}_i\big) \cdot \mathbf{e}_y\Big] \mathbf{e}_z \quad \text{for} \quad \alpha = 3, 4 \tag{5.5}$$

$$\boldsymbol{\Omega}_{i}^{(1)} = \sum_{\alpha=3,4} \frac{F_\alpha}{8\pi\mu l_{\alpha i}^3} \Big[\big(\mathbf{x}_i - \mathbf{x}_\alpha\big) \cdot \mathbf{e}_{y'}\Big] \mathbf{e}_{z'} \quad \text{for} \quad i = 1, 2. \tag{5.6}$$

In addition, the system should satisfy the volume conservation condition

$$\sum_{i=1,2} R_i^3(t) \equiv \frac{3}{4\pi} V_I, \quad \sum_{\alpha=3,4} R_\alpha^3(t) \equiv \frac{3}{4\pi} V_{II} \tag{5.7}$$

and the force- and torque-free conditions

$$\begin{aligned} &\text{Force-free:} \quad \mathbf{F}_1 + \mathbf{F}_2 = \mathbf{0}, \quad \mathbf{F}_3 + \mathbf{F}_4 = \mathbf{0} \\ &\text{Torque-free:} \quad \mathbf{x}_1 \times \mathbf{F}_1 + \mathbf{x}_2 \times \mathbf{F}_2 = \mathbf{0}, \quad \mathbf{x}_3 \times \mathbf{F}_3 + \mathbf{x}_4 \times \mathbf{F}_4 = \mathbf{0}. \end{aligned}$$

The latter constraints require that

$$\mathbf{F}_i = F_i \mathbf{e}_x \ (i = 1, 2), \quad \mathbf{F}_\alpha = F_\alpha \mathbf{e}_{x'} \ (\alpha = 3, 4)$$

and

$$\sum_{i=1,2} \mathbf{F}_i = \sum_{i=1,2} F_i \mathbf{e}_x \equiv \mathbf{0}, \quad \sum_{\alpha=3,4} \mathbf{F}_\alpha = \sum_{\alpha=3,4} F_\alpha \mathbf{e}_{x'} \equiv \mathbf{0}. \tag{5.8}$$

Finally the rigid motions of the spheres in each PMPY should satisfy:

$$\big(\mathbf{U}_2 - \mathbf{U}_1\big) \cdot \mathbf{e}_x = \dot{l}_{12}, \quad \big(\mathbf{U}_4 - \mathbf{U}_3\big) \cdot \mathbf{e}_{x'} = \dot{l}_{34} \tag{5.9}$$

Equations (5.1–5.9) define the system that determines the swimming of the two PMPY models.

We set

$$R_M = \max_t \{R_i(t)\}_{i=1,2,3,4}, \quad L_m = \min_t \{l_{ij}(t)\}_{i,j=1,2,3,4}, \quad \delta = \frac{R_M}{L_m},$$

and we use the nondimensionalization given in Sect. 3.1. A simple analysis similar to that in Sect. 4.2 gives the following leading order estimate

$$\mathbf{U}_i^{(0)} \sim O(1), \quad \mathbf{U}_i^{(1)} \sim O(\delta), \quad \boldsymbol{\Omega}_i^{(1)} \sim O(\delta^3)$$

From this we see that when $\delta \ll 1$, the rotational effect of the PMPYs is much smaller as compared to the translational effect.

5.2 Hydrodynamic interactions between two PMPY swimmers in a line

To proceed further we must specify how the pair moves, and we first consider the configuration in which they lie in the same line, specifically, suppose that the centers of all spheres lie along the x-axis. In addition, we place PMPY II in front of PMPY I, hence from negative to positive direction along the x-axis, the spheres are ordered from sphere 1 to sphere 4 (Fig. 15il).

Equations (5.2, 5.3) show that the hydrodynamic interactions between the two PMPYs arise at $O(\delta)$. A simple perturbation analysis gives the non-dimensionalized forces exerted on the spheres (again with hat notation omitted):

$$\begin{aligned}
-F_1 = F_2 \sim{}& \frac{R_1 R_2}{R_1 + R_2}\xi_I + 3\frac{\delta}{l_{12}}\Big(\frac{R_1 R_2}{R_1 + R_2}\Big)^2 \xi_I \\
&+ \frac{3}{2}\delta \frac{R_1 R_2 R_3 R_4}{(R_1 + R_2)(R_3 + R_4)}\Big(\frac{1}{l_{23}} - \frac{1}{l_{24}} - \frac{1}{l_{13}} + \frac{1}{l_{14}}\Big)\xi_{II} + O(\delta^2) \\
-F_3 = F_4 \sim{}& \frac{R_3 R_4}{R_3 + R_4}\xi_{II} + 3\frac{\delta}{l_{34}}\Big(\frac{R_3 R_4}{R_3 + R_4}\Big)^2 \xi_{II} \\
&+ \frac{3}{2}\delta \frac{R_1 R_2 R_3 R_4}{(R_1 + R_2)(R_3 + R_4)}\Big(\frac{1}{l_{23}} - \frac{1}{l_{24}} - \frac{1}{l_{13}} + \frac{1}{l_{14}}\Big)\xi_I + O(\delta^2)
\end{aligned}$$

and the translational velocities of the spheres:

$$
\begin{aligned}
U_1 \sim & -\frac{R_2}{R_1+R_2}\xi_I + \delta\frac{R_1R_2(R_1-R_2)}{2(R_1+R_2)^2 l_{12}}\xi_I \\
& -\frac{3}{2}\delta\frac{R_3R_4}{(R_1+R_2)(R_3+R_4)}\xi_{II}\Big[R_1\Big(\frac{1}{l_{13}}-\frac{1}{l_{14}}\Big)+R_2\Big(\frac{1}{l_{23}}-\frac{1}{l_{24}}\Big)\Big]+O(\delta^2) \\
U_3 \sim & -\frac{R_4}{R_3+R_4}\xi_{II} + \delta\frac{R_3R_4(R_3-R_4)}{2(R_3+R_4)^2 l_{34}}\xi_{II} \\
& -\frac{3}{2}\delta\frac{R_1R_2}{(R_1+R_2)(R_3+R_4)}\xi_I\Big[R_3\Big(\frac{1}{l_{13}}-\frac{1}{l_{23}}\Big)+R_4\Big(\frac{1}{l_{14}}-\frac{1}{l_{24}}\Big)\Big]+O(\delta^2)
\end{aligned}
$$

where $\xi_I,\ \xi_{II}$ are $\dot{l}_I,\ \dot{l}_{II}$ after non-dimensionalization. Reference to Eqs. (3.27, 3.28), and taking into consideration the geometric condition at Eq. (5.9), leads to the following estimate of the hydrodynamic interaction effects on the velocities of the PMPYs.

$$
\begin{aligned}
U^{\text{hydro}}_{II\to I} = & -\frac{3}{2}\delta\frac{R_3R_4}{(R_1+R_2)(R_3+R_4)}\xi_{II}\Big[R_1\Big(\frac{1}{l_{13}}-\frac{1}{l_{14}}\Big) \\
& +R_2\Big(\frac{1}{l_{23}}-\frac{1}{l_{24}}\Big)\Big]+O(\delta^2) \qquad (5.10) \\
U^{\text{hydro}}_{I\to II} = & \frac{3}{2}\delta\frac{R_1R_2}{(R_1+R_2)(R_3+R_4)}\xi_I\Big[R_3\Big(\frac{1}{l_{23}}-\frac{1}{l_{13}}\Big) \\
& +R_4\Big(\frac{1}{l_{24}}-\frac{1}{l_{14}}\Big)\Big]+O(\delta^2) \qquad (5.11)
\end{aligned}
$$

The geometric relations give

$$
\frac{1}{l_{13}}-\frac{1}{l_{14}},\ \frac{1}{l_{23}}-\frac{1}{l_{24}},\ \frac{1}{l_{23}}-\frac{1}{l_{13}},\ \frac{1}{l_{24}}-\frac{1}{l_{14}} > 0
$$

and thus the leading order of $U^{\text{hydro}}_{II\to I}$ has the opposite sign of ξ_{II} while that of $U^{\text{hydro}}_{I\to II}$ has the same sign as ξ_I:

$$
U^{\text{hydro}}_{II\to I}\xi_{II} < 0, \quad U^{\text{hydro}}_{I\to II}\xi_I > 0
$$

This can be understood as follows. Since PMPY II is leading, when it lengthens it impedes the swimming of PMPY I, which follows; on the other hand, when PMPY I lengthens, it enhances the swimming of PMPY II in front of it.

The full expressions of the $O(\delta^2)$ term of $U^{\text{hydro}}_{II\to I},\ U^{\text{hydro}}_{I\to II}$ are lengthy, however, by taking $\xi_I = \xi_{II} = 0$, we can easily obtain the hydrodynamic interactions on the sphere velocities that result from the sphere expansion/contraction of the other PMPY only (Appendix F.2):

$$
U^{\text{hydro}}_{II\to I}\{\dot{R}\} = -R_3^2\zeta_3\delta^2\Big[\frac{R_1}{R_1+R_2}\Big(\frac{1}{l_{13}^2}-\frac{1}{l_{14}^2}\Big)+\frac{R_2}{R_1+R_2}\Big(\frac{1}{l_{23}^2}-\frac{1}{l_{24}^2}\Big)\Big]+O(\delta^3)
$$

$$U^{\text{hydro}}_{I\to II}\{\dot{R}\} = -R_1^2\zeta_1\delta^2\Big[\frac{R_3}{R_3+R_4}\Big(\frac{1}{l_{23}^2}-\frac{1}{l_{13}^2}\Big)+\frac{R_4}{R_3+R_4}\Big(\frac{1}{l_{24}^2}-\frac{1}{l_{14}^2}\Big)\Big]+O(\delta^3)$$

The geometry of the system also dictates that the leading order term of $U^{\text{hydro}}_{II\to I}\{\dot{R}\}$ has the opposite sign of ζ_3, while that of $U^{\text{hydro}}_{I\to II}\{\dot{R}\}$ has the opposite sign of ζ_1:

$$\big(U^{\text{hydro}}_{II\to I}\{\dot{R}\}\big)\zeta_3 < 0, \quad \big(U^{\text{hydro}}_{I\to II}\{\dot{R}\}\big)\zeta_1 < 0$$

The first relation is easy to understand: the expansion of sphere 3, which is the closer of 3 and 4 to PMPY I, will impede the swimming of PMPY I, which follows PMPY II. For the second relation, recall that the volume conservation constraint gives $R_1^2\zeta_1 = -R_2^2\zeta_2$, thus we have $\big(U^{\text{hydro}}_{I\to II}\{\dot{R}\}\big)\zeta_2 > 0$, that is, the leading order of $U^{\text{hydro}}_{I\to II}\{\dot{R}\}$ has the same sign as ζ_2. In other words, the expansion of sphere 2, which is the sphere in PMPY I that is near PMPY II, will enhance the swimming of PMPY II.

When $\delta \ll 1$ the hydrodynamic effect that results from sphere expansion/contraction ($U^{\text{hydro}}\{\dot{R}\} \sim O(\delta^2)$) can certainly be neglected compared to the total hydrodynamic effect due to expansion/contraction of the rod, which is $U^{\text{hydro}} \sim O(\delta)$. Here we consider the hydrodynamic effects when the spheres are allowed to come closer, i.e., $\delta < 1$ but not too small. We first consider the instantaneous behavior of the system, and then the period-average behavior. For example, we consider an instantaneous system configuration in which $R_1 = R_2 = R_3 = R_4 = R$ and $l_{12} = l_{23} = l_{34} = L$, and for this we have for the leading order terms

$$\big|U^{\text{hydro}}_{II\to I}\big| = \frac{R}{4L}\delta|\xi_{II}|, \quad \big|U^{\text{hydro}}_{II\to I}\{\dot{R}\}\big| = \frac{4R^2}{9L^2}\delta^2|\zeta_3|.$$

Recalling that the non-dimensionalization of our system guarantees that $R \le 1,\ L \ge 1$ [Eq. (3.6)], in the case of $R = L = 1$, we have the relation

$$\frac{\big|U^{\text{hydro}}_{II\to I}\{\dot{R}\}\big|}{\big|U^{\text{hydro}}_{II\to I}\big|} \sim \frac{16}{9}\delta\Big|\frac{\zeta_3}{\xi_{II}}\Big|.$$

For a system with $\delta \sim 0.5$ where the spheres are close to each other, the coefficient of the above equation is 8/9, and in this case the hydrodynamic effects that result from sphere expansion/contraction must be included, together with higher order terms in U^{hydro}.

Figure 14 gives the instantaneous fluid velocity field around a system of two linear PMPYs, where the instantaneous system profile is $R_1 = R_2 = R_3 = R_4 = 2\,\mu\text{m}$, $l_{12} = l_{34} = 6\,\mu\text{m}$, $l_{23} = 8\,\mu\text{m}$. Figure 14a, b give the velocity fields when only the rod lengths vary, while in Fig. 14c–f we include both rod and sphere changes. A comparison of the two cases shows that for a linear system in which δ is not too small, the $O(\delta^2)$ terms that result from the sphere changes give rise to a large perturbation of the surrounding fluid near the swimmers.

To obtain some insight into the swimming behavior of a linear system of two PMPYs over a period, we consider the following two systems.

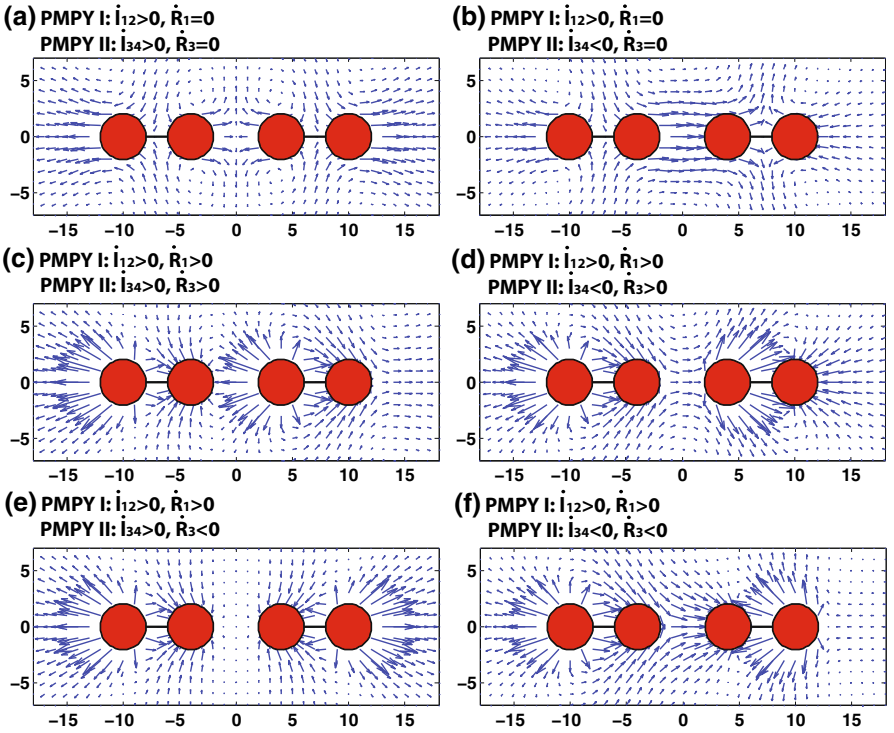

Fig. 14 The instantaneous fluid velocity field around two linear PMPYs, with $R_1 = R_2 = R_3 = R_4 = 2$, $l_{12} = l_{34} = 6$, $l_{23} = 8$. **a** Both swimmers undergo expansion and contraction of their connecting rods, but no volume changes. For I, $\dot{l}_{12} = 2\pi$, $\dot{R}_1 = 0$, and for II, $\dot{l}_{34} = 2\pi$, $\dot{R}_3 = 0$; **b** As in **a**, but with $\dot{l}_{34} = -2\pi$; **c** For I, $\dot{l}_{12} = 2\pi$, and $\dot{R}_1 = 2\pi$, and for II, $\dot{l}_{34} = 2\pi$, $\dot{R}_3 = 2\pi$; **d** As in **c**, but with $\dot{l}_{34} = -2\pi$; **e** For I, $\dot{l}_{12} = 2\pi$, $\dot{R}_1 = 2\pi$, and for II $\dot{l}_{34} = 2\pi$, $\dot{R}_3 = -2\pi$; **f** As in **e** but with $\dot{l}_{34} = -2\pi$, $\dot{R}_3 = -2\pi$. The system is with classic units μm and min

– System i:

$$\begin{aligned} &\text{PMPY I:} \quad R_1(t) = 2 - \sin 2\pi t, \quad R_2(0) = 3, \quad l_{12} = l_0 + \cos 2\pi t \\ &\text{PMPY II:} \quad R_3(t) = 2 - \sin(2\pi t + \psi_0), \quad l_{34} = l_0 + \cos(2\pi t + \psi_0) \end{aligned}$$

– System ii:

$$\begin{aligned} &\text{PMPY I:} \quad R_1(0) = 3, \quad R_2(t) = 2 + \sin 2\pi t, \quad l_{12} = l_0 + \cos 2\pi t \\ &\text{PMPY II:} \quad R_4(t) = 2 + \sin(2\pi t + \psi_0), \quad l_{34} = l_0 + \cos(2\pi t + \psi_0), \end{aligned}$$

both with the following constraint and initial condition:

$$\begin{aligned} &\text{Equal volume conservation:} \quad \frac{4\pi}{3}\left(R_1^3 + R_2^3\right) = \frac{4\pi}{3}\left(R_3^3 + R_4^3\right) \equiv \text{Const.} \\ &\text{Initial distance between the two PMPY models:} \quad l_{23}(0) = d_0 \end{aligned}$$

and the system is with classic units μm and min. In either system the two PMPYs undergo the same loop in the control space $(\dot{l}, \dot{R}_1)$ except for a phase difference ψ_0.

We solve the linear system Eqs. (5.1–5.9), with Eqs. (5.5, 5.6) for the angular motions removed due to the linear geometry (Appendix E). We take $l_0 = 8\,\mu\text{m}$, thus $R_M \sim 3.24\,\mu\text{m}$, $l_m = 7\,\mu\text{m}$, $\delta \sim 0.46$ and with $\delta^4 \sim 4.5E-2$. Simulation results of the two systems for the translation and performance are shown in Fig. 15, and for comparison we show the results for a single swimmer undergoing the same cyclic deformations (black dotted line in Fig. 15a–f, j, k, and black solid line in Fig. 15g, h). From these results we can draw the following conclusions.

1. Figure 15a–c show that in system i the one in front (PMPY II) gets pushed forward (red line), while the one that follows (PMPY I, blue line) gets pushed backward, and Fig. 15d–f show that the performance of the PMPY in front increased while that of the one that follows is decreased. On the other hand, in system ii we observe the reverse effect: the one in front gets pulled back and its performance decreased, while the one that follows gets pushed forward and its performance enhanced (Fig. 15j, k). Therefore we see that in system i the two PMPYs are repelling one another, while in system ii they are attracting each other. In short, *when two PMPYs that are identical except for a phase difference in their shape deformations swim in a line, they may repel or attract each other with a small amplitude, depending on their initial configuration and shape deformations.*
2. Regarding the phase difference, in the repelling system i, when $\psi_0 = 0$, PMPY II gets the maximum increase while PMPY I gets the minimum decrease in both net translation and performance; on the other hand when $\psi = \pi$, PMPY II gets the minimum increase while PMPY I gets the maximum decrease in both net translation and performance (Fig. 15a, d). In the attracting system ii we observe the similar effect (Fig. 15j, k).

Next we compute the scaled distance change $l_{23}(1) - l_{23}(0)$ between the two PMPYs after one period for systems with different values of l_0 and d_0, the initial rod length and the distance between spheres 2 and 3, resp. This measures the drag/propulsion between the two PMPYs due to hydrodynamic interaction: if there is no hydrodynamic interaction between them, $l_{23}(1) - l_{23}(0)$ is identically zero, but otherwise the difference will generally be non-zero, and will reflect the strength of the interaction. This raises the question as to how accurately the asymptotic approximation can capture this interaction. In simulations to examine this, we allow $l_{23} < L_m$ as long as all spheres are always kept separated. Figure 16 shows the results for $l_0 = 8\,\mu\text{m}$, and different values of d_0, with the translation either calculated up to the first reflection [Eqs. (5.1–5.4), Fig. 16 blue lines], or with leading terms from the second reflection included (Fig. 16 black dots, for computation details, see Appendix E), or by asymptotic approximation to $O(\delta)$ (Fig. 16 green lines). From this we see that when l_0 and d_0 are both small, i.e., the spheres are close, there is a clear difference in magnitude between the asymptotic solution and the solution that results from the first reflection or the second reflection but only with the leading terms, although they are qualitatively similar.

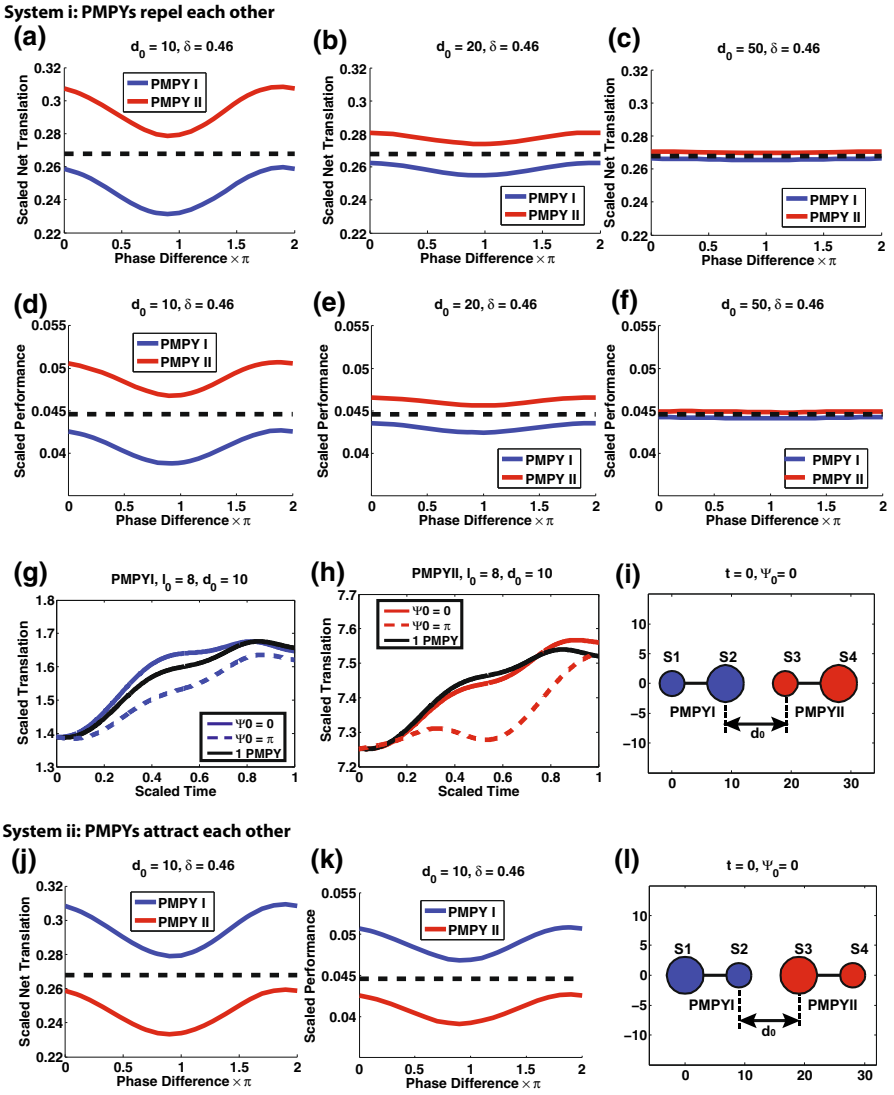

Fig. 15 Two PMPYs swim in a line. In panels **a**–**f** and **j**, **k** the dashed black line gives either the scaled net translation X or the scaled performance $\mathscr{P}$ of a single PMPY undergoing the same sequence of shape changes. **a**–**i** Simulation results for system i, **j**–**l** simulation results for system ii. **a**–**c**, **j** The relation between the scaled net translations of the two PMPYs (X_I, PMPY I, blue line; X_{II}, PMPY II, red line) and the phase difference Ψ_0 for $d_0 = 10, 20, 50\,\mu$m and $l_0 = 8\,\mu$m. **d**–**f**, **k** The relation between the scaled performance of the two PMPYs ($\mathscr{P}_I$, PMPY I, blue line; $\mathscr{P}_{II}$, PMPY II, red line) and the phase difference Ψ_0 for $d_0 = 10, 20, 50\,\mu$m and $l_0 = 8\,\mu$m. **g** The scaled trajectory X_I ($0\,\text{min} \le t \le 1\,\text{min}$) of PMPY I with $l_0 = 8\,\mu$m, $d_0 = 10\,\mu$m and phase difference $\Psi_0 = 0$ (blue solid line) or π (blue dashed line), comparing to the scaled trajectory of a single PMPY undergoing the same sequence of shape deformations (black solid line). **h** As in **g**, but for PMPY II. **i**, **l** The initial profile of the system with $l_0 = 8\,\mu$m, $d_0 = 10\,\mu$m, $\Psi_0 = 0$ (color figure online)

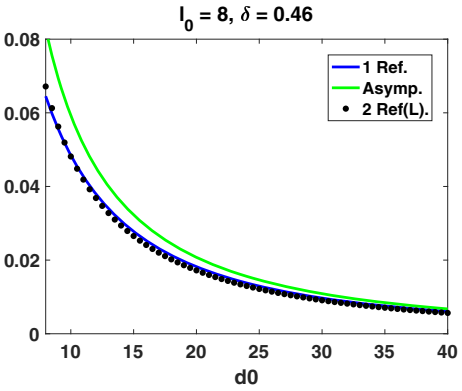

Fig. 16 Scaled $l_{23}(1) - l_{23}(0)$ for system i, with different values of l_0 and d_0, where the translation is either calculated up to the first reflection (blue lines), or with leading terms from the second reflection included (black dots), or by asymptotic approximation to $O(\delta)$ (green lines) (color figure online)

6 Extended scallop theorem and mixed controls

A widely-quoted principle in LRN swimming is that *any reciprocal stroke gives no net motion*, which is known as the "scallop theorem" (Purcell 1977). An immediate corollary of this theorem is: if a self-propelled swimmer has only one degree of freedom in its shape deformations, any cyclic stroke must be reciprocal and hence it cannot swim at LRN. However, a group of reciprocal swimmers, none of which can swim in isolation, may coordinate their shape deformations such that the aggregate shape deformations of the group are not reciprocal. Thus, by taking advantage of the hydrodynamic interactions, they may swim. This phenomenon is referred to as "no many scallop theorem" in the existing literature (Koiller et al. 1996; Lauga and Bartolo 2008; Alexander and Yeomans 2008; Lauga 2011). We quote from (Lauga 2011): "Although a body undergoing reciprocal motion cannot swim, two bodies undergoing reciprocal motion with nontrivial phase differences are able to take advantage of the unsteady hydrodynamic flows they create to undergo nonzero collective and relative dynamics; there is thus no many-scallop theorem."

In previous sections each PMPY could swim by itself, but here we modify the PMPY model into a scallop-type swimmer and study the collective behavior. In particular, we focus on how well the collection can swim by taking advantage of hydrodynamic interactions. As we discussed earlier, a PMPY has two degrees of freedom in its shape deformations, namely $\dot{l}$ and $\dot{R}_1$, and to make it a scallop-type swimmer, we can disable either of them. Thus for two hobbled PMPYs swimming together, there are three possibilities for their controls: $(\dot{l}_I, \dot{l}_{II})$, $(\dot{R}_{I,1}, \dot{R}_{II,1})$, or a mixed control $(\dot{l}_I, \dot{R}_{II,1})$. The first case, i.e., $(\dot{l}_I, \dot{l}_{II})$, in which each PMPY is a simple dumb-bell with an extensible connecting rod, has been studied previously (Lauga and Bartolo 2008; Alexander and Yeomans 2008), while the other combinations of controls have not. Recall that for a single active LRN swimmer, three linked-sphere models have been designed according to these three different combinations of controls: Najafi–Golestanian three-sphere model in $(\dot{l}_1, \dot{l}_2)$ (Alexander et al. 2009; Najafi and Golestanian 2004), PMPY in $(\dot{l}, \dot{R}_1)$ (Avron et al. 2005) and the three-sphere volume-exchange model $(\dot{R}_1, \dot{R}_3)$ (Wang et al. 2012). It was shown that a PMPY adopting the mixed control is superior

Table 1 Simulation results of scaled net translation X and performance $\mathscr{P}$ of the three systems of two degraded PMPYs

	X_I	X_{II}	$\mathscr{P}_I$	$\mathscr{P}_{II}$
System A	-0.8×10^{-3}	-1.1×10^{-3}	5.25×10^{-4}	6.94×10^{-4}
System B	3.3×10^{-3}	4.0×10^{-3}	6.66×10^{-4}	7.84×10^{-4}
System C	0.5×10^{-3}	-17.5×10^{-3}	3.39×10^{-4}	34×10^{-4}

than the other two by order $O(L^2)$ in both net translation and performance, where L is the typical length of the swimmers (Wang and Othmer 2015). Here we ask the question: will a mixed control strategy of deformations lead to better LRN swimming for two hobbled PMPYs, as it does for a single active swimmer?

Again we consider two PMPYs lying along the x-axis, with PMPY II in front. We design three systems according to different types of controls, again with classic units μm and min.

– System A in $(\dot{l}_I, \dot{l}_{II})$ (two dumb-bells):

$$R_1 = R_2 = R_3 = R_4 = 3.24, \quad l_{12} = l_0 + \cos(2\pi t), \quad l_{34} = l_0 + \sin(2\pi t)$$

– System B in $(\dot{R}_{I,1}, \dot{R}_{II,1})$:

$$R_1(t) = 2 + \cos(2\pi t), \quad R_2(0) = 2, \quad R_3(t) = 2 + \sin(2\pi t),$$
$$R_4(0) = 3 \quad l_{12} = l_{34} = l_0 - 1$$

– System C in $(\dot{l}_I, \dot{R}_{II,1})$:

$$R_1 = R_2 = 3, \quad R_3(t) = 2 + \sin(2\pi t), \quad R_4(0) = 3,$$
$$l_{12}(t) = l_0 + \cos(2\pi t), \quad l_{34} = l_0$$

– Initial condition: $l_{23}(0) = d_0$

Therefore the three systems have the same scales: $R_M \sim 3.24\,\mu$m, $L_m = (l_0 - 1)\,\mu$m. We perform simulations with $l_0 = d_0 = 12\,\mu$m, which gives $\delta \sim 0.29$, and the scaled net translations X_I, X_{II} and scaled performances $\mathscr{P}_I$, $\mathscr{P}_{II}$ are given in Table 1.

First, from Table 1 we see that all three systems can swim, although none is as effective as a single active PMPY, which typically swims a scaled net translation of $X \sim O(10^{-1})$ and with a scaled performance of $\mathscr{P} \sim O(10^{-2})$ under this protocol (see Sect. 3.4). Next, we find that the swimming behaviors of systems A and B, i.e., the two with the same type of shape deformations, are quite similar: both PMPYs in both systems have scaled net translations and scaled performances of the orders $X \sim O(10^{-3})$ and $\mathscr{P} \sim O(10^{-4})$. On the other hand, system C, which adopts the mixed controls, behaves very differently. The PMPY with shape deformations in $\dot{l}$ (i.e., PMPY I) swims much less effectively than the one using an $\dot{R}$ control (PMPY II) , with scaled net translations and scaled performance ratios $X_{II}/X_I \sim 35$ and

$\mathscr{P}_{II}/\mathscr{P}_I \sim 10$. Also, PMPY II in system C clearly swims better than either of the two PMPYs in system A or B, while the poorer one (PMPY I) swims slightly worse than the two PMPYs in system A or B . A detailed asymptotic analysis of the three systems is given in Appendix F.

The reasons for this difference in outcome for different control choices are: (1) $\dot{l}$ gives rise to lower-order terms in the translational velocity than does $\dot{R}$ [Eq. 3.23]; (2) to guarantee that the lower-order terms resulting from $\dot{l}$ do not vanish in the net translation, it is necessary that the coefficients that depend on the radii be time-dependent, otherwise the temporal integral will be path-independent, or at best only result in higher order terms. To be more specific:

1. Controls in $(\dot{R}_{I,1}, \dot{R}_{II,1})$ will result in terms no lower than $O(\delta^2)$ in velocity and net translation.
2. Controls in $(\dot{l}_I, \dot{l}_{II})$ will result in leading order term of $O(1)$ or $O(\delta)$ in velocity, depending on the geometry of the model. However, their coefficients are either of the form $\Phi(R_{1,2,3,4})$ or $\Phi(R_{1,2,3,4})/l(t)$, where the radii are all constants. In the former case, it gives rise to a path-independent integral when computing the net translation; in the latter case, when integrated, it only gives higher order terms. For details, see the discussion in Appendix F.1.
3. Only with mixed controls in $(\dot{l}_I, \dot{R}_{II,1})$ and for the PMPY with shape deformation $\dot{R}$, the leading order in velocity is of $O(\delta)$ order and of the from $\Phi(R_{1,2,3,4}(t))/l(t)$, which neither vanishes nor degrades when integrated.

Finally we summarize previous studies on the *scallop theorem* (Purcell 1977; Lauga 2011) together with our discussions from Sects. 4 and 5 as follows. In an LRN Newtonian flow,

1. a scallop cannot swim (*Purcell's scallop theorem*);
2. a living scallop surrounded by a few dead scallops cannot swim;
3. a group of living scallops can swim, but in an energy-inefficient manner.

The precise mathematical interpretation of the above generalization is as follows. At low Reynolds number,

1. a self-deformable swimmer with only one degree of freedom cannot swim—which is the statement of the original scallop theorem.
2. A self-deformable swimmer with only one degree of freedom cannot swim efficiently in the presence of passive rigid objects. This can be seen from Sect. 4, as the presence of a rigid object that cannot deform itself has no effect on the swimmer up to the first reflection. When further reflections are considered, the presence of the rigid objects nearby will indeed affect the swimmer, but the effect would be too small to have a significant effect on the swimmer.
3. A group of self-deformable swimmers, all with only one degree of freedom, can swim by taking advantage of hydrodynamic interactions. However, both the translation and performance are much worse than one swimmer with multiple degrees of freedom.

7 Discussion

Herein we used a basic PMPY model to study the LRN swimming characteristics of both single and multiple swimmers, so as to understand the effect of hydrodynamic interactions on the translation and performance of such swimmers. One significant result is that the PMPY model is an efficient LRN swimmer whose swimming behavior approximates that of swimming Dd amoebae. This suggests that the PMPY model may provide a good first-order model for the study of microorganisms swimming at LRN. As was shown, to better approximate the characteristics of LRN swimming microorganisms one must allow the spheres to approach more closely than in previous analyses, in which case the asymptotic solution for $\delta \sim 0$ is inadequate and higher-terms in the interactions must be included. When a PMPY is swimming with a passive object, the swimming PMPY has a clear effect on the passive object, while the existence of the latter has little effect on the PMPY, as long as the size of this object is comparable to or less than the spheres in the PMPY. If the passive object is directly ahead of the PMPY, the PMPY can catch up with it within a few cycles, using a reasonable amount of energy. If the freely buoyant object is not directly in the PMPY's path, its long-term trajectory approximates a closed-triangle when it is far away from the PMPY's swimming path, or it will be pushed forward if it is close to the PMPY's swimming path. In this case the higher-order terms in the solution of the translational velocity of the PMPY contribute significantly to this entrainment effect, and again, an asymptotic solution does not capture this effect. Moreover, a longer PMPY will enhance the entrainment effect.

When there are two PMPYs swimming together collinearly, the hydrodynamic interactions among them may cause some attraction or repulsion between them, depending on the stroke. However, this effect is small compared with the net translation of the PMPYs, but again, higher-order terms should be taken into consideration, particularly if one is interested in either the instantaneous or long-term behavior of the system. A scallop-type swimmer cannot swim at LRN on its own or in the presence of non-deformable buoyant objects, but with an intricate coordination of their strokes, two or more of them can swim by taking advantage of hydrodynamic interactions. Although swimming in this manner is generally not efficient, a pair of scallop-type swimmers that use a mixed $(\dot{l}, \dot{R})$ control may enhance the swimming of one of the pair as compared to pairs in which both use either a pure $(\dot{l})$ or $(\dot{R})$ control.

Computationally, we use the *reflection method*, which is shown to be an efficient computation method for linked-sphere type of LRN swimmers, in particular, PMPY. Although an approximation approach, we show that when the spheres are not touching, the reflection method is quite accurate. In some of our simulations, we can push the system to $\delta \sim 1/2$, yet by comparing with the results obtained with the leading terms from the second reflection included, we show that the results are still trustworthy, at least for qualitative results. However, if the spheres are drawing even closer or even touching each other, the lubrication effect becomes dominant and the validity of the reflection method is greatly limited. Other computational approaches should be adopted in this regime.

In the biological context the surrounding material may be non-Newtonian, and in particular, is often viscoelastic. Some results for this case are known (Qiu et al. 2014; Curtis and Gaffney 2013), but much remains to be done.

Appendices

A Newtonian flow produced by the translation and radial expansion of a sphere

Here we derive the velocity field $\mathbf{u}(\mathbf{x})$ of a LRN flow produced by a sphere of radius R, pulled by a force $\mathbf{F}$ and expanding radially at a rate $\dot{R} = \mathrm{d}R/\mathrm{d}t$. Due to the linearity of LRN flows, the velocity field is the sum of two terms: that resulting from the drag force—$\mathbf{u}\{\mathbf{F}\}$, and that resulting from the radial expansion—$\mathbf{u}\{\dot{R}\}$:

$$\mathbf{u} = \mathbf{u}\{\mathbf{F}\} + \mathbf{u}\{\dot{R}\} \tag{A.1}$$

The flow produced by the translation of a solid sphere is a classical result (Pozrikidis 1992). It can be represented in terms of a Stokeslet and dipole with poles at the center of the sphere that are given by

$$\mathbf{G} = \frac{\mathbf{I}}{r} + \frac{\mathbf{rr}}{r^3} \tag{A.2}$$

$$\mathbf{D} = -\frac{\mathbf{I}}{r^3} + 3\frac{\mathbf{rr}}{r^5} \tag{A.3}$$

where $\mathbf{x}_0$ is the center of the sphere, $\mathbf{r} = \mathbf{x} - \mathbf{x}_0$ and $r = |\mathbf{r}|$. $\mathbf{G}$ is called the Oseen tensor. The velocity field is then

$$u_i(\mathbf{x}) = G_{ij}(\mathbf{x}, \mathbf{x}_0)\Big(\frac{3}{4}RU_j\Big) - D_{ij}(\mathbf{x}, \mathbf{x}_0)\Big(\frac{1}{4}R^3U_j\Big). \tag{A.4}$$

Here $\mathbf{U}$ is the translational velocity of the sphere, i.e., $\mathbf{U}(t) = \dot{\mathbf{x}}_0(t)$. The relation between the drag force $\mathbf{F}$ and $\mathbf{U}$ is

$$\mathbf{F} = 6\pi\mu R\mathbf{U} \tag{A.5}$$

Using the above one obtains the fluid velocity

$$\begin{aligned} u_i &= \frac{1}{24\pi\mu}\Big[3\Big(\frac{\delta_{ij}}{r} + \frac{r_i r_j}{r^3}\Big)F_j - \Big(-\frac{\delta_{ij}}{r^3} + 3\frac{r_i r_j}{r^5}\Big)R^2F_j\Big] \\ &= \frac{1}{24\pi\mu}\Big[3\Big(\frac{F_i}{r} + \frac{(\mathbf{F}\cdot\mathbf{r})r_i}{r^3}\Big) + \Big(\frac{F_i}{r^3} - 3\frac{(\mathbf{F}\cdot\mathbf{r})r_i}{r^5}\Big)R^2\Big] \\ &= \frac{1}{24\pi\mu r}\Big[\Big(3 + \frac{R^2}{r^2}\Big)F_i + 3(\frac{1}{r^2} - \frac{R^2}{r^4})(\mathbf{F}\cdot\mathbf{r})r_i\Big] \end{aligned}$$

or alternatively

$$\mathbf{u}\{\mathbf{F}\} = \frac{1}{24\pi\mu r}\Big[\Big(3+\frac{R^2}{r^2}\Big)\mathbf{F} + 3\Big(1-\frac{R^2}{r^2}\Big)(\mathbf{F}\cdot\hat{\mathbf{r}})\hat{\mathbf{r}}\Big] \tag{A.6}$$

where $\hat{\mathbf{r}} = \mathbf{r}/|\mathbf{r}|$.

The velocity field $\mathbf{u}\{\dot{R}\}$ of the flow produced by a radially expanding sphere can be represented by a point source with pole at the center $\mathbf{x}_0$ of the sphere, and thus has the form

$$\mathbf{u} = \alpha\frac{\hat{\mathbf{r}}}{r^2} \tag{A.7}$$

where the strength of the source (α) is a constant to be determined. The no-slip boundary condition on the sphere surface implies that

$$\mathbf{u}(\mathbf{x}) = \frac{\mathrm{d}R}{\mathrm{d}t}\hat{\mathbf{r}}. \tag{A.8}$$

From (A.7, A.8) we find that $\alpha = \dot{R}R^2$, and therefore

$$\mathbf{u}\{\dot{R}\} = \dot{R}\Big(\frac{R}{r}\Big)^2\hat{\mathbf{r}}. \tag{A.9}$$

If we represent it in terms of the sphere volume $v = 4\pi R^3/3$ this reads

$$\mathbf{u}\{\dot{R}\} = \frac{\dot{v}}{4\pi r^2}\hat{\mathbf{r}} \tag{A.10}$$

This leads to the combined flow Eq. (3.16):

$$\mathbf{u}\big(\mathbf{r};\, R, \mathbf{F}, \dot{R}\big) = \frac{1}{24\pi\mu r}\Big[\big(3+\frac{R^2}{r^2}\big)\mathbf{F} + 3\big(1-\frac{R^2}{r^2}\big)\big(\mathbf{F}\cdot\widehat{\mathbf{r}}\big)\widehat{\mathbf{r}}\Big] + \dot{R}\Big(\frac{R}{r}\Big)^2\widehat{\mathbf{r}}.$$

B Accuracy of $U_i^{(e)}$ after incorporating the second reflection

Next we determine how a second reflection contributes to the rigid motions of two radially expanding spheres.

0th reflection We consider two spheres with radii $R_1(t)$ and $R_2(t)$ resp., centered at $\mathbf{x}_1(t)$ and $\mathbf{x}_2(t)$ so that $\mathbf{x}_2 - \mathbf{x}_1$ points in the $\mathbf{e}_x$ direction. The radial expansion of the ith sphere alone generates a flow

$$\mathbf{u}_i^{(0)}(\mathbf{x}) = R_i^2\dot{R}_i\frac{\mathbf{x}-\mathbf{x}_i}{|\mathbf{x}-\mathbf{x}_i|^3} \tag{B.1}$$

and the rigid motion of the sphere vanishes

$$\mathbf{U}_i^{(0)} = \mathbf{0}, \quad \omega_i^{(0)} = \mathbf{0}. \tag{B.2}$$

1**st Reflection.** Next we put sphere 1 into the flow $\mathbf{u}_2$ generated by the radially expanding sphere 2. We calculate the resulting *translational velocity* $\mathbf{U}_1^{(1)}$, *angular velocity* $\omega_1^{(1)}$, and the *stresslet* $\mathbf{S}_1^{(1)}$, from which we obtain the velocity field $\mathbf{u}_{21}(\mathbf{x})$.

Translational velocity $\mathbf{U}_1^{(1)}$.

$$\begin{aligned}\mathbf{U}_1^{(1)} &= \Big(1 + \frac{R_1^2}{6}\nabla^2\Big)\mathbf{u}_2^{(0)}\Big|_{\mathbf{x}=\mathbf{x}_1} = R_2^2\dot{R}_2\Big[\frac{\mathbf{x}_1 - \mathbf{x}_2}{|\mathbf{x}_1 - \mathbf{x}_2|^3} + \frac{R_1^2}{6}\nabla^2\Big(\frac{\mathbf{x} - \mathbf{x}_2}{|\mathbf{x} - \mathbf{x}_2|^3}\Big)\Big|_{\mathbf{x}=\mathbf{x}_1}\Big] \\ &= R_2^2\dot{R}_2\Big[-\frac{\mathbf{e}_z}{l^2} + \frac{R_1^2}{6}\nabla^2\Big(\frac{\mathbf{x} - \mathbf{x}_2}{|\mathbf{x} - \mathbf{x}_2|^3}\Big)\Big|_{\mathbf{x}=\mathbf{x}_1}\Big]\end{aligned}$$

Letting $\mathbf{r} = \mathbf{x} - \mathbf{x}_2$ and $r = |\mathbf{r}|$, we must calculate

$$\nabla^2\Big(\frac{\mathbf{r}}{r^3}\Big) = \partial_k\partial_k\frac{r_i}{r^3}$$

Since

$$\partial_k\Big(\frac{1}{r^n}\Big) = -\frac{nr_k}{r^{n+2}}$$

we have

$$\begin{aligned}\partial_k\Big(\frac{r_i}{r^3}\Big) &= \frac{\delta_{ik}}{r^3} - \frac{3r_ir_k}{r^5} \\ \partial_k\partial_k\Big(\frac{r_i}{r^3}\Big) &= -\frac{3\delta_{ik}r_k}{r^5} - \frac{3\delta_{ik}r_k}{r^5} - \frac{3r_i\partial_k r_k}{r^5} + \frac{15r_ir_kr_k}{r^7} = 0.\end{aligned}$$

Thus

$$\nabla^2\Big(\frac{\mathbf{r}}{r^3}\Big) = \mathbf{0}$$

and

$$\mathbf{U}_1^{(1)} = -\frac{R_2^2\dot{R}_2}{l^2}\mathbf{e}_x \tag{B.3}$$

Angular velocity $\omega_1^{(1)}$.

$$\omega_1^{(1)} = \frac{1}{2}\nabla\times\mathbf{u}_2^{(0)}\Big|_{\mathbf{x}=\mathbf{x}_1} = \mathbf{0} \tag{B.4}$$

Stresslet $\mathbf{S}_1^{(1)}$. The rate of deformation that results from $\mathbf{u}_2$ is

$$\begin{aligned}\mathbf{E}_2^{(0)} &= \frac{1}{2}\Big[\nabla\mathbf{u}_2^{(0)} + \big(\nabla\mathbf{u}_2^{(0)}\big)^T\Big] - \frac{1}{3}\mathbf{I}\Big(\nabla\cdot\mathbf{u}_2^{(0)}\Big)\\ &= \dot{R}_2 R_2^2\Big[\frac{1}{2}\Big(\nabla\frac{\hat{\mathbf{r}}}{r^2} + \big(\nabla\frac{\hat{\mathbf{r}}}{r^2}\big)^T\Big) - \frac{1}{3}\mathbf{I}\Big(\nabla\cdot\frac{\hat{\mathbf{r}}}{r^2}\Big)\Big]\end{aligned}$$

where $\hat{\mathbf{r}} = \mathbf{r}/r$. Using spherical coordinates, we have

$$\begin{aligned}\nabla\frac{\hat{\mathbf{r}}}{r^2} &= \Big(\hat{\mathbf{r}}\frac{\partial}{\partial r} + \frac{1}{r}\hat{\theta}\frac{\partial}{\partial\theta} + \frac{1}{r\sin\theta}\hat{\phi}\frac{\partial}{\partial\phi}\Big)\Big(\frac{\hat{\mathbf{r}}}{r^2}\Big) = \Big(\frac{\partial}{\partial r}\frac{1}{r^2}\Big)\hat{\mathbf{r}}\hat{\mathbf{r}} = -\frac{2}{r^3}\hat{\mathbf{r}}\hat{\mathbf{r}}\\ \nabla\cdot\frac{\hat{\mathbf{r}}}{r^2} &= \frac{\partial}{\partial r}\frac{1}{r^2} + \frac{2}{r}\frac{1}{r^2} = 0.\end{aligned}$$

Thus

$$\mathbf{E}_2^{(0)} = -\frac{2R_2^2\dot{R}_2}{r^3}\hat{\mathbf{r}}\hat{\mathbf{r}} = -\frac{2R_2^2\dot{R}_2}{r^5}\mathbf{r}\mathbf{r}, \tag{B.5}$$

and the stresslet is given by

$$\begin{aligned}\mathbf{S}_1^{(1)} &= \frac{20}{3}\pi\mu R_1^3\Big(1 + \frac{R_1^2}{10}\nabla^2\Big)\mathbf{E}_2^{(0)}\Big|_{\mathbf{x}=\mathbf{x}_1}\\ &= -\frac{40}{3}\pi\mu R_1^3 R_2^2\dot{R}_2\Big[\frac{\mathbf{e}_x\mathbf{e}_x}{l^3} + \frac{R_1^2}{10}\nabla^2\Big(\frac{\mathbf{r}\mathbf{r}}{r^5}\Big)\Big|_{\mathbf{x}=\mathbf{x}_1}\Big]\end{aligned}$$

We need to calculate

$$\begin{aligned}\nabla^2\Big(\frac{\mathbf{r}\mathbf{r}}{r^5}\Big) &= \partial_k\partial_k\Big(\frac{r_i r_j}{r^5}\Big)\\ \partial_k\Big(\frac{r_i r_j}{r^5}\Big) &= \frac{\delta_{ik}r_j}{r^5} + \frac{\delta_{jk}r_i}{r^5} - \frac{5r_i r_j r_k}{r^7}\\ \partial_k\partial_k\Big(\frac{r_i r_j}{r^5}\Big) &= \Big(\frac{\delta_{ik}\delta_{jk}}{r^5} - \frac{5\delta_{ik}r_j r_k}{r^7}\Big) + \Big(\frac{\delta_{jk}\delta_{ik}}{r^5} - \frac{5\delta_{jk}r_i r_k}{r^7}\Big)\\ &\quad + \Big(-\frac{5\delta_{ik}r_j r_k}{r^7} - \frac{5\delta_{jk}r_i r_k}{r^7} - \frac{5r_i r_j\partial_k r_k}{r^7} + \frac{35r_i r_j r_k r_k}{r^9}\Big) = \frac{2\delta_{ij}}{r^5}\end{aligned}$$

Thus

$$\mathbf{S}_1^{(1)} = -\frac{40}{3}\pi\mu R_1^3 R_2^2\dot{R}_2\Big[\frac{\mathbf{e}_x\mathbf{e}_x}{l^3} + \frac{R_1^2}{5l^5}\mathbf{I}\Big] \tag{B.6}$$

Finally, the velocity field $\mathbf{u}_{21}^{(1)}(\mathbf{x})$ is given by

$$\mathbf{u}_{21}^{(1)}(\mathbf{x}) = \Big(\mathbf{S}_1^{(1)}\cdot\nabla\Big)\cdot\frac{\mathbf{G}(\mathbf{x}-\mathbf{x_1})}{8\pi\mu} + \cdots \tag{B.7}$$

From Eqs. (B.6, A.2) we have that near $\mathbf{x}_1$,

$$\mathbf{S}_1^{(1)} \sim O\Big(\frac{1}{l^3}\Big), \quad \mathbf{G} \sim O\Big(\frac{1}{l}\Big)$$

and thus the velocity near $\mathbf{x}_1$ scales as $\mathbf{u}_{21}^{(1)} \sim O(l^{-5})$.

2nd Reflection. Now we reflect once again and consider sphere 1 immersed in the flow $\mathbf{u}_{12}^{(1)}$. The translational velocity $\mathbf{U}_1^{(2)}$ that results is given by

$$\mathbf{U}_1^{(2)} = \Big(1 + \frac{R_1^2}{6}\nabla^2\Big)\mathbf{u}_{12}^{(1)}\Big|_{\mathbf{x}=\mathbf{x}_1} \tag{B.8}$$

From the discussion of the first reflection we know that near $\mathbf{x}_1$ the velocity field $\mathbf{u}_{12}^{(1)}$ is $O(l^{-5})$, and thus $\mathbf{U}_1^{(2)} \sim O(l^{-5})$ as well.

C Extended analysis and computation of a PMPY of small separation.

C.1 Results with the second reflection involved and accurate up to $O(\delta^5)$.

From Sect. 3.2, the translational velocities of the spheres after two reflections can be approximated as:

$$U_1 = \frac{F_1}{6\pi\mu R_1}\Big(1 - \frac{15R_1R_2^3}{4l^4}\Big) + \frac{F_2}{4\pi\mu l}\Big(1 - \frac{R_1^2+R_2^2}{3l^2}\Big) - \dot{R}_2\Big(\frac{R_2}{l}\Big)^2 + O\Big(\frac{1}{l^5}\Big)$$
$$U_2 = \frac{F_2}{6\pi\mu R_2}\Big(1 - \frac{15R_1^3R_2}{4l^4}\Big) + \frac{F_1}{4\pi\mu l}\Big(1 - \frac{R_1^2+R_2^2}{3l^2}\Big) + \dot{R}_1\Big(\frac{R_1}{l}\Big)^2 + O\Big(\frac{1}{l^5}\Big)$$

After non-dimensionalization, they read:

$$U_1 = \frac{F_1}{R_1}\Big(1 - \frac{15R_1R_2^3}{4l^4}\delta^4\Big) + \frac{3F_2}{2l}\delta\Big(1 - \frac{R_1^2+R_2^2}{3l^2}\delta^2\Big) - \delta^2\Big(\frac{R_2}{l}\Big)^2\zeta_2 + O(\delta^5)$$
$$U_2 = \frac{F_2}{R_2}\Big(1 - \frac{15R_1^3R_2}{4l^4}\delta^4\Big) + \frac{3F_1}{2l}\delta\Big(1 - \frac{R_1^2+R_2^2}{3l^2}\delta^2\Big) + \delta^2\Big(\frac{R_1}{l}\Big)^2\zeta_1 + O(\delta^5)$$

and the coefficient matrix in the system Eq. (3.24) becomes

$$\begin{pmatrix} -1 & 0 & \alpha_1 & \Gamma \\ 0 & -1 & \Gamma & \alpha_2 \\ 1 & -1 & 0 & 0 \\ 0 & 0 & 1 & 1 \end{pmatrix} \tag{B.1}$$

where

$$\alpha_1 = \frac{1}{R_1}\Big(1 - \frac{15R_1R_2^3}{4l^4}\delta^4\Big),$$

$$\alpha_2 = \frac{1}{R_2}\Big(1 - \frac{15R_1^3R_2}{4l^4}\delta^4\Big),$$
$$\Gamma = \delta\frac{3}{2l}\Big(1 - \frac{R_1^2 + R_2^2}{3l^2}\delta^2\Big)$$

We consider the stroke in Eq. (3.35) again, but with solution obtained with the first reflection [Eq. (3.24), Fig. 4 black dots] or with both the first and the leading order term from second reflections [Eq. (3.24) with coefficient matrix in Eq. (B.1), Fig. 4 green crosses]—the former is truncated from the δ^4 term while the latter is from the δ^5 term. For small separation of the PMPY with $l_0 = 7$, $\delta = 0.54$, simulation of the scaled translation and power are shown in Fig. 4, from which we see them match well. For this system, the first reflection is correct to $O(\delta^4)$ where $\delta^4 \sim 8.5E-2$, while with the leading order term from the second reflection included, it is correct to $O(\delta^5)$ where $\delta^5 \sim 4.6E-2$. However, in the simulation, the difference between the net translation after one cycle ($X(1)$) obtained by the two approximations is:

$$|X_{1\text{stRef}}(1) - X_{2\text{ndRef}}(1)| \sim 8.9E-3$$

When comparing with δ, this difference gives the estimation of

$$|X_{1\text{stRef}}(1) - X_{2\text{ndRef}}(1)| \sim \delta^{7.7}$$

This implies that with δ as large as 0.54, the solution obtained from the first reflection is accurate to the order of $O(10^{-3})$ which approximates $O(\delta^{7.7})$.

C.2 Comparing the contributions of P_D and P_V to the power P.

As is discussed in Sect. 3.3, the power expended to propel a PMPY consists of two parts: P_D that results from the drag force on the spheres, and P_V that results from the radial expansion of the spheres. In addition, Eq. (3.31) shows that the higher-order corrections to P only exists in P_D. We repeat the simulations in Fig. 3 with different values of l_0 and show the results for P_D and P_V in Fig. 17, where P_D and P_V calculated by the first reflection are shown by green and blue solid lines, resp., and P_D calculated by Avron's asymptotic approximation is shown by black dots.

D Calculation of $\boldsymbol{\Omega}_{3,i}^{(1)}$

The angular velocity of sphere 3 (i.e., the free-floating sphere) $\boldsymbol{\Omega}_{3,i}^{(1)}$ consists of two parts: $\boldsymbol{\Omega}_{3,i}^{(1,f)}$ that results from the drag force on sphere i, and $\boldsymbol{\Omega}_{3,i}^{(1,e)}$ that results from the expansion of sphere i. Here we calculate them separately.

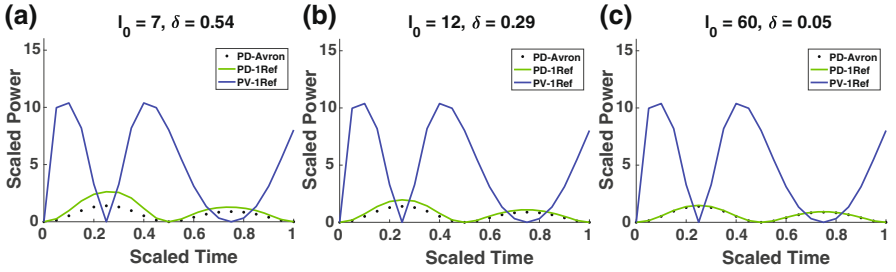

Fig. 17 Comparing the contributions of P_D and P_V to the power P. Simulations are set up the same as in Fig. 3, with $l_0 = 7, 12, 60\,\mu$m (color figure online)

First, $\boldsymbol{\Omega}_{3,i}^{(1,e)}$, which results from the flow generated by the expansion of sphere i is:

$$\mathbf{u}_i^{(0,e)} = R_i^2 \dot{R}_i \frac{\mathbf{x} - \mathbf{x}_i}{|\mathbf{x} - \mathbf{x}_i|^3},$$

and therefore

$$\boldsymbol{\Omega}_{3,i}^{(1,e)} = \frac{1}{2}\nabla \times \mathbf{u}_i^{(e)}\Big|_{\mathbf{x}=\mathbf{x}_3} = \frac{R_i^2 \dot{R}_i}{2}\nabla \times \left(\frac{\mathbf{x} - \mathbf{x}_i}{|\mathbf{x} - \mathbf{x}_i|^3}\right)\Big|_{\mathbf{x}=\mathbf{x}_3}. \tag{D.1}$$

Let $\mathbf{r} = \mathbf{x} - \mathbf{x}_i$ and $r = |\mathbf{x} - \mathbf{x}_i|$, then the antisymmetric part in Eq. (D.1) is

$$\partial_j\left(\frac{r_k}{r^3}\right) - \partial_k\left(\frac{r_j}{r^3}\right) = \left(\frac{\delta_{jk}}{r^3} - \frac{3r_j r_k}{r^5}\right) - \left(\frac{\delta_{kj}}{r^3} - \frac{3r_k r_j}{r^5}\right) = 0$$

and therefore $\boldsymbol{\Omega}_{3,i}^{(1,e)} = 0$.

Next, $\boldsymbol{\Omega}_{3,i}^{(1,f)}$, which results from the flow generated by the drag force $\mathbf{F}_i = F_i \mathbf{e}_x$ on sphere i, is given by

$$\begin{aligned}
\boldsymbol{\Omega}_{3,i}^{(1,f)} &= \frac{1}{2}\nabla \times \mathbf{u}\{\mathbf{F}_i\}\Big|_{\mathbf{x}=\mathbf{x}_3} \\
&= \frac{1}{16\pi\mu}\nabla \times \left[\left(\frac{1}{r} + \frac{1}{3r^3}\right)F_i\mathbf{e}_x + \left(\frac{1}{r} - \frac{1}{r^3}\right)(F_i\mathbf{e}_x \cdot \frac{\mathbf{r}}{r})\frac{\mathbf{r}}{r}\right]\Big|_{\mathbf{x}=\mathbf{x}_3} \\
&= \frac{F_i}{16\pi\mu}\nabla \times \left[\left(\frac{1}{r} + \frac{1}{3r^3}\right)\mathbf{e}_x + \left(\frac{1}{r} - \frac{1}{r^3}\right)\frac{r_x\mathbf{r}}{r^2}\right].
\end{aligned}$$

Since

$$\begin{aligned}
\nabla \times \left(\frac{1}{r^n}\mathbf{e}_x\right) &= -\frac{nr_z}{r^{n+2}}\mathbf{e}_y + \frac{nr_y}{r^{n+2}}\mathbf{e}_z \\
\nabla \times \left(\frac{r_x}{r^n}\mathbf{r}\right) &= -\frac{r_z}{r^n}\mathbf{e}_y + \frac{r_y}{r^n}\mathbf{e}_z
\end{aligned}$$

we have

$$\boldsymbol{\Omega}_{3,i}^{(1,f)} = \frac{F_i}{8\pi\mu r^3}\Big[-r_z\mathbf{e}_y + r_y\mathbf{e}_z\Big]\Big|_{\mathbf{r}=\mathbf{x}_3-\mathbf{x}_i} = \frac{F_i}{8\pi\mu l_{i3}^3}\big(\mathbf{x}_3-\mathbf{x}_i\big)_y\mathbf{e}_z \tag{D.2}$$

and therefore

$$\boldsymbol{\Omega}_3^{(1)} = \sum_{i=1,2}\boldsymbol{\Omega}_{3,i}^{(1,f)} + \boldsymbol{\Omega}_{3,i}^{(1,e)} = \sum_{i=1,2}\frac{F_i}{8\pi\mu l_{i3}^3}\big(\mathbf{x}_3-\mathbf{x}_i\big)_y\mathbf{e}_z. \tag{D.3}$$

E Numerical scheme of two PMPY models

The following numerical scheme is written in terms of unscaled variables.

When the two PMPY models both lie along the x-axis, and the spheres are numbered 1, 2, 3, 4 from the negative to the positive x-direction, the Eqs. (5.1–5.9) reduce to

$$\begin{pmatrix} A_{11} & A_{12} \\ A_{21} & A_{22} \end{pmatrix}\begin{pmatrix} \mathbf{U} \\ \mathbf{F} \end{pmatrix} = \begin{pmatrix} \mathbf{B}_1 \\ \mathbf{B}_2 \end{pmatrix} \tag{E.1}$$

where

$$\mathbf{U} = \begin{pmatrix} U_1 \\ U_2 \\ U_3 \\ U_4 \end{pmatrix}, \quad \mathbf{F} = \mu^{-1}\begin{pmatrix} F_1 \\ F_2 \\ F_3 \\ F_4 \end{pmatrix}.$$

Here $A_{11} = -I_4$, where I_4 is the 4×4 identity matrix, $A_{12} = (a_{ij})$ is a symmetric 4×4 matrix, with

$$a_{ii} = \frac{1}{6\pi R_i}, \quad a_{ij} = \frac{1}{4\pi l_{ij}}\Big(1 - \frac{R_i^2+R_j^2}{3l_{ij}^2}\Big) \tag{E.2}$$

and

$$\big(A_{21}\ A_{22}\big) = \begin{pmatrix} 1 & -1 & 0 & 0 & 0 & 0 & 0 & 0 \\ 0 & 0 & 1 & -1 & 0 & 0 & 0 & 0 \\ 0 & 0 & 0 & 0 & 1 & 1 & 0 & 0 \\ 0 & 0 & 0 & 0 & 0 & 0 & 1 & 1 \end{pmatrix}.$$

$\mathbf{B}_1 \in \mathbb{R}^4$, is given by

$$(\mathbf{B}_1)_i = -\sum_{j\neq i}\operatorname{sign}(i-j)\dot{R}_j\Big(\frac{R_j}{l_{ij}}\Big)^2$$

and

$$\mathbf{B}_2 = \begin{pmatrix} -\dot{l}_{12} \\ -\dot{l}_{34} \\ 0 \\ 0 \end{pmatrix}.$$

With the second reflection considered, the leading term in $\mathbf{U}_i^{(2)}$ is of order δ^4, which results from the drag forces and can be computed from the following equations:

$$\mathbf{U}_i^{(2,f)} = \Big(1 + \frac{R_i^2}{6}\Big)\nabla^2 \sum_{j,k}^{k\neq i,j} \mathbf{u}_{jk}^{(1)}\Big|_{\mathbf{x}=\mathbf{x}_i}$$

where

$$\mathbf{u}_{jk}^{(1)} = \big(\mathbf{S}_{k,j}^{(1)} \cdot \nabla\big) \cdot \frac{\mathbf{G}(\mathbf{x}-\mathbf{x}_k)}{8\pi\mu} + \cdots$$

and the stresslet $\mathbf{S}_{k,j}^{(1)}$ is

$$\mathbf{S}_{k,j}^{(1)} = \frac{20}{3}\pi\mu R_k^3\big(1 + \frac{R_k^2}{10}\nabla^2\big)\mathbf{E}_j^{(0)}\Big|_{\mathbf{x}=\mathbf{x}_k}$$

where $\mathbf{E}_j^{(0)}$ is the rate of deformation resulting from $\mathbf{u}_j$.

To compute $\mathbf{U}_i^{(2,f)}$, we follow the computation framework provided in (Kim and Karrila 1991), with the algebra reduced from the system geometry. First we have

$$\begin{aligned}\mathbf{S}_{k,j}^{(1)} = &\Big[-\frac{5}{2}\frac{R_k^3}{l_{kj}^2} + \frac{3}{2}\frac{R_k^5}{l_{kj}^4}\Big(1 + \frac{5}{3}\frac{R_j^2}{R_k^2}\Big)\Big]\big(\mathbf{d}_{jk}\mathbf{d}_{jk} - \frac{1}{3}\mathbf{I}\big)\mathbf{d}_{jk}\cdot\mathbf{F}_j \\ &- \frac{1}{2}\frac{R_k^5}{l_{kj}^4}\Big(1 + \frac{5}{3}\frac{R_j^2}{R_k^2}\Big)\Big(\mathbf{F}_j\mathbf{d}_{jk} + \mathbf{d}_{jk}\mathbf{F}_j - 2\mathbf{d}_{jk}\mathbf{d}_{jk}\mathbf{d}_{jk}\cdot\mathbf{F}_j\Big)\end{aligned}$$

where

$$\mathbf{d}_{jk} = \frac{\mathbf{x}_k - \mathbf{x}_j}{l_{kj}} = \mathrm{sign}(k-j)\mathbf{e}_x, \quad \mathbf{F}_j = F_j\mathbf{e}_x$$

thus

$$\mathbf{S}_{k,j}^{(1)} = F_j\,\mathrm{sign}(k-j)\Big[-\frac{5}{2}\frac{R_k^3}{l_{kj}^2} + \frac{3}{2}\frac{R_k^5}{l_{kj}^4}\Big(1 + \frac{5}{3}\frac{R_j^2}{R_k^2}\Big)\Big]\big(\mathbf{e}_x\mathbf{e}_x - \frac{1}{3}\mathbf{I}\big)$$

Let

$$\Lambda_{k,j} = \mathrm{sign}(k-j)\Big[-\frac{5}{2}\frac{R_k^3}{l_{kj}^2} + \frac{3}{2}\frac{R_k^5}{l_{kj}^4}\Big(1+\frac{5}{3}\frac{R_j^2}{R_k^2}\Big)\Big]$$

after some direct calculation, we obtain

$$\mathbf{u}_{jk}^{(1)} = \Big[F_j\Lambda_{k,j}\Big(\mathbf{e}_x\mathbf{e}_x - \frac{1}{3}\mathbf{I}\Big)\cdot\nabla\Big]\cdot\frac{\mathbf{G}(\mathbf{x}-\mathbf{x}_k)}{8\pi\mu} = \frac{F_j\Lambda_{k,j}}{8\pi\mu}\Big(\frac{\mathbf{r}}{r^3} - \frac{3r_x^2}{r^5}\mathbf{r}\Big)$$

thus

$$\begin{aligned}
&\Big(1+\frac{R_i^2}{6}\Big)\nabla^2\mathbf{u}_{jk}^{(1)}\Big|_{\mathbf{x}=\mathbf{x}_i}\\
&= \frac{F_j\Lambda_{k,j}}{8\pi\mu}\Big[\frac{\mathbf{x}_i-\mathbf{x}_k}{|\mathbf{x}_i-\mathbf{x}_k|^3} - \frac{3\big((\mathbf{x}_i-\mathbf{x}_k)\cdot\mathbf{e}_x\big)^2}{|\mathbf{x}_i-\mathbf{x}_k|^5}(\mathbf{x}_i-\mathbf{x}_k) + \frac{R_i^2}{6}\nabla^2\Big(\frac{\mathbf{r}}{r^3} - \frac{3r_x^2}{r^5}\mathbf{r}\Big)\Big|_{\mathbf{x}=\mathbf{x}_i}\Big]\\
&\sim \frac{F_j}{8\pi\mu}\mathrm{sign}(k-j)\Big(-\frac{5}{2}\frac{R_k^3}{l_{kj}^2} + O\Big(\frac{1}{l_{kj}^4}\Big)\Big)\Big(-\frac{2\mathrm{sign}(i-k)}{l_{ik}^2}\mathbf{e}_x + O\Big(\frac{1}{l_{ik}^4}\Big)\Big)\\
&= \frac{F_j}{8\pi\mu}\mathrm{sign}(k-j)\mathrm{sign}(i-k)\frac{5R_k^3}{l_{kj}^2 l_{ik}^2}\mathbf{e}_x + O\Big(\frac{1}{l^6}\Big)
\end{aligned}$$

Finally we get

$$\begin{aligned}
\mathbf{U}_i^{(2,f)} &= \Big(1+\frac{R_i^2}{6}\Big)\nabla^2\sum_{j,k}^{k\neq i,j}\mathbf{u}_{jk}^{(1)}\Big|_{\mathbf{x}=\mathbf{x}_i}\\
&= \sum_j\frac{F_j}{8\pi\mu}\sum_{k\neq i,j}\mathrm{sign}(k-j)\mathrm{sign}(i-k)\frac{5R_k^3}{l_{kj}^2 l_{ik}^2}\mathbf{e}_x + O\Big(\frac{1}{l^6}\Big)
\end{aligned}$$

after non-dimensionalization, it gives

$$\begin{aligned}
\mathbf{U}_i^{(2,f)} &= \Big(1+\frac{R_i^2}{6}\Big)\nabla^2\sum_{j,k}^{k\neq i,j}\mathbf{u}_{jk}^{(1)}\Big|_{\mathbf{x}=\mathbf{x}_i}\\
&= \sum_j\frac{15}{4}F_j\delta^4\sum_{k\neq i,j}\mathrm{sign}(k-j)\mathrm{sign}(i-k)\frac{R_k^3}{l_{kj}^2 l_{ik}^2}\mathbf{e}_x + O\big(\delta^6\big)
\end{aligned}$$

Our analysis in Appendix B shows that $\mathbf{U}_i^{(2,e)} \sim O(\delta^5)$, therefore

$$\mathbf{U}_i^{(2)} = \sum_j\frac{15}{4}F_j\delta^4\sum_{k\neq i,j}\mathrm{sign}(k-j)\mathrm{sign}(i-k)\frac{R_k^3}{l_{kj}^2 l_{ik}^2}\mathbf{e}_x + O\big(\delta^5\big)$$

With the leading terms from the second reflection added to the system, the algorithm given at the beginning of this part is modified as $A_{12} = (a_{ij} + \widetilde{a}_{ij})$, where a_{ij} is given by Eq. (E.2) and

$$\widetilde{a}_{ij} = \frac{5}{8\pi} \sum_{k \neq i,j} \text{sign}(k-j)\text{sign}(i-k) \frac{R_k^3}{l_{kj}^2 l_{ik}^2}$$

F Asymptotic analysis of the three systems consisting of two hobbled PMPYs

For simplicity, we denote the distance between any two spheres i and j by l_{ij}. For example, $l_{13} = l_{12} + l_{23}$.

F.1 System A (two dumb-bells) with controls in $(\dot{l}_I, \dot{l}_{II})$

The asymptotic behavior of the velocity of the spheres is

$$\begin{aligned}
U_1 &\sim \frac{F_1}{6\pi\mu R_1} + \frac{F_2}{4\pi\mu l_{12}} + \frac{F_3}{4\pi\mu l_{13}} + \frac{F_4}{4\pi\mu l_{14}} \\
U_2 &\sim \frac{F_1}{4\pi\mu l_{12}} + \frac{F_2}{6\pi\mu R_2} + \frac{F_3}{4\pi\mu l_{23}} + \frac{F_4}{4\pi\mu l_{24}} \\
U_3 &\sim \frac{F_1}{4\pi\mu l_{13}} + \frac{F_2}{4\pi\mu l_{23}} + \frac{F_3}{6\pi\mu R_3} + \frac{F_4}{4\pi\mu l_{34}} \\
U_4 &\sim \frac{F_1}{4\pi\mu l_{14}} + \frac{F_2}{4\pi\mu l_{24}} + \frac{F_3}{4\pi\mu l_{34}} + \frac{F_4}{6\pi\mu R_4}
\end{aligned}$$

with relations and constraints

$$\begin{aligned}
&U_2 - U_1 = \dot{l}_{12} = \xi_I, \quad U_4 - U_3 = \dot{l}_{34} = \xi_{II} \\
&F_1 + F_2 = 0, \quad F_3 + F_4 = 0.
\end{aligned}$$

After scaling with hat notation omitted, the system becomes

$$\begin{aligned}
U_1 &\sim \frac{F_1}{R_1} + \frac{3}{2}\left[\frac{F_2}{l_{12}} + \frac{F_3}{l_{13}} + \frac{F_4}{l_{14}}\right]\delta \\
U_2 &\sim \frac{F_2}{R_2} + \frac{3}{2}\left[\frac{F_1}{l_{12}} + \frac{F_3}{l_{23}} + \frac{F_4}{l_{24}}\right]\delta \\
U_3 &\sim \frac{F_3}{R_3} + \frac{3}{2}\left[\frac{F_1}{l_{13}} + \frac{F_2}{l_{23}} + \frac{F_4}{l_{34}}\right]\delta \\
U_4 &\sim \frac{F_4}{R_4} + \frac{3}{2}\left[\frac{F_1}{l_{14}} + \frac{F_2}{l_{24}} + \frac{F_3}{l_{34}}\right]\delta \\
U_2 - U_1 &= \dot{l}_{12} = \xi_I, \quad U_4 - U_3 = \dot{l}_{34} = \xi_{II} \\
F_1 + F_2 &= 0, \quad F_3 + F_4 = 0.
\end{aligned}$$

With $F_2 = -F_1,\ F_4 = -F_3$, the system is simplified to

$$\begin{aligned}
U_1 &\sim F_1\Big(\frac{1}{R_1} - \frac{3\delta}{2l_{12}}\Big) + \frac{3}{2}F_3\delta\Big(\frac{1}{l_{13}} - \frac{1}{l_{14}}\Big)\\
U_2 &\sim F_1\Big(\frac{3\delta}{2l_{12}} - \frac{1}{R_2}\Big) + \frac{3}{2}F_3\delta\Big(\frac{1}{l_{23}} - \frac{1}{l_{24}}\Big)\\
U_3 &\sim \frac{3}{2}F_1\delta\Big(\frac{1}{l_{13}} - \frac{1}{l_{23}}\Big) + F_3\Big(\frac{1}{R_3} - \frac{3\delta}{2l_{34}}\Big)\\
U_4 &\sim \frac{3}{2}F_1\delta\Big(\frac{1}{l_{14}} - \frac{1}{l_{24}}\Big) + F_3\Big(\frac{3\delta}{2l_{34}} - \frac{1}{R_3}\Big).
\end{aligned}$$

When $R_1 = R_2 = R_3 = R_4 = R$,

$$\begin{aligned}
\xi_I = U_2 - U_1 \sim -F_1\Big(\frac{1}{R_1} + \frac{1}{R_2}\Big) \quad &\Rightarrow \quad F_1 = -\frac{R}{2}\xi_I\\
\xi_{II} = U_4 - U_3 \sim -F_3\Big(\frac{1}{R_3} + \frac{1}{R_4}\Big) \quad &\Rightarrow \quad F_3 = -\frac{R}{2}\xi_{II}.
\end{aligned}$$

Velocities of the PMPYs:

$$\begin{aligned}
\overline{U}_I &= \frac{1}{2}\big(U_1 + U_2\big) = \frac{1}{2}F_1\Big(\frac{1}{R_1} - \frac{1}{R_2}\Big) + \frac{3}{4}F_3\delta\Big(\frac{1}{l_{13}} - \frac{1}{l_{14}} + \frac{1}{l_{23}} - \frac{1}{l_{24}}\Big)\\
&\sim -\frac{3}{8}R\xi_{II}\delta\Big(\frac{1}{l_{13}} - \frac{1}{l_{14}} + \frac{1}{l_{23}} - \frac{1}{l_{24}}\Big)\\
\overline{U}_{II} &= \frac{1}{2}\big(U_3 + U_4\big) = \frac{3}{4}F_1\delta\Big(\frac{1}{l_{13}} - \frac{1}{l_{23}} + \frac{1}{l_{14}} - \frac{1}{l_{24}}\Big) + \frac{1}{2}F_1\Big(\frac{1}{R_3} - \frac{1}{R_4}\Big)\\
&\sim -\frac{3}{8}R\xi_I\delta\Big(\frac{1}{l_{13}} - \frac{1}{l_{23}} + \frac{1}{l_{14}} - \frac{1}{l_{24}}\Big)
\end{aligned}$$

Power of the PMPYs:

$$\begin{aligned}
P_I &= F_1U_1 + F_2U_2 = F_1\big(U_1 - U_2\big) = -F_1\xi_I = \frac{R}{2}\xi_I^2\\
P_{II} &= F_3U_3 + F_4U_4 = F_3\big(U_3 - U_4\big) = -F_3\xi_{II} = \frac{R}{2}\xi_{II}^2
\end{aligned}$$

However, we observe that although $\overline{U}_I, \overline{U}_{II}$ scale like $O(\delta)$, the net translations X_I, X_{II} do not. Without loss of generality, we consider the first integral term in X_I:

$$\int \overline{U}_I dt = -\frac{3}{8}R\delta\int_0^1 \frac{\xi_{II}(t)}{l_{13}(t)}dt$$

l_{13} can be written as $l_{13} = l_{12} + l_{23} = 2 + \Delta l_{12} + \Delta l_{23}$, where $\Delta l_{12}, \Delta l_{23} \sim O(\delta)$, thus

$$\frac{1}{l_{13}} = \frac{1}{2 + \Delta l_{12} + \Delta l_{23}} = \frac{1}{2} - \frac{\Delta l_{12} + \Delta l_{23}}{4} + O(\delta^2)$$

and

$$-\frac{3}{8}R\delta\int_0^1\frac{\xi_{II}(t)}{l_{13}(t)}dt=-\frac{3}{8}R\delta\int_0^1\xi_{II}\Big(\frac{1}{2}-\frac{\Delta l_{12}+\Delta l_{23}}{4}\Big)dt+O(\delta^3)$$
$$=-\frac{3}{16}R\delta\int_0^1\xi_{II}dt+\frac{3}{32}R\delta\int_0^1\xi_{II}(\Delta l_{12}+\Delta l_{23})dt+O(\delta^3).$$

The first integral vanishes since it is path-independent, the second one is an $O(\delta^2)$ term, hence

$$-\frac{3}{8}R\delta\int_0^1\frac{\xi_{II}(t)}{l_{13}(t)}dt\sim O(\delta^2).$$

A similar argument applies to all other integrals in X_I, X_{II}, thus at most X_I, $X_{II}\sim O(\delta^2)$.

When the radii are not all equal, the leading order term of $\overline{U}_I$, $\overline{U}_{II}$ scales as $O(1)$, but this does not contribute to the net translations and we still have X_I, $X_{II}\sim O(\delta^2)$. This is because the leading order terms are of the form $\Phi\xi(t)$, where the coefficient Φ depends on the radii only, thus $\int\Phi\xi dt$ is again path-independent. Also in this case, the $O(\delta)$ terms in $\overline{U}_I$, $\overline{U}_{II}$ become more complicated, but they are still of the form $\Phi\xi/l_{ij}$, where Φ depends on the radii only, and the same argument above applies, thus in the end we have X_I, $X_{II}\sim O(\delta^2)$.

F.2 System B with controls in $(\dot{R}_1, \dot{R}_3)$

The asymptotic behavior of the velocity of each sphere is

$$U_1\sim\frac{F_1}{6\pi\mu R_1}+\Big[\frac{F_2}{4\pi\mu l_{12}}-\Big(\frac{R_2}{l_{12}}\Big)^2\dot{R}_2\Big]+\Big[\frac{F_3}{4\pi\mu l_{13}}-\Big(\frac{R_3}{l_{13}}\Big)^2\dot{R}_3\Big]$$
$$+\Big[\frac{F_4}{4\pi\mu l_{14}}-\Big(\frac{R_4}{l_{14}}\Big)^2\dot{R}_4\Big]$$
$$U_2\sim\frac{F_2}{6\pi\mu R_2}+\Big[\frac{F_1}{4\pi\mu l_{12}}+\Big(\frac{R_1}{l_{12}}\Big)^2\dot{R}_1\Big]+\Big[\frac{F_3}{4\pi\mu l_{23}}-\Big(\frac{R_3}{l_{23}}\Big)^2\dot{R}_3\Big]$$
$$+\Big[\frac{F_4}{4\pi\mu l_{24}}-\Big(\frac{R_4}{l_{24}}\Big)^2\dot{R}_4\Big]$$
$$U_3\sim\frac{F_3}{6\pi\mu R_3}+\Big[\frac{F_1}{4\pi\mu l_{13}}+\Big(\frac{R_1}{l_{13}}\Big)^2\dot{R}_1\Big]+\Big[\frac{F_2}{4\pi\mu l_{23}}+\Big(\frac{R_2}{l_{23}}\Big)^2\dot{R}_2\Big]$$
$$+\Big[\frac{F_4}{4\pi\mu l_{34}}-\Big(\frac{R_4}{l_{34}}\Big)^2\dot{R}_4\Big]$$
$$U_4\sim\frac{F_4}{6\pi\mu R_4}+\Big[\frac{F_1}{4\pi\mu l_{14}}+\Big(\frac{R_1}{l_{14}}\Big)^2\dot{R}_1\Big]+\Big[\frac{F_2}{4\pi\mu l_{24}}+\Big(\frac{R_2}{l_{24}}\Big)^2\dot{R}_2\Big]$$
$$+\Big[\frac{F_3}{4\pi\mu l_{34}}+\Big(\frac{R_3}{l_{34}}\Big)^2\dot{R}_3\Big]$$

with relations

$$\begin{aligned} U_2 - U_1 = 0, \quad & U_4 - U_3 = 0 \\ F_1 + F_2 = 0, \quad & F_3 + F_4 = 0 \\ R_1^2\dot{R}_1 + R_2^2\dot{R}_2 = 0 \quad \Rightarrow \quad & R_2^2\zeta_2 = -R_1^2\zeta_1 \\ R_3^2\dot{R}_3 + R_4^2\dot{R}_4 = 0 \quad \Rightarrow \quad & R_4^2\zeta_4 = -R_3^2\zeta_3. \end{aligned}$$

After scaling with hat notation omitted

$$\begin{aligned} U_1 \sim\ & \frac{F_1}{R_1} + \Big[\frac{3F_2}{2l_{12}}\delta - \Big(\frac{R_2}{l_{12}}\Big)^2\zeta_2\delta^2\Big] + \Big[\frac{3F_3}{2l_{13}}\delta - \Big(\frac{R_3}{l_{13}}\Big)^2\zeta_3\delta^2\Big] \\ & + \Big[\frac{3F_4}{2l_{14}}\delta - \Big(\frac{R_4}{l_{14}}\Big)^2\zeta_4\delta^2\Big] \\ U_2 \sim\ & \frac{F_2}{R_2} + \Big[\frac{3F_1}{2l_{12}}\delta + \Big(\frac{R_1}{l_{12}}\Big)^2\zeta_1\delta^2\Big] + \Big[\frac{3F_3}{2l_{23}}\delta - \Big(\frac{R_3}{l_{23}}\Big)^2\zeta_3\delta^2\Big] \\ & + \Big[\frac{3F_4}{2l_{24}}\delta - \Big(\frac{R_4}{l_{24}}\Big)^2\zeta_4\delta^2\Big] \\ U_3 \sim\ & \frac{F_3}{R_3} + \Big[\frac{3F_1}{2l_{13}}\delta + \Big(\frac{R_1}{l_{13}}\Big)^2\zeta_1\delta^2\Big] + \Big[\frac{3F_2}{2l_{23}}\delta + \Big(\frac{R_3}{l_{23}}\Big)^2\zeta_2\delta^2\Big] \\ & + \Big[\frac{3F_4}{2l_{34}}\delta - \Big(\frac{R_4}{l_{34}}\Big)^2\zeta_4\delta^2\Big] \\ U_4 \sim\ & \frac{F_4}{R_4} + \Big[\frac{3F_1}{2l_{14}}\delta + \Big(\frac{R_1}{l_{14}}\Big)^2\zeta_1\delta^2\Big] + \Big[\frac{3F_2}{2l_{24}}\delta + \Big(\frac{R_3}{l_{24}}\Big)^2\zeta_2\delta^2\Big] \\ & + \Big[\frac{3F_3}{2l_{34}}\delta + \Big(\frac{R_3}{l_{34}}\Big)^2\zeta_3\delta^2\Big]. \end{aligned}$$

With $F_2 = -F_1,\ F_4 = -F_3$, the system becomes

$$\begin{aligned} U_1 \sim\ & F_1\Big(\frac{1}{R_1} - \frac{3\delta}{2l_{12}}\Big) + \frac{3F_3}{2}\delta\Big(\frac{1}{l_{13}} - \frac{1}{l_{14}}\Big) \\ & + \delta^2\Big[-\Big(\frac{R_2}{l_{12}}\Big)^2\zeta_2 - \Big(\frac{R_3}{l_{13}}\Big)^2\zeta_3 - \Big(\frac{R_4}{l_{14}}\Big)^2\zeta_4\Big] \\ U_2 \sim\ & F_1\Big(-\frac{1}{R_2} + \frac{3\delta}{2l_{12}}\Big) + \frac{3F_3}{2}\delta\Big(\frac{1}{l_{23}} - \frac{1}{l_{24}}\Big) \\ & + \delta^2\Big[\Big(\frac{R_1}{l_{12}}\Big)^2\zeta_1 - \Big(\frac{R_3}{l_{23}}\Big)^2\zeta_3 - \Big(\frac{R_4}{l_{24}}\Big)^2\zeta_4\Big] \\ U_3 \sim\ & \frac{3F_1}{2}\delta\Big(\frac{1}{l_{13}} - \frac{1}{l_{23}}\Big) + F_3\Big(\frac{1}{R_3} - \frac{3\delta}{2l_{34}}\Big) \\ & + \delta^2\Big[\Big(\frac{R_1}{l_{13}}\Big)^2\zeta_1 + \Big(\frac{R_2}{l_{23}}\Big)^2\zeta_2 - \Big(\frac{R_4}{l_{34}}\Big)^2\zeta_4\Big] \end{aligned}$$

$$U_4 \sim \frac{3F_1}{2}\delta\Big(\frac{1}{l_{14}} - \frac{1}{l_{24}}\Big) + F_3\Big(-\frac{1}{R_4} + \frac{3\delta}{2l_{34}}\Big) + \delta^2\Big[\Big(\frac{R_1}{l_{14}}\Big)^2\zeta_1 + \Big(\frac{R_2}{l_{24}}\Big)^2\zeta_2 + \Big(\frac{R_3}{l_{34}}\Big)^2\zeta_3\Big].$$

Expand F_1, F_3 as

$$F_1 = F_1^0 + \delta F_1^1 + \delta^2 F_1^2 + O(\delta^3), \quad F_3 = F_3^0 + \delta F_3^1 + \delta^2 F_3^2 + O(\delta^3);$$

then

$$\begin{aligned}
U_1 \sim\ & \frac{F_1^0}{R_1} + \delta\frac{F_1^1}{R_1} - \delta\frac{3F_1^0}{2l_{12}} + \delta^2\frac{F_1^2}{R_1} - \delta^2\frac{3F_1^1}{2l_{12}} + \frac{3}{2}\delta F_3^0\Big(\frac{1}{l_{13}} - \frac{1}{l_{14}}\Big) \\
& + \frac{3}{2}\delta^2 F_3^1\Big(\frac{1}{l_{13}} - \frac{1}{l_{14}}\Big) \\
& + \delta^2\Big[-\Big(\frac{R_2}{l_{12}}\Big)^2\zeta_2 - \Big(\frac{R_3}{l_{13}}\Big)^2\zeta_3 - \Big(\frac{R_4}{l_{14}}\Big)^2\zeta_4\Big] + O(\delta^3) \\
U_2 \sim\ & -\frac{F_1^0}{R_2} - \delta\frac{F_1^1}{R_2} + \delta\frac{3F_1^0}{2l_{12}} - \delta^2\frac{F_1^2}{R_2} + \delta^2\frac{3F_1^1}{2l_{12}} \\
& + \frac{3}{2}\delta F_3^0\Big(\frac{1}{l_{23}} - \frac{1}{l_{24}}\Big) + \frac{3}{2}\delta^2 F_3^1\Big(\frac{1}{l_{23}} - \frac{1}{l_{24}}\Big) \\
& + \delta^2\Big[\Big(\frac{R_1}{l_{12}}\Big)^2\zeta_1 - \Big(\frac{R_3}{l_{23}}\Big)^2\zeta_3 - \Big(\frac{R_4}{l_{24}}\Big)^2\zeta_4\Big] + O(\delta^3) \\
U_3 \sim\ & \frac{F_3^0}{R_3} + \delta\frac{F_3^1}{R_3} - \delta\frac{3F_3^0}{2l_{34}} + \delta^2\frac{F_3^2}{R_3} - \delta^2\frac{3F_3^1}{2l_{34}} \\
& + \frac{3}{2}\delta F_1^0\Big(\frac{1}{l_{13}} - \frac{1}{l_{23}}\Big) + \frac{3}{2}\delta^2 F_1^1\Big(\frac{1}{l_{13}} - \frac{1}{l_{23}}\Big) \\
& + \delta^2\Big[\Big(\frac{R_1}{l_{13}}\Big)^2\zeta_1 + \Big(\frac{R_2}{l_{23}}\Big)^2\zeta_2 - \Big(\frac{R_4}{l_{34}}\Big)^2\zeta_4\Big] + O(\delta^3) \\
U_4 \sim\ & -\frac{F_3^0}{R_4} - \delta\frac{F_3^1}{R_4} + \delta\frac{3F_3^0}{2l_{34}} - \delta^2\frac{F_3^2}{R_4} + \delta^2\frac{3F_3^2}{2l_{34}} \\
& + \frac{3}{2}\delta F_1^0\Big(\frac{1}{l_{14}} - \frac{1}{l_{24}}\Big) + \frac{3}{2}\delta^2 F_1^1\Big(\frac{1}{l_{14}} - \frac{1}{l_{24}}\Big) \\
& + \delta^2\Big[\Big(\frac{R_1}{l_{14}}\Big)^2\zeta_1 + \Big(\frac{R_2}{l_{24}}\Big)^2\zeta_2 + \Big(\frac{R_3}{l_{34}}\Big)^2\zeta_3\Big] + O(\delta^3).
\end{aligned}$$

Compare the $O(1)$ terms:

$$U_1^0 = U_2^0 \ \Rightarrow\ \frac{F_1^0}{R_1} = -\frac{F_1^0}{R_2} \ \Rightarrow\ F_1^0 = 0, \quad \text{similarly,} \quad F_3^0 = 0.$$

Compare the $O(\delta)$ terms:

$$U_1^1 = U_2^1 \;\Rightarrow\; \frac{F_1^1}{R_1} = -\frac{F_1^1}{R_2} \;\Rightarrow\; F_1^1 = 0, \quad \text{similarly,} \quad F_3^1 = 0.$$

Compare the $O(\delta^2)$ terms:

$$\begin{aligned} U_1^2 &= \frac{F_1^2}{R_1} + \Big[-\Big(\frac{R_2}{l_{12}}\Big)^2\zeta_2 - \Big(\frac{R_3}{l_{13}}\Big)^2\zeta_3 - \Big(\frac{R_4}{l_{14}}\Big)^2\zeta_4\Big] \\ U_2^2 &= -\frac{F_1^2}{R_2} + \Big[\Big(\frac{R_1}{l_{12}}\Big)^2\zeta_1 - \Big(\frac{R_3}{l_{23}}\Big)^2\zeta_3 - \Big(\frac{R_4}{l_{24}}\Big)^2\zeta_4\Big] \\ U_1^2 = U_2^2 \Rightarrow F_1^2 &= \frac{R_1R_2}{R_1+R_2}\Big(\frac{1}{l_{13}^2} - \frac{1}{l_{23}^2} - \frac{1}{l_{14}^2} + \frac{1}{l_{24}^2}\Big)R_3^2\zeta_3 \end{aligned}$$

and similarly,

$$\begin{aligned} U_3^2 &= \frac{F_3^2}{R_3} + \Big[\Big(\frac{R_1}{l_{13}}\Big)^2\zeta_1 + \Big(\frac{R_2}{l_{23}}\Big)^2\zeta_2 - \Big(\frac{R_4}{l_{34}}\Big)^2\zeta_4\Big] \\ U_4^2 &= -\frac{F_3^2}{R_4} + \Big[\Big(\frac{R_1}{l_{14}}\Big)^2\zeta_1 + \Big(\frac{R_2}{l_{24}}\Big)^2\zeta_2 + \Big(\frac{R_3}{l_{34}}\Big)^2\zeta_3\Big] \\ U_3^2 = U_4^2 \Rightarrow F_3^2 &= \frac{R_3R_4}{R_3+R_4}\Big(\frac{1}{l_{14}^2} - \frac{1}{l_{13}^2} - \frac{1}{l_{24}^2} + \frac{1}{l_{23}^2}\Big)R_1^2\zeta_1. \end{aligned}$$

Velocities of the PMPYs:

$$\begin{aligned} U_I = U_1 = U_2 &= \frac{R_1^2}{l_{12}^2}\zeta_1\delta^2 + R_3^2\zeta_3\delta^2\Big[\frac{R_1}{R_1+R_2}\Big(\frac{1}{l_{14}^2} - \frac{1}{l_{13}^2}\Big) \\ &\quad + \frac{R_2}{R_1+R_2}\Big(\frac{1}{l_{24}^2} - \frac{1}{l_{23}^2}\Big)\Big] \\ U_{II} = U_3 = U_4 &= \frac{R_3^2}{l_{34}^2}\zeta_3\delta^2 + R_1^2\zeta_1\delta^2\Big[\frac{R_3}{R_3+R_4}\Big(\frac{1}{l_{13}^2} - \frac{1}{l_{23}^2}\Big) \\ &\quad + \frac{R_4}{R_3+R_4}\Big(\frac{1}{l_{14}^2} - \frac{1}{l_{24}^2}\Big)\Big] \end{aligned}$$

Power of the PMPYs:

$$\begin{aligned} P_I &= \frac{8}{3}\big(R_1\zeta_1^2 + R_2\zeta_2^2\big) = \frac{8}{3}R_1\frac{R_1^3+R_2^3}{R_2^3}\zeta_1^2 \\ P_{II} &= \frac{8}{3}\big(R_3\zeta_3^2 + R_4\zeta_4^2\big) = \frac{8}{3}R_3\frac{R_3^3+R_4^3}{R_4^3}\zeta_3^2 \end{aligned}$$

F.3 System C with controls in $(\dot{l}_I, \dot{R}_3)$

The asymptotic behavior of the velocity of each sphere is

$$
\begin{aligned}
U_1 &\sim \frac{F_1}{6\pi\mu R_1} + \frac{F_2}{4\pi\mu l_{12}} + \Big[\frac{F_3}{4\pi\mu l_{13}} - \Big(\frac{R_3}{l_{13}}\Big)^2 \dot{R}_3\Big] + \Big[\frac{F_4}{4\pi\mu l_{14}} - \Big(\frac{R_4}{l_{14}}\Big)^2 \dot{R}_4\Big] \\
U_2 &\sim \frac{F_2}{6\pi\mu R_2} + \frac{F_1}{4\pi\mu l_{12}} + \Big[\frac{F_3}{4\pi\mu l_{23}} - \Big(\frac{R_3}{l_{23}}\Big)^2 \dot{R}_3\Big] + \Big[\frac{F_4}{4\pi\mu l_{24}} - \Big(\frac{R_4}{l_{24}}\Big)^2 \dot{R}_4\Big] \\
U_3 &\sim \frac{F_3}{6\pi\mu R_3} + \frac{F_1}{4\pi\mu l_{13}} + \frac{F_2}{4\pi\mu l_{23}} + \Big[\frac{F_4}{4\pi\mu l_{34}} - \Big(\frac{R_4}{l_{34}}\Big)^2 \dot{R}_4\Big] \\
U_4 &\sim \frac{F_4}{6\pi\mu R_4} + \frac{F_1}{4\pi\mu l_{14}} + \frac{F_2}{4\pi\mu l_{24}} + \Big[\frac{F_3}{4\pi\mu l_{34}} + \Big(\frac{R_3}{l_{34}}\Big)^2 \dot{R}_3\Big]
\end{aligned}
$$

with relations

$$
\begin{gathered}
U_2 - U_1 = \dot{l}_{12} = \xi_I, \quad U_4 - U_3 = 0 \\
F_1 + F_2 = 0, \quad F_3 + F_4 = 0 \\
R_3^2\zeta_3 + R_4^2\zeta_4 = 0 \;\Rightarrow\; R_4^2\zeta_4 = -R_3^2\zeta_3.
\end{gathered}
$$

After scaling

$$
\begin{aligned}
U_1 &\sim \frac{F_1}{R_1} + \frac{3F_2}{2l_{12}}\delta + \Big[\frac{2F_3}{2l_{13}}\delta - \Big(\frac{R_3}{l_{13}}\Big)^2\zeta_3\delta^2\Big] + \Big[\frac{3F_4}{2l_{14}}\delta - \Big(\frac{R_4}{l_{14}}\Big)^2\zeta_4\delta^2\Big] \\
U_2 &\sim \frac{F_2}{R_2} + \frac{3F_1}{2l_{12}}\delta + \Big[\frac{2F_3}{2l_{23}}\delta - \Big(\frac{R_3}{l_{23}}\Big)^2\zeta_3\delta^2\Big] + \Big[\frac{3F_4}{2l_{24}}\delta - \Big(\frac{R_4}{l_{24}}\Big)^2\zeta_4\delta^2\Big] \\
U_3 &\sim \frac{F_3}{R_3} + \frac{3F_1}{2l_{13}}\delta + \frac{3F_2}{2l_{23}}\delta + \Big[\frac{3F_4}{2l_{34}}\delta - \Big(\frac{R_4}{l_{34}}\Big)^2\zeta_4\delta^2\Big] \\
U_4 &\sim \frac{F_4}{R_4} + \frac{3F_1}{2l_{14}}\delta + \frac{3F_2}{2l_{24}}\delta + \Big[\frac{3F_3}{2l_{34}}\delta + \Big(\frac{R_3}{l_{34}}\Big)^2\zeta_3\delta^2\Big].
\end{aligned}
$$

With $F_2 = -F_1,\ F_4 = -F_3$, the system is simplified to

$$
\begin{aligned}
U_1 &\sim \frac{F_1}{R_1} - \frac{3F_1}{2l_{12}}\delta + \Big[\frac{3F_3}{2l_{13}}\delta - \Big(\frac{R_3}{l_{13}}\Big)^2\zeta_3\delta^2\Big] + \Big[-\frac{3F_3}{2l_{14}}\delta + \Big(\frac{R_3}{l_{14}}\Big)^2\zeta_3\delta^2\Big] \\
U_2 &\sim -\frac{F_1}{R_2} + \frac{3F_1}{2l_{12}}\delta + \Big[\frac{3F_3}{2l_{23}}\delta - \Big(\frac{R_3}{l_{13}}\Big)^2\zeta_3\delta^2\Big] + \Big[-\frac{3F_3}{2l_{24}}\delta + \Big(\frac{R_3}{l_{24}}\Big)^2\zeta_3\delta^2\Big] \\
U_3 &\sim \frac{F_3}{R_3} + \frac{3F_1}{2l_{13}}\delta - \frac{3F_1}{2l_{23}}\delta + +\Big[-\frac{3F_3}{2l_{34}}\delta + \Big(\frac{R_3}{l_{34}}\Big)^2\zeta_3\delta^2\Big] \\
U_4 &\sim -\frac{F_3}{R_4} + \frac{3F_1}{2l_{14}}\delta - \frac{3F_1}{2l_{24}}\delta + +\Big[\frac{3F_3}{2l_{34}}\delta + \Big(\frac{R_3}{l_{34}}\Big)^2\zeta_3\delta^2\Big].
\end{aligned}
$$

For PMPY I,

$$
\xi_I = U_2 - U_1 \sim -F_1\Big(\frac{1}{R_1} + \frac{1}{R_2}\Big) \;\Rightarrow\; F_1 = -\frac{R_1R_2}{R_1 + R_2}\xi_I,
$$

thus for PMPY II,

$$U_3 \sim \frac{F_3}{R_3} - \frac{3}{2}\frac{R_1R_2}{R_1+R_2}\xi_I\delta\Big(\frac{1}{l_{13}} - \frac{1}{l_{23}}\Big) - \frac{3F_3}{2l_{34}}\delta + \Big(\frac{R_3}{l_{34}}\Big)^2\zeta_3\delta^2$$
$$U_4 \sim -\frac{F_3}{R_4} - \frac{3}{2}\frac{R_1R_2}{R_1+R_2}\xi_I\delta\Big(\frac{1}{l_{14}} - \frac{1}{l_{24}}\Big) + \frac{3F_3}{2l_{34}}\delta + \Big(\frac{R_3}{l_{34}}\Big)^2\zeta_3\delta^2.$$

Expand F_3 as $F_3 = F_3^0 + \delta F_3^1 + \delta^2 F_3^2 + O(\delta^3)$,

$$U_3 \sim \frac{F_3^0}{R_3} + \delta\frac{F_3^1}{R_3} + \delta^2\frac{F_3^2}{R_3} - \frac{3}{2}\frac{R_1R_2}{R_1+R_2}\xi_I\delta\Big(\frac{1}{l_{13}} - \frac{1}{l_{23}}\Big) - \frac{3F_3^0}{2l_{34}}\delta - \frac{3F_3^1}{2l_{34}}\delta^2 + \Big(\frac{R_3}{l_{34}}\Big)^2\zeta_3\delta^2$$
$$U_4 \sim -\frac{F_3^0}{R_4} - \delta\frac{F_3^1}{R_4} - \delta^2\frac{F_3^2}{R_4} - \frac{3}{2}\frac{R_1R_2}{R_1+R_2}\xi_I\delta\Big(\frac{1}{l_{14}} - \frac{1}{l_{24}}\Big) + \frac{3F_3^0}{2l_{34}}\delta + \frac{3F_3^1}{2l_{34}}\delta^2 + \Big(\frac{R_3}{l_{34}}\Big)^2\zeta_3\delta^2$$

Compare the $O(1)$ terms

$$U_3^0 = U_4^0 \;\Rightarrow\; \frac{F_3^0}{R_3} = -\frac{F_3^0}{R_4} \;\Rightarrow\; F_3^0 = 0.$$

Compare the $O(\delta)$ terms

$$U_3^1 = U_4^1 \;\Rightarrow\; F_3^1 = \frac{3}{2}\frac{R_1R_2}{R_1+R_2}\frac{R_3R_4}{R_3+R_4}\xi_I\Big(\frac{1}{l_{13}} - \frac{1}{l_{23}} - \frac{1}{l_{14}} + \frac{1}{l_{24}}\Big)$$

Velocities of the PMPYs:

$$\begin{aligned}\overline{U}_I &= \frac{1}{2}(U_1+U_2)\\ &= \frac{9}{8}\frac{R_1R_2R_3R_4}{(R_1+R_2)(R_3+R_4)}\xi_I\delta^2\Big(\frac{1}{l_{13}} - \frac{1}{l_{14}} + \frac{1}{l_{23}} - \frac{1}{l_{24}}\Big)^2\\ &\quad + \frac{1}{2}R_3^2\zeta_3\delta^2\Big(\frac{1}{l_{14}^2} - \frac{1}{l_{13}^2} + \frac{1}{l_{24}^2} - \frac{1}{l_{23}^2}\Big)\\ \overline{U}_{II} &= U_3 = U_4\\ &\sim \frac{3}{2}\frac{R_1R_2}{R_1+R_2}\xi_I\delta\Big[\frac{R_3}{R_3+R_4}\Big(\frac{1}{l_{23}} - \frac{1}{l_{13}}\Big) + \frac{R_4}{R_3+R_4}\Big(\frac{1}{l_{24}} - \frac{1}{l_{14}}\Big)\Big]\end{aligned}$$

Power of the PMPYs:

$$P_I = F_1U_1 + F_2U_2 = F_1(U_1 - U_2) = -F_1\xi_I = \frac{R_1R_2}{R_1+R_2}\xi_I^2$$

$$P_{II} = \frac{8}{3}(R_3\zeta_3^2 + R_4\zeta_4^2) = \frac{8}{3}R_3\frac{R_3^3 + R_4^3}{R_4^3}\zeta_3^2$$

References

Alexander G, Pooley C, Yeomans J (2009) Hydrodynamics of linked sphere model swimmers. J Phys Condens Matter 21(20):204108

Alexander GP, Yeomans JM (2008) Dumb-bell swimmers. EPL (Eur Lett) 83(3):34006

Avron J, Kenneth O, Oaknin D (2005) Pushmepullyou: an efficient micro-swimmer. New J Phys 7:234

Barry NP, Bretscher MS (2010) Dictyostelium amoebae and neutrophils can swim. Proc Natl Acad Sci 107(25):11376

Bergert M, Chandradoss SD, Desai RA, Paluch E (2012) Cell mechanics control rapid transitions between blebs and lamellipodia during migration. Proc Natl Acad Sci 109(36):14434–14439

Binamé F, Pawlak G, Roux P, Hibner U (2010) What makes cells move: requirements and obstacles for spontaneous cell motility. Mol BioSyst 6(4):648–661

Brennen CE (2013) Cavitation and bubble dynamics. Cambridge University Press, Cambridge

Brenner H (1961) The slow motion of a sphere through a viscous fluid towards a plane surface. Chem Eng Sci 16(3–4):242–251

Charras G, Paluch E (2008) Blebs lead the way: how to migrate without lamellipodia. Nat Rev Mol Cell Biol 9(9):730–736

Childress S (1977) Mechanics of swimming and flying. Courant Institute of Mathematical Sciences, New York

Cooley M, O'Neill M (1969a) On the slow motion generated in a viscous fluid by the approach of a sphere to a plane wall or stationary sphere. Mathematika 16(01):37–49

Cooley M, O'Neill M (1969b) On the slow motion of two spheres in contact along their line of centres through a viscous fluid. Math Proc Cambr Philos Soc 66(2):407–415 Cambridge Univ Press

Curtis MP, Gaffney EA (2013) Three-sphere swimmer in a nonlinear viscoelastic medium. Phys Rev E 87(4):043006

Dunkel J, Putz VB, Zaid IM, Yeomans JM (2010) Swimmer–tracer scattering at low Reynolds number. Soft Matter 6(17):4268–4276

Elgeti J, Winkler RG, Gompper G (2015) Physics of microswimmers—single particle motion and collective behavior: a review. Rep Prog Phys 78(5):056601

Fackler OT, Grosse R (2008) Cell motility through plasma membrane blebbing. J Cell Biol 181(6):879–884

Friedl P, Alexander S (2011) Cancer invasion and the microenvironment: plasticity and reciprocity. Cell 147(5):992–1009

Friedl P, Wolf K (2003) Plasticity of cell migration: a multiscale tuning model. Nat Rev Cancer 3(5):362–74

Hancock G (1953) The self-propulsion of microscopic organisms through liquids. Proc R Soc Lond Ser A 217(1128):96–121

Higdon JJL (1979) The hydrodynamics of flagellar propulsion: helical waves. J Fluid Mech 94:331–351

Ishikawa T, Locsei J, Pedley T (2010) Fluid particle diffusion in a semidilute suspension of model micro-organisms. Phys Rev E 82(2):021408

Kim S, Karrila SJ (1991) Microhydrodynamics: principles and selected applications. Butterworth-Heinemann, New York

Koiller J, Ehlers K, Montgomery R (1996) Problems and progress in microswimming. J Nonlinear Sci 6(6):507–541

Kurtuldu H, Guasto JS, Johnson KA, Gollub JP (2011) Enhancement of biomixing by swimming algal cells in two-dimensional films. Proc Natl Acad Sci 108(26):10391–10395

Lämmermann T, Bader BL, Monkley SJ, Worbs T, Wedlich-Söldner R, Hirsch K, Keller M, Förster R, Critchley DR, Fässler R et al (2008) Rapid leukocyte migration by integrin-independent flowing and squeezing. Nature 453(7191):51–55

Lauga E, Powers TR (2009) The hydrodynamics of swimming microorganisms. Rep Prog Phys 72(9):096601

Lauga E (2011) Life around the scallop theorem. Soft Matter 7(7):3060–3065

Lauga E, Bartolo D (2008) No many-scallop theorem: collective locomotion of reciprocal swimmers. Phys Rev E 78(3):030901

Leptos KC, Guasto JS, Gollub JP, Pesci AI, Goldstein RE (2009) Dynamics of enhanced tracer diffusion in suspensions of swimming eukaryotic microorganisms. Phys Rev Lett 103(19):198103
Liang Z, Gimbutas Z, Greengard L, Huang J, Jiang S (2013) A fast multipole method for the Rotne–Prager–Yamakawa tensor and its applications. J Comput Phys 234:133–139
Lin Z, Thiffeault J-L, Childress S (2011) Stirring by squirmers. J Fluid Mech 669:167–177
Luke JH (1989) Convergence of a multiple reflection method for calculating Stokes flow in a suspension. SIAM J Appl Math 49(6):1635–1651
Maiuri P, Rupprecht J-F, Wieser S, Ruprecht V, Bénichou O, Carpi N, Coppey M, Beco SD, Gov N, Heisenberg C-P et al (2015) Actin flows mediate a universal coupling between cell speed and cell persistence. Cell 161(2):374–386
Miño G, Mallouk TE, Darnige T, Hoyos M, Dauchet J, Dunstan J, Soto R, Wang Y, Rousselet A, Clement E (2011) Enhanced diffusion due to active swimmers at a solid surface. Phys Rev Lett 106(4):048102
Najafi A, Golestanian R (2004) Simple swimmer at low Reynolds number: three linked spheres. Phys Rev E 69(6):062901
Phan-Thien N, Tran-Cong T, Ramia M (1987) A boundary-element analysis of flagellar propulsion. J Fluid Mech 184:533–549
Pozrikidis C (1992) Boundary integral and singularity methods for linearized viscous flow. Cambridge Univ Press, Cambridge
Purcell EM (1977) Life at low Reynolds number. Am J Phys 45(1):3–11
Pushkin DO, Shum H, Yeomans JM (2013) Fluid transport by individual microswimmers. J Fluid Mech 726:5–25
Qiu T, Lee T-C, Mark AG, Morozov KI, Münster R, Mierka O, Turek S, Leshansky AM, Fischer P (2014) Swimming by reciprocal motion at low Reynolds number. Nat Commun 5:5119
Renkawitz J, Schumann K, Weber M, Lämmermann T, Pflicke H, Piel M, Polleux J, Spatz JP, Sixt M (2009) Adaptive force transmission in amoeboid cell migration. Nat Cell Biol 11(12):1438–1443
Renkawitz J, Sixt M (2010) Mechanisms of force generation and force transmission during interstitial leukocyte migration. EMBO Rep 11(10):744–750
Ruprecht V, Wieser S, Callan-Jones A, Smutny M, Morita H, Sako K, Barone V, Ritsch-Marte M, Sixt M, Voituriez R et al (2015) Cortical contractility triggers a stochastic switch to fast amoeboid cell motility. Cell 160(4):673–685
Rushkin I, Kantsler V, Goldstein RE (2010) Fluid velocity fluctuations in a suspension of swimming protists. Phys Rev Lett 105(18):188101
Shum H, Gaffney E, Smith D (2010) Modelling bacterial behaviour close to a no-slip plane boundary: the influence of bacterial geometry. Proc R Soc Lond A Math Phys Eng Sci 466:1725–1748 The Royal Society
Sokolov A, Goldstein RE, Feldchtein FI, Aranson IS (2009) Enhanced mixing and spatial instability in concentrated bacterial suspensions. Phys Rev E 80(3):031903
Stimson M, Jeffery G (1926) The motion of two spheres in a viscous fluid. Proc R Soc Lond Ser A 111(757):110–116
Stone HA, Samuel ADT (1996) Propulsion of microorganisms by surface distortions. Phys Rev Lett 77(19):4102–4104
Taylor G (1952) The action of waving cylindrical tails in propelling microscopic organisms. Proc R Soc Lond Ser A 211(1105):225–239
Underhill PT, Hernandez-Ortiz JP, Graham MD (2008) Diffusion and spatial correlations in suspensions of swimming particles. Phys Rev Lett 100(24):248101
Van Haastert PJ (2011) Amoeboid cells use protrusions for walking, gliding and swimming. PLoS ONE 6(11):e27532
van Zijl F, Krupitza G, Mikulits W (2011) Initial steps of metastasis: cell invasion and endothelial transmigration. Rev Mutat Res 728(1):23–34
Wajnryb E, Mizerski KA, Zuk PJ, Szymczak P (2013) Generalization of the Rotne–Prager–Yamakawa mobility and shear disturbance tensors. J Fluid Mech 731:R5
Wang Q, Hu J, Othmer H (2012) Models of low reynolds number swimmers inspired by cell blebbing. In: Natural locomotion in fluids and on surfaces. Springer, Berlin, pp 185–195
Wang Q, Othmer HG (2015) The performance of discrete models of low Reynolds number swimmers. Math Biosci Eng 12(6):1303–1320
Wang Q, Othmer HG (2016) Computational analysis of amoeboid swimming at low Reynolds number. J Math Biol 72(7):1893–1926

Welch MD (2015) Cell migration, freshly squeezed. Cell 160(4):581–582
Wolf K, Mazo I, Leung H, Engelke K, Andrian UHV, Deryugina EI, Strongin AY, Bröcker EB, Friedl P (2003) Compensation mechanism in tumor cell migration: mesenchymal-amoeboid transition after blocking of pericellular proteolysis. J Cell Biol 160(2):267–277
Wu X-L, Libchaber A (2000) Particle diffusion in a quasi-two-dimensional bacterial bath. Phys Rev Lett 84(13):3017
Yamakawa H (1970) Transport properties of polymer chains in dilute solution: hydrodynamic interaction. J Chem Phys 53(1):436–443
Yeomans JM, Pushkin DO, Shum H (2014) An introduction to the hydrodynamics of swimming microorganisms. Eur Phys J Spec Topics 223(9):1771–1785
Zaid IM, Dunkel J, Yeomans JM (2011) Lévy fluctuations and mixing in dilute suspensions of algae and bacteria. J R Soc Interface 8(62):1314–1331
Zatulovskiy E, Tyson R, Bretschneider T, Kay RR (2014) Bleb-driven chemotaxis of Dictyostelium cells. J Cell Biol 204(6):1027–1044
Zuk P, Wajnryb E, Mizerski K, Szymczak P (2014) Rotne–Prager–Yamakawa approximation for different-sized particles in application to macromolecular bead models. J Fluid Mech 741:R5